BUDOWNICTWO
I ARCHITEKTURA

Vol. 20(4) 2021

ISSN 1899-0665

SPIS TREŚCI
CONTENTS

Crossref
Similarity Check
Powered by iThenticate

Orginal Article

Comparison of methods of monitoring structure deformations based on tests of a flat plate slab

Damian Nykiel

*Department of Building Structures; Faculty of Civil and Environmental Engineering
and Architecture; Rzeszow University of Technology;
2 Poznańska St., 35-084 Rzeszów, Poland;
d.nykiel@prz.edu.pl* (iD) *0000-0003-2259-5917*

Abstract: This work includes a comparison of the methods of monitoring the deformations of a structure on the example of a flat plate slab test. Classic ESG (electrofusion strain gauges) and modern DFOS (distributed fiber optic sensors) were compared. During the research, both types of sensors were used on some of the reinforcing bars. The study aims to indicate the differences between the compared monitoring methods, both in terms of the obtained results and their utility values.

Keywords: measurement, deformation, strains, flat plate slab, electrofusion strain gauge, fibre optic gauge

1. Introduction

The evolution of measurement techniques provides us with increasingly more opportunities to obtain information on the behaviour of the structure during use or destruction [6]. This includes reinforced concrete structures, where the reinforcing steel embedded in concrete into a large area invisible to the observer. Therefore, for this type of construction, it is important to use measurement techniques that ensure the obtained results are reliable and as extensive as possible. In the case of large and complex elements, the results of experimental tests obtained on research models are the basis for the validation of numerical models. This is of particular importance in reinforced concrete structures, where many processes are not yet fully explained, and the results obtained from FEM models are often inconsistent with test results. Correct measurement and analysis of the obtained results, apart from experimental tests, are also very important during the continuous monitoring of deformations of real structures [1], [4], [7].

This article aims to compare two methods of deformation measurement that can be used in research and continuous monitoring of structures. Based on the conducted research, particular attention was paid to showing the advantages and disadvantages of these methods in the case of measurements of reinforcing bars deformation in reinforced concrete structures.

The inspiration for this comparison was research conducted at the Rzeszów University of Technology under a contract concluded with CELSA Huta Ostrowiec, a part of project no. POIR.01.02.00-00-0223/-17 entitled: "Manufacture of innovative bars and rings for concrete reinforcement, made in the new class of steel B600B with the implementation of a proprietary technology demonstrator". The conducted research concerned the issue of verification of the influence of reinforcing bars made of B600B steel on the development of a progressive catastrophe caused by the removal of the edge support in the flat plate system.

2. Description of the tested model

The tested model presented in fig. 1, was a sixteen-section flat plate slab, reflecting the work of the real structure.

Fig. 1.   View of the research model. *Source*: author

The tested model was made on a scale of 1:3 so that it replicated the real object as accurately as possible. The model assumed a support spacing of 2.4 m, which corresponds to a ceiling span of 7.2 m commonly used in construction in scale 1:3. The slab thickness was assumed to be 80 mm and the dimension of prefabricated columns 300x300 mm. The total dimension of the tested slab was 9.9 x 9.9 m. The research model of the slab was monolithic. The upper part of the columns was monolithized with the slab plate in the laboratory – fig. 2. The slab reinforcement was designed assuming the ceiling loads had the following values: permanent load $g_k = 3$ kN/m^2 and variable load $q_k = 3$ kN/m^2. Different bonding reinforcement was used in the tested element to create a secondary load-bearing structure in the event of local damage to the edge columns.

Fig. 2.   Prefabricated reinforced concrete columns attached to the strength floor. *Source*: author

Two methods of ceiling loading were used. In method 1, concrete weights of 200 kg each were suspended on steel ropes passing through holes prepared in the slab and anchored on its upper surface with washers. These weights were used to simulate permanent and variable loads occurring in this type of structure.

In method 2, after removing the edge column (under full load from method 1), the load with the actuator was implemented. The force from the actuator was transferred to the place of the removed support by a cubic reinforced concrete block imitating the upper storey column.

The results were read with a constant interval determined by lifting weights (method 1) and increasing the force on the actuator every 5 kN (method 2).

During the conducted research, various measuring techniques, from traditional to modern, were used to measure strains of concrete and steel. The strains of concrete and steel were measured using ESG (electrofusion strain gauges) and DFOS (distributed fiber optic strain) gauges located along the entire length of tested elements.

Electrofusion strain gauges have several advantages that determine their wide range of applications. They are used in tests under static and dynamic loads. The strain gauges are sensitive and their very low weight that does not affect the accuracy of the measurements. Direct transmission of strains to the resistance wire eliminates errors in transmission inaccuracy or slippage that may occur in other strain gauges. Measurements do not depend on the base adopted because result readings are dimensionless. Experience with monitoring systems based on strain measurements shows that there are issues with the interpretation of measurement results and their reliability [9]. As for the strain sensors, an exact connection with monitored elements and stability of their indications is essential. Electrofusion strain gauges are sensitive to operation in a complex state of stress and temperature, therefore improper positioning of the sensors may result in erroneous and unreliable results.

DFOS is a type of fiberoptic sensor that, apart from interferometric sensors and sensors with Bragg grating, is increasingly used in monitoring structures [4]. The fiberoptic measurement technique enables quasi-continuous measurements, consisting of the distribution of up to a dozen measurement points along the sensor of a single fiber (Bragg grating). From an engineering point of view, these distributed measurements, in which the lengths of virtual

sensors and their distances are so small (row 5-10 mm), can be considered geometrically continuous [5]. This approach allows replacing thousands of traditional sensors with a single optical fiber. For example, on a length of 1 m, it is possible to obtain information about the strain's value even at 200 measurement points. This measurement technique also allows recording and locating cracks in the concrete [3].

3. Methods of deformation measurement

During the conducted studies, electrofusion strain gauges and fiberoptic strain gauges were used to measure strains. In the tested element, more than 100 electrofusion strain gauges were glued onto reinforcing steel and about 50 onto concrete. 19 fiberoptic strain gauges were also glued onto reinforcing steel and 4 onto concrete. Fig. 3 and fig. 4 show a strain gauges arrangement scheme used only on reinforcing steel.
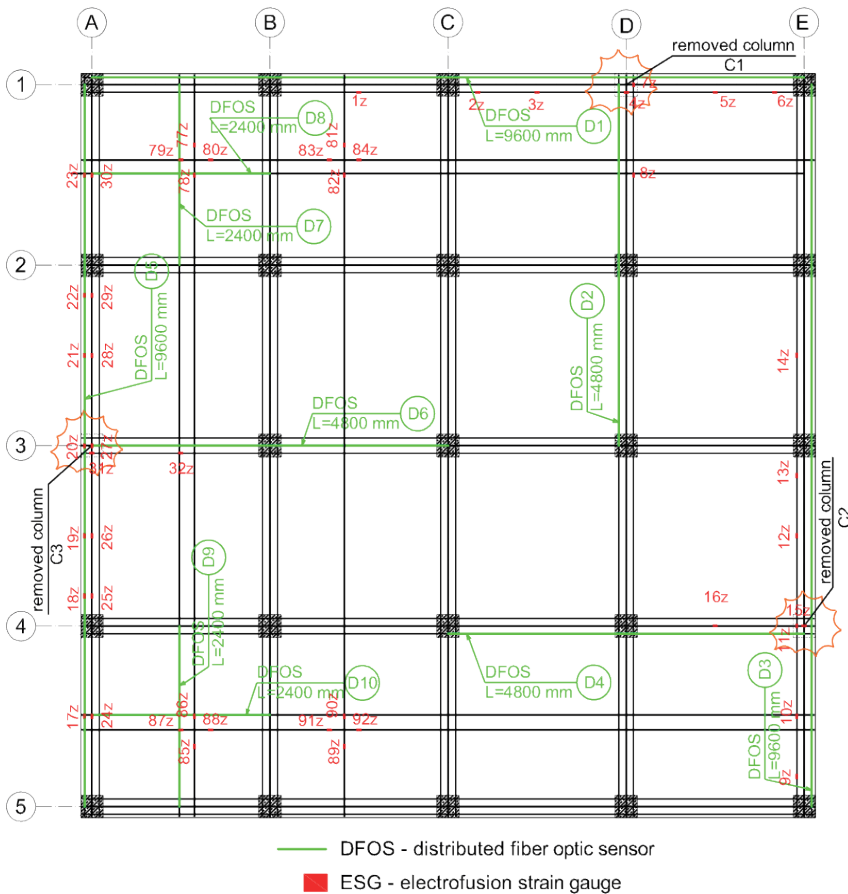
Fig. 3.   Strain gauges arrangement scheme on the bottom reinforcement. *Source*: author
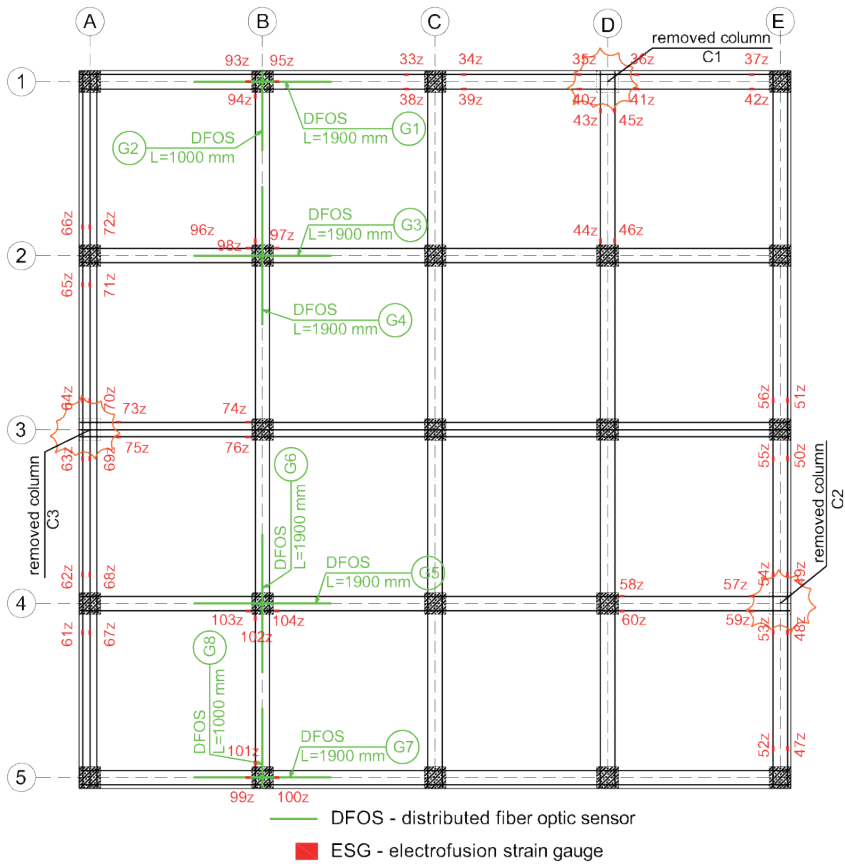
Fig. 4.   Strain gauges arrangement scheme on the top reinforcement. *Source*: author

TFs 5/120 electrofusion film strain gauges were used to measure the strains of reinforcing steel and TFs 60/120 to measure the strains of concrete produced by TENMEX. The strain gauges were glued to the reinforcement in accordance with the manufacturer's instructions. The strain gauges bonding was performed on the already prepared reinforcement of the slab. The surface of the rod was cleaned by grinding, then smoothed with sandpaper no. 300-400 in two mutually perpendicular directions. The surface was degreased with ATEPO Z-12 remover and WBT-500 swabs used once. A drop of ATEPO Z-03 neutralizer was applied, spread out and allowed to dry. A strain gauge was glued onto the prepared surface with cyanoacrylate adhesive TB-1731. Then, the cables were soldered to the ends of the strain gauge and secured against adverse weather conditions and mechanical damage with self-adhesive ALG-2 shielding and protection tape. For each strain gauge, temperature compensation strain gauges were used, glued on the same material and surface-connected to the tested element. Fig. 5 shows the prepared electrofusion strain gauges before concreting.
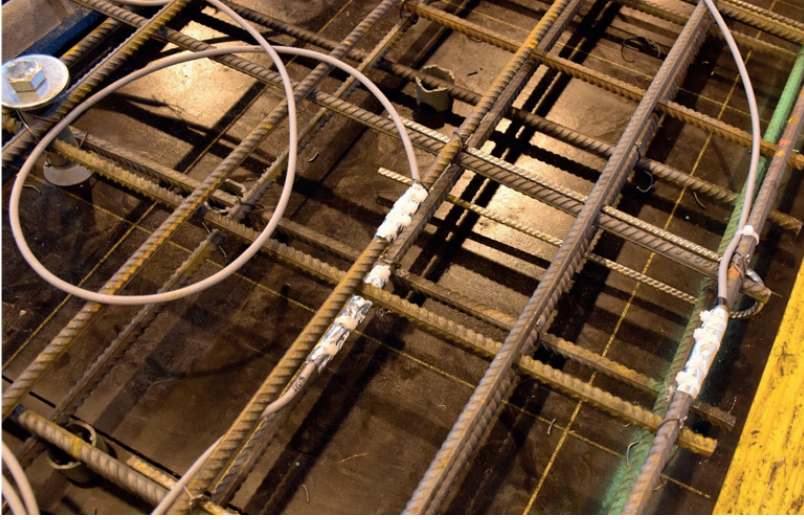
Fig. 5.   View of electrofusion strain gauges glued to the reinforcement. *Source*: author

Another group of sensors used to measure strains are optical fiber strain gauges, in which the basic element is a standard optical fiber, a thin glass fiber transmitting light in its core. DFOS (distributed fiber optic sensors) were used in the conducted research – fig. 6.
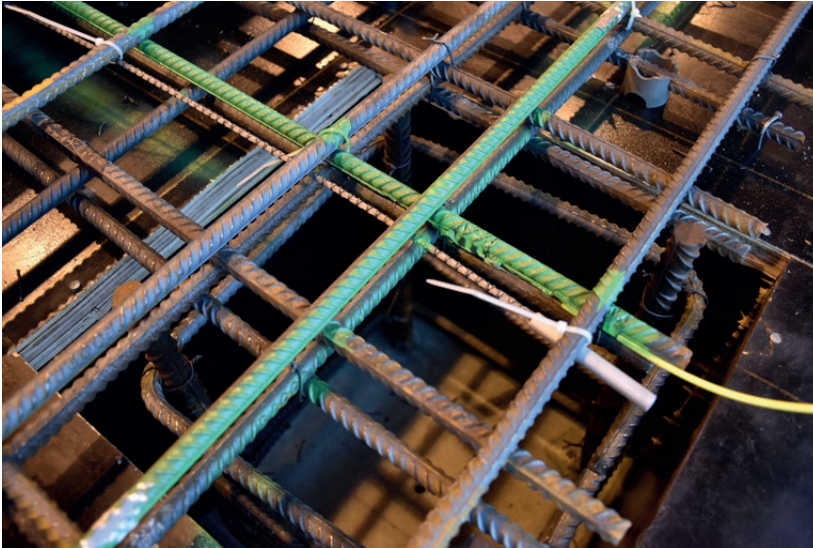
Fig. 6.   View of fibre optic strain gauge glued to the reinforcement. *Source*: author

The installation and recording of results from fiberoptic sensors were handled by an external company – SHM System. SM 9/125, OFS, ITU-G657.A1 fiber sensors were glued to the longitudinal ribs of rebars with a thin layer of epoxy resin. Strain results were recorded using OBR4600 reflectometer manufactured by LUNA Technologies in the unit:

$\mu\varepsilon = 10^{-6} = 0.0001\% = 0.001‰ = 0.001$ mm/m. The scan range was from 1,545,518 to 1,588,258 nm, the group refractive index was 1.47, and the gain was 24 dB. Optical fiber spatial resolution – 10 mm, meaning 100 sensors per 1 m of fiber. The optical fibers were glued on selected rods which, after the resin had dried, were inserted into the formwork and tied to the remaining reinforcement.

Before concreting, the operation of all strain gauges on reinforcing steel was checked and no damage was noted. A few days after concreting, another check was made. It turned out that all electrofusion strain gauges work well, while some fiber optic sensors were damaged. A more thorough inspection showed damage (or partial damage) of sensors: D1, D4, D5, D10, G2, G4, and G7. This represents 40% of all DFOS sensors used.

4. Results obtained

Examples of the strain measuring results of reinforcing steel with electrofusion strain gauges are shown in fig. 7. These are the results of several measurement points located on the bottom reinforcement, located in the tested slab.
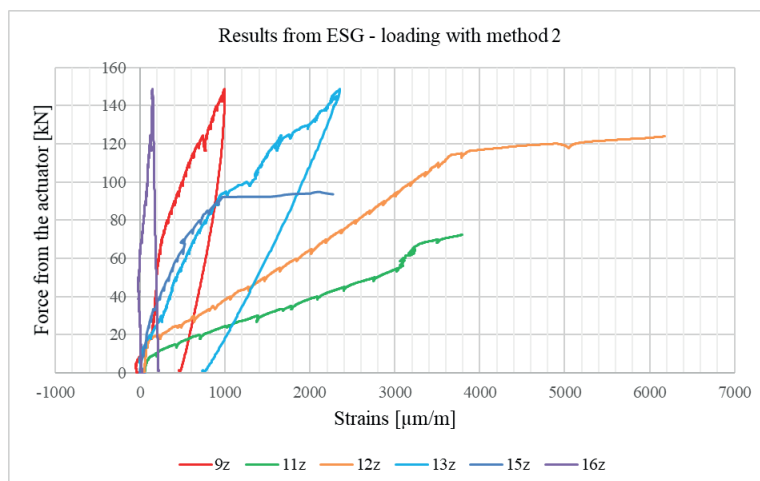
Fig. 7.   Results from electrofusion strain gauges. Strain gauges glued to different bars of the bottom rein-
forcement – loading method 2. *Source*: author

As can be seen, three strain gauges broke during the tests. The 15z strain gauge was damaged with relatively small strains amounting to only 0.1%, while the 11z and 12z strain gauges with strains of about 0.4%, which can be equated with reaching the yield point by the reinforcing steel. The failure mechanism at 0.4% strains presented in fig. 7. was typical for most strain gauges used in the research.

Fig. 9 shows the results of strain measurements for the selected two points placed on the rebar, obtained with electrofusion strain gauges. On the other hand, fig. 8. shows the results of strains measurements with the use of fiberoptic sensors. Obtained results are for the entire length of the tested reinforcing bar, the same one in which the strain gauges shown in fig. 9. were placed. The result of deformation is presented depending on 9 load stages, determined by the suspension of concrete weights simulating permanent and variable loads (method 1).
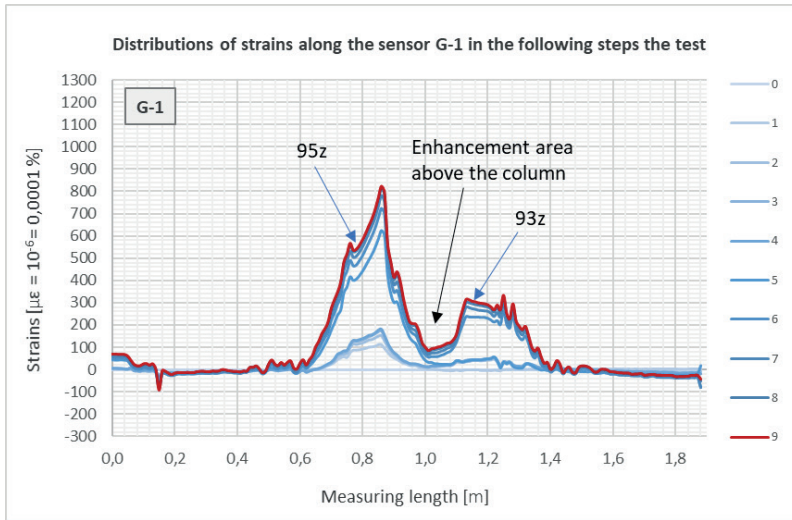
Fig. 8.   Results from the DFOS-G1 – loading method 1. *Source*: author
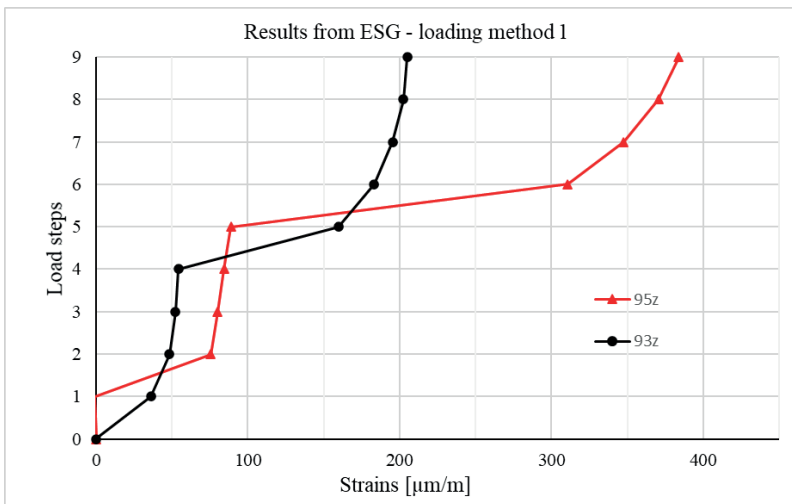
Fig. 9.   Results from the 93z and 95z electrofusion strain gauge. Strain gauges on the top reinforcement
           bar at a distance of 75 cm and 115 cm from the beginning of the bar (5 cm behind the face of the
           column) – loading method 1. *Source*: author

As can be seen, the strains obtained, e.g., step 9, are different depending on the meas-
urement technique. From electrofusion strain gauges, the strains for points 93z and 95z are
respectively: approximately 380 μm/m and 200 μm/m, while those obtained from fiberoptic
sensors are larger and amount to 95z = 530 μm/m, 93z = 300 μm/m. When analysing the strains
of the entire length of the bar, more interesting processes can be noticed, such as a decrease

in strains associated with the enhancement area above the column, or the complete loss of strains in the initial and end areas of the bar.

Continuous measurement allows you to see differences in the deformability of bars, which seem to be the same. This process was observed during tests carried out on three bars perpendicular to the removed supports. Fig. 10, fig. 11, and fig. 12 show strains diagrams obtained from fiber optic sensors placed on the analysed reinforcement bars during a load of 90 kN.
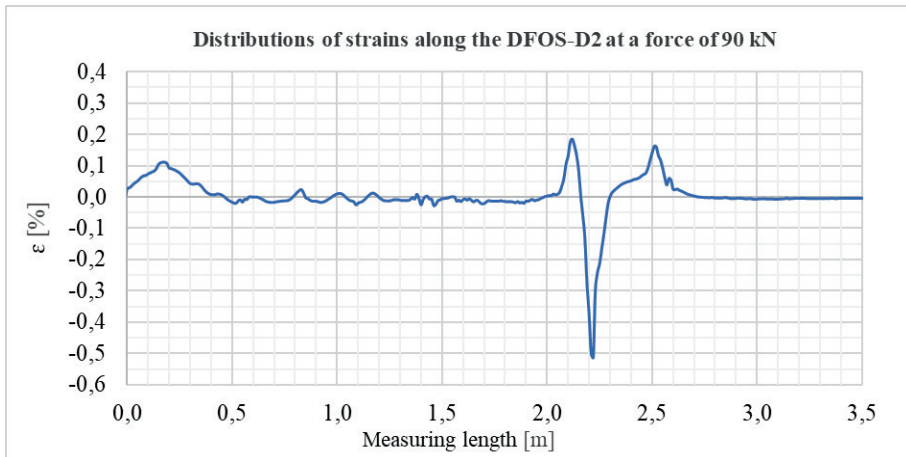
Fig. 10. Distribution of strains on the bottom reinforcement bar obtained from the DFOS-D2 sensor with an actuator load of 90 kN. *Source*: author
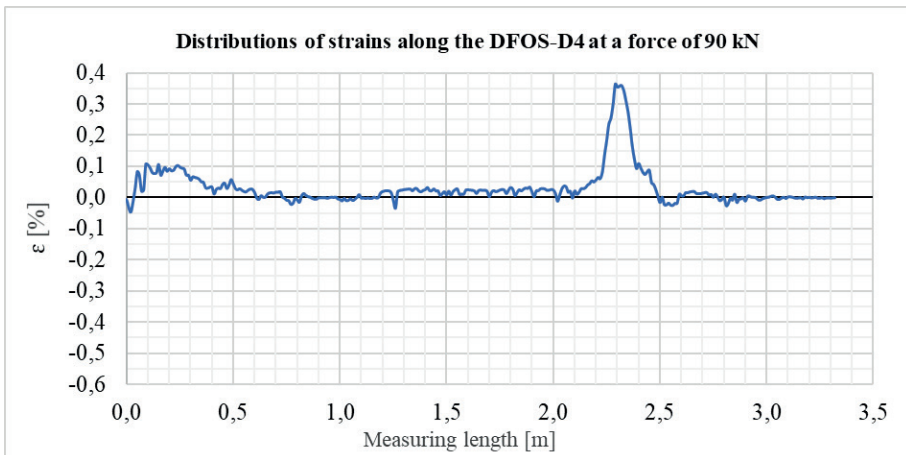
Fig. 11. Distribution of strains on the bottom reinforcement bar obtained from the DFOS-D4 sensor with an actuator load of 90 kN. *Source*: author
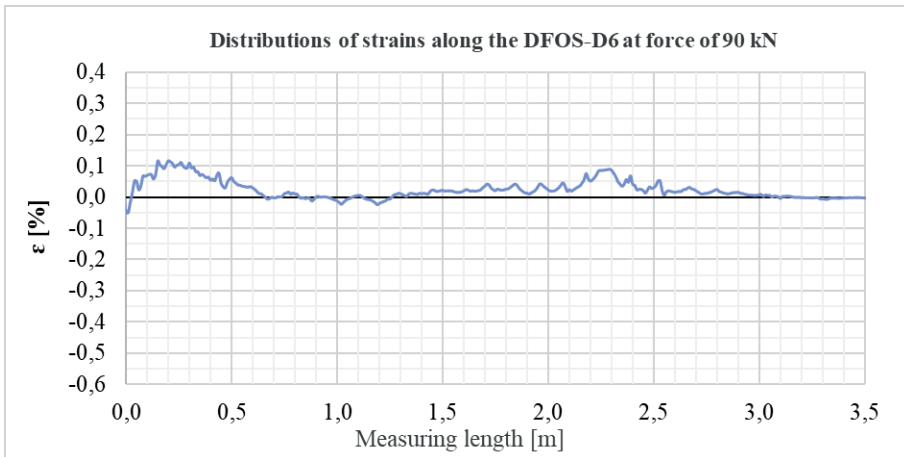
Fig. 12.   Distribution of strains on the bottom reinforcement bar obtained from the DFOS-D6 sensor with an
actuator load of 90 kN. *Source*: author

The charts presented above allow to read the tensile strains in the place where the actuator is applied, amounting to approximately 0.1% in each case. The situation is different over the support. In the case of the DFOS-D4 sensor, the expected deformation course of almost 0.4% can be seen. However, the DFOS-D2 sensor shows a completely different course. The rapid jump of strains in the compression direction to the value of -0.5% could be caused by the local influence of transverse reinforcement or the local pressure of the aggregate against the sensor. The local nature of this process highlights the fact strains before and after the "jump" amount to approximately 0.4% – similar to the DFOS-D4 sensor. The strains above the support obtained from the sensor DFOS-D6 are significantly lower. This seemingly insignificant fact had an impact on the change in the strains of the DFOS-D6 bar in relation to DFOS-D2 and DFOS-D4. During the tests, the reinforced concrete central column was removed and replaced with a steel column loosely connected to the slab. The lack of a rigid connection enabled the slab to rotate over the support and, as a result, the measured deformation of the bar was 4 times smaller.

As shown, the analysis of the results obtained from continuous measurements over the entire length of the test bar has allowed the observation of the processes impossible to detect with point strain gauges. Another disadvantage of commonly used electrofusion strain gauges is their high sensitivity when working in a complex stress state.

To analyse the processes that were impossible to capture directly during the research, a numerical model of the tested flat plate slab was created. The numerical model was devised in the ATENA program and validated based on the results obtained from experimental measurements. Fig. 13 shows the deformation of reinforcement bars during tests, obtained from numerical simulations.
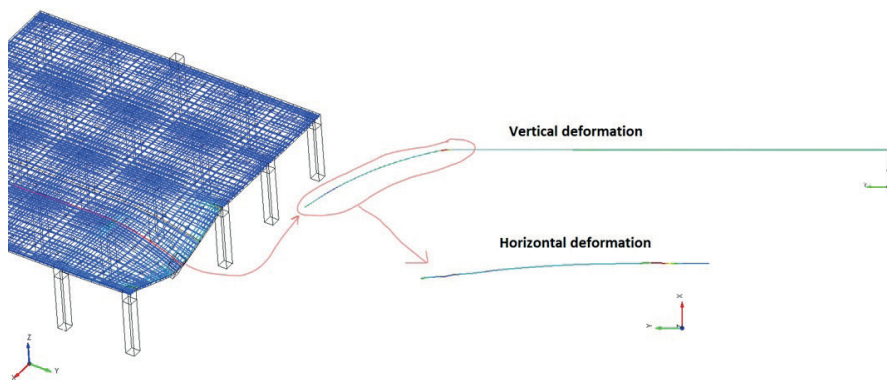
Fig. 13.   Images of reinforcing bar deformation obtained from the numerical model using the ATENA program. *Source*: author

As shown in the figure, the reinforcement bars have undergone deformations along the bar axis as well as lateral deformations. This means that the tested element works in a complex state of stress. Therefore, electrofusion strain gauges adapted to work in the uniaxial state of stress can provide erroneous results. Conducted tests confirmed that the results obtained in many cases were defective and strain gauges were destroyed at the limit strain values lower than those provided by the manufacturer. This process was not observed in the case of fiberoptic strain gauges. Conducted research and obtained results have shown one more important aspect that should be taken into account when planning the measurements – the place on the bar to which the fiberoptic strain gauge will be glued. In conducted research, the fiberoptic strain gauges were glued onto the longitudinal ribs of the reinforcing bars and then placed in the plate in such a way, that the strain gauge was located on the side edge. During formwork and concrete pouring, it is possible to rotate the bar around its axis and the glued sensor will be located on the lower or upper edge, and this may have a significant impact on obtained results and their comparison.

5. Summary and conclusions

Summarizing presented methods of monitoring the deformation of the structure, it can be noticed that new measurement techniques are superior to the traditional ones. The obtained results of strains of reinforcing steel from DFOS provide more information than classic electrofusion strain gauges. The fiberoptic sensor enables strain analysis along the entire length of the rebar, capturing the places of maximum strains and enhancement areas. During the measurements, a greater limiting strain of the DFOS sensors was also noticed, practically in every measured element, the measurement was possible up to the strains of about 4%. Measurement of such large strains in the case of electrofusion strain gauges was impossible, most of them were destroyed at strains of about 0.4%, i.e., when the reinforcing steel became plastic or cracks appeared in the concrete. In contrast, a disadvantage of optical fiber sensors is their high sensitivity to mechanical factors. A significant part of the fiber optic sensors located on the reinforcing steel was damaged during pouring and vibrating the concrete of the slab and during auxiliary works related to it. Therefore, when using fiber optic sensors, special attention should be paid to the manufacturing technology and measures to protect the sensor against

mechanical damage. Table 1 summarizes the advantages and disadvantages of the methods used to measure deformation.

Table 1.   Collective summary of advantages and disadvantages of electrofusion and fiber optic strain gauges

ESG	DFOS
Point results	Results along the entire length of the element
Lower strains limit ≈ 0.4%	Higher strains limit > 4%
No crack detection	Possibility to locate and analyse cracks
Hardiness to mechanical factors	Sensitivity to mechanical factors
Low cost of recording the results	High cost of recording the results
Sensitivity to working in a complex stress state	Hardiness to work in a complex stress state

References

[1]   Chróścielewski J. et al., "Badania wiaduktu nad torami kolejowymi przy PGE Arena w Gdańsku podczas jego realizacji", *Budownictwo i Architektura*, vol. 12(2), 2013, s. 015–022. https://doi.org/10.35784/bud-arch.2065

[2]   Bado, M.F. and Casas, J.R., "A Review of Recent Distributed Optical Fiber Sensors Applications for Civil Engineering Structural Health Monitoring", *Sensors*, vol. 21, 2021, 1818. https://doi.org/10.3390/s21051818

[3]   Bassil A. et al., *Distributed Fiber Optics Sensing and Coda Wave Interferometry Techniques for Damage Monitoring in Concrete Structures*, *Sensors*, vol. 19, 2019, 356. https://doi.org/10.3390/s19020356

[4]   Kulpa, M. and Siwowski T., "Badania pomostów kompozytowych do zastosowań w mostach drogowych", *Budownictwo i Architektura*, 13(2), 2014, pp. 231–238. https://doi.org/10.35784/bud-arch.1900

[5]   López-Higuera J., Cobo L., Incera A., Cobo A., "Fiber optic sensors in structural health monitoring", *Journal of Lightwave Technology,* vol. 29, no. 4, 15 Feb. 2011, pp. 587–608. https://doi.org/10.1109/JLT.2011.2106479.

[6]   Mesquita, E. et al., "Global overview on advances in structural health monitoring platforms", *J Civil Struct Health Monit*, vol. 6(3), 2016, pp. 461–475. https://doi.org/10.1007/s13349-016-0184-5

[7]   Poneta P., and Siwowski T., "Badania dźwigara mostowego z kompozytów FRP pod obciążeniem statycznym", *Budownictwo i Architektura*, 13(2), 2014, pp. 291–298. https://doi.org/10.35784/bud-arch.1907

[8]   Siwowski T., Sieńko R., Bednarski Ł., "System monitorowania mostów kompozytowych z wykorzystaniem światłowodowych czujników odkształceń", *Most*, May 2017, pp. 24–27.

[9]   Wierzbicki S., "Monitoring konstrukcji stalowych. Część 3 – Metody pomiarowe – pomiary odkształceń", *Builder,* R. 20, September 2016, pp. 82–84.

Crossref
Similarity Check
Powered by iThenticate

Acoustic analysis of selected sacred buildings in Szczecin

Agata Stolarska[1], Jarosław Strzałkowski[2], Agata Kandybowicz[3]

[1] *Department of Building Physics and Building Materials; Faculty of Civil and Environmental Engineering; West Pomeranian University of Technology; 50 Piastów Av., 70-311 Szczecin, Poland; siwinska@zut.edu.pl* (iD) *0000-0003-1923-2920*
[2] *Department of Building Physics and Building Materials; Faculty of Civil and Environmental Engineering; West Pomeranian University of Technology; 50 Piastów Av., 70-311 Szczecin, Poland; jaroslaw.strzalkowski@zut.edu.pl* (iD) *0000-0001-7001-9303*
[3] *Department of Building Physics and Building Materials; Faculty of Civil and Environmental Engineering; West Pomeranian University of Technology; 50 Piastów Av., 70-311 Szczecin, Poland; agata.kandybowicz@gmail.com*

Abstract: The aim of this study was to acoustically assess selected sacred buildings located in Szczecin. The research part contains the research methodology and the results obtained. The research was carried out using two methods. The first one is the integrated impulse response method where, using a bursting balloon, the time of sound pressure drop was measured at selected points of the object. In the second research method, the interrupted noise method, the sound pressure drop was measured after the noise generated by the omnidirectional loudspeaker had ceased. Reverberation time was calculated for the results obtained, which is the main and basic parameter determining the interior acoustics. On the basis of the above-mentioned measurements, the reverberation indicators for the temples were also calculated. When analysing the components of the reverberation indicator, it was noticed that poor acoustics in the sanctuary concerns speech, while interior acoustics is good for the reception of organ music. In the analysed church, the reception of liturgical music is also better than the reception of speech, but the differences between these values are small.

Keywords: acoustics, sacred buildings, reverberation time, sound pressure

1. Introduction

The acoustic profile of a room depends primarily on its shape and the absorbing materials used, as well as the arrangement of sound-reflecting materials. The acoustic field in a room consists of the waves that run directly from the source of sound and the waves which overlap each other once or repeatedly.

When designing spaces with their sound quality in mind, attention is paid to the relationship between specular and diffused reflection. Fully diffused reflection is desirable as it covers

a wide range of sound frequencies; however, partial diffusion occurs more often. In practice, the propagation of sounds in an enclosed space is influenced by its shape. The mutual location of the walls and ceilings can differentiate the directions of reflected waves that reach the audience. In order to improve the propagation of sound in geometrically simple interiors, acoustic structures or systems are also used, with a defined number of cavities; the task is to disperse a wide range of sound frequencies, depending on the size of the blocks used to produce it. It is one of the many types of distractor in the group of sound diffusing acoustic systems. It was invented by the German acoustician Manfred R. Schroeder [1]. The significance of acoustics is closely related to sacred buildings. The builders of the first churches used the principles of sound propagation in order to make sure that the acoustics of the interior is good enough for the music accompanying the liturgy to sound properly and the speech to be clearly heard by the congregation. This approach can be observed in a multitude of temples all over the world. They largely differ in terms of the external appearance, form, interior fittings, ornaments and building materials. The arrangement of the interior of the temple has great impact on its acoustics. When it comes to acoustics, the interior of the building is more important aspect than its external shape. With this in mind, the authors [2] categorized churches according to the shape of their interior. In large buildings with geometric shapes and simple décor, the effect of reverberation is observed. In buildings with more elaborate geometry, with aisles, chapels or a series of columns, the acoustics is much better due to the fact that these elements reduce reverberation and improve sound transmission. However, the more complicated the layout of the interior, the more difficult it is to predict the acoustic phenomena occurring inside and take them into account when designing a church [2]. The authors of a previous study have pointed out that the great variety of temple shapes is one of the most unsteady factors when comparing both their acoustics and measurements of different assemblies at the same site [3]. A comparative analysis of the acoustics of sacred buildings from different eras, based on experimental research by scientists on the acoustic qualities of churches from around the world, was described in the article [4].

Engel and colleagues, based on many years of research, have defined the conclusions regarding the field of acoustics in sacred buildings [2]. The findings show that unfavourable acoustic phenomena occur in spaces with oval and round bases and in interiors with domes. This is because the concentration of sound waves occur in one or more spots. Standing waves are generated in buildings with a rectangular or square plan, which causes local amplification or weakening of the acoustic signal. The most complex in terms of architecture and acoustics are composite interiors with side chapels, naves and recesses because when designing them, the theory of coupled rooms must be taken into account.

Carbonari and colleagues have proposed a set of guidelines for the selection of the location of sound sources and receivers and suggests appropriate equipment combinations for acoustic measurements in churches [5]. Measurements of reverberation time at various locations of sound sources and receivers done as part of a large survey of Roman Catholic churches in Portugal have been investigated previously [6], [7]. In the article [7], they presented the acoustic qualities of the interior of the Basilica of the Holy Trinity in Fatima, designed for 9,000 people. The reverberation time was also tested. On the other hand, the work [8] contains the results of measurements of the real reverberation time in the 125–8000 Hz band, made in the Dominican Order church in Krakow. Detailed analyses and comparison of the reverberation time as a function of frequency in Orthodox churches in Poland have been carried out previously in [9]. The recent article [10] discusses the acoustic problems in a contemporary Catholic church in Poznań and presents a study of the impact of the ceiling structure on its acoustics.

The paper [11] reported two examples of sacred buildings in Italy (S. Dominic, Imola) and the acoustic design specifically developed for using these spaces as concert halls. The topic of using the church as a temporary auditorium is also presented in [12]many of the ancient buildings, especially sacred architecture, are subject to renovation projects by converting their initial occupation type for temporary exposition. In particular, the demand for assisting to live musical performance is increased considerably in Italy because of the missing of places dedicated to the performing arts. As such, one of the churches of Imola (i.e. San Domenico.

Many methods can be used to assess the interior acoustics based on various measurement parameters. The basic and most important parameter is the reverberation time T. There are many indirect and direct methods to measure reverberation time in a space. The standard [13] describes the measurement procedures, irregularities, the scope of reports for the interrupted noise and impulse response methods. It also specifies the requirements for the equipment to be used for the correct performance of such measurements. The methods mentioned above have been used in this work. Measurements of acoustic parameters in Spanish churches according to [13] standard was presented in the work [14].

Bearing in mind the above information, the objective of the current study was to examine the acoustic measurements in two religious buildings located in Szczecin and to evaluate them in terms of sound quality. This study was carried out using two methods; integrated impulse response and interrupted noise methods. Based on the obtained results, reverberation time was calculated, which is the main and basic parameter determining the acoustics of the interior.

2. Materials and methods

2.1. Description of the analysed buildings

Two acoustics properties of two type of sacred buildings, the church and the sanctuary, located in Poland in Szczecin at Rydla Street was analysed.

Fig. 1.   Church at the parish of the Immaculate Heart of the Blessed Virgin Mary in Szczecin. *Source: own study [*15]

The church was built on a rectangular plan (Fig. 1). It is a single-storey reinforced concrete structure building without a basement. The structure is supported by reinforced concrete pillars elliptically arranged inside. On both sides of the church, there are lower aisles behind the pillars. Thanks to the large span between the pillars, the aisles form an integral part of the nave. The entrances to the church are: the main entrance portal with double brass doors, and 3 side entrances with wooden doors. Above the porch there is a gallery for the choir and the organist. From the level of the gallery there is a spiral staircase leading to the belfry topped with a dome. The interior of the church is unfinished. In the presbytery the walls and the floor

are made of wooden boards. In other parts of the church, there is only a concrete screed on the floor. In the center of the presbytery there is a wooden altar and two pulpits made of solid bricks with wooden stands. In the main nave there are 4 rows of wooden benches on a wooden landing. In the aisles there are benches parallel to the wall. The volume of the building is 12258.5 m³ and the floor usable area is 997.5 m². Based on the volume of the building, it was classified as a mid-sized church with a volume between 1500 and 15000 m³. The geometry of the church was classified as a complex multi-body (multi-block) non-dome sacred object.

Fig. 2.   Chapel of the Immaculate Heart of the Blessed Virgin Mary in Szczecin. *Source: own study [*15]

The sanctuary (Fig. 2) is a two-storey brick structure, without a basement, it has a shape of a twelve-sided polygon circumscribed to the circle. Its first floor is a lowered ground floor. The upper storey is elevated above the ground and it forms the main nave of the sanctuary. There is an organ gallery in the chapel that can be accessed by reinforced concrete stairs. There are two pairs of stairs circumscribed to the circle, leading to the interior of the sanctuary. The skeletal structure of the building, consisting of columns fastened with binders and wreaths, is made of reinforced concrete, and the walls are made of solid brick. The inter-storey ceiling is made as a reinforced concrete slab. The skeletal frame is crowned with a reinforced concrete dome. The interior of the sanctuary is simple and there are not many sculptures or ornaments. There is a marble altar and a pulpit in the presbytery, as well as a lectern and seats for the members of the liturgical service. The tabernacle is surrounded by a stone wall. In the main part of the building, there are wooden benches with fabric cushions on the seats for the congregation. The chapel is a contemporary structure with a volume of 4681.5 m³, and therefore it can be classified as a mid-size church, even though its volume is almost three times smaller than that of the church described previously. The geometry of the block is complex, varied, single-dome. Despite the fact that both analysed buildings have been classified as sacred objects of complex geometry, the form of the chapel is more problematic due to its dome and rounding of the external walls. The interior of the chapel is finished but does not abound with decorative elements.

2.2. Measurement methods

The reverberation time tests were performed in accordance with [13] standard. First, the measurement of the impulse response was done. To generate the required sound pressure, inflated balloons up to a diameter of about 18 cm were burst, which caused a total sound level of approx. 92 dB (filter A). The acoustic tests in the church were preceded by the

charting out a grid of measuring points with dimensions of 4.0 by 4.5 m in the main nave of the church (Fig. 3).
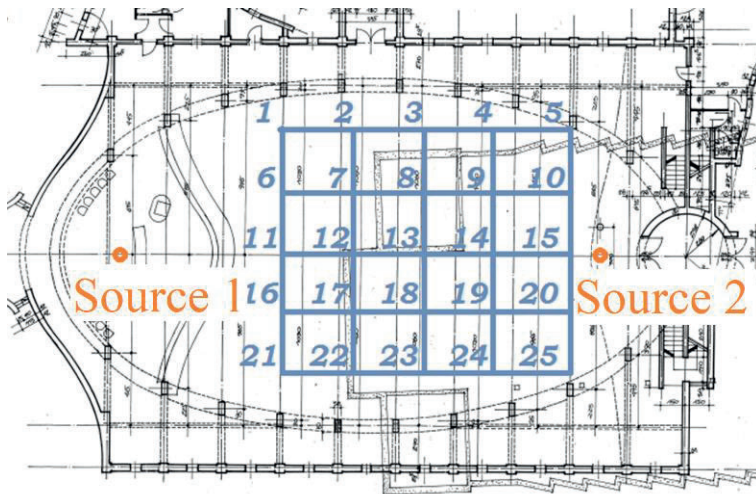
Fig. 3.   The church plan with a sketched measurement grid and the location of sources no. 1 and no. 2. *Source: own study*

The selected points were located between the benches for the congregation to recreate the auditory impression for the audience during the mass. The location of source 1 was based on the nature of the structure, as the most important point during the liturgy and as the main place from which the sound is emitted. A similar approach to the selection of the sound source location has been presented in the article [16]. The impulse reactions were determined for the following locations of the sound source: the main altar, the pulpit, the choir and the organ, which correspond to the places where liturgical, musical and cultural activities take place in the temple under study. Source 2 was located in the central part of the choir, next to the organ. The choir is the second, after the presbytery, the most important place from which sound is directed to the faithful. It is mainly singing and, in most cases, organ music. At these sound source locations, the balloons were burst. Each of them was burst at a height of approx. 1.2 m above the ground. The other person recorded the impulse response of the exploding balloon. Each measurement was performed in the direction of the presbytery and at the height of approx. 1.2 m.

The balloon was burst each time after approx. 5 seconds from activation of the sound level meter. The purpose of this procedure was to record the background noise level at a given point of the temple before the balloon explosion. The measurement itself was long enough to register the pressure drop to the value indicated on the screen at the beginning of the test. The same steps were performed for the sound source 2, which was situated in the central part of the gallery, next to the organ.

After the measurements in the church using the impulse response method were done, acoustic analysis was performed using the interrupted noise method. The spherical loudspeaker was placed on the floor, at the location of the sound source 1. Before turning the loudspeaker on, the sound intensity of the exploding balloon was measured at a distance of 1 m from the

sound source 1. The intensity level of approx. 80 dB was noted on the sound level meter. This measurement was used to set the same noise level generated by the loudspeaker. The interrupted noise test was performed using pink noise. As in the first method, measurements were made at a height of about 1.2 m at grid points. Before the sound generator was turned on, background noise had been measured for about 5 seconds, and then the loudspeaker was activated at the previously set sound intensity values for approx. 5 seconds. This time allowed the temple to be fully filled with the given noise, which was evidenced by the constant reading of the meter. About 5 seconds after activating the loudspeaker, the noise was turned off and the acoustic drop at a given measuring point was measured. The total measurement time at one point was 20 seconds.

Acoustic measurements in the sanctuary were performed in accordance with the previously described rules. Due to the specific shape of the chapel, the grid of measurement points was arranged in a different way. In this case, the measuring points are situated in an arc, among the benches. 16 measurement points were provided for sound source 1, and the 17th point was sound source 1 itself. 16 measurements were performed for sources 2 and 3, except that the last measuring point was in the presbytery. The arrangement of measuring points in the chapel is shown in the Fig. 4.
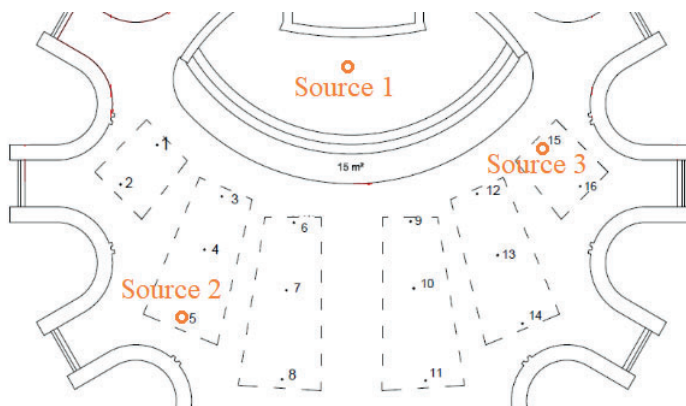
Fig. 4.   Chapel plan with sketched location of measurements and locations of sources. *Source: own study*

The tests in the chapel were performed using both the interrupted noise method and the impulse response method. Measurements for both methods were made at a height of about 1.2 m above the floor, and each time in the direction of the presbytery. Due to the nature of the location, source 1 was located in the presbytery behind the altar, while other sound sources were positioned among the benches for the congregation. This approach resulted from the acoustic reception of sounds in the chapel during the liturgy and the most resounding voices of other members of congregation in selected points.

3. Results

3.1. Measuring devices

Two methods were used: the interrupted noise method, in which an omnidirectional loudspeaker was used as an impulse generator, and the integrated impulse response method,

for which the increase in the sound pressure level was caused by a balloon explosion. Balloon explosion as a source of sound is used, among others, in works [17]. To measure the reverberation time in the room, it was necessary to use an omnidirectional sound source and a sound meter. The sound level meter SVAN 979 and DL 203 spherical loudspeaker were used to perform the tests.

In the studied temples, the places with the sound source were designated (in the church – 2 spots, in the chapel – 3 spots) and measurements were made using both methods in each location of the source. Each measurement was performed for 7 frequencies ranging from 125 Hz to 8000 Hz, and for overall level with a correction filter A - Total A. In total, 1568 charts were obtained illustrating the sound pressure drop in the tested point for a given frequency. Due to the huge number of results, only selected points will be described in detail and global statements for both structures will be presented.

3.2. Church results

The first analysed subject is the comparison of the results obtained for both methods. The point 13 will be interpreted as the central point of the grid for source 1. The charts (Fig. 5) present the obtained values of the sound pressure level with the specification of individual frequencies.
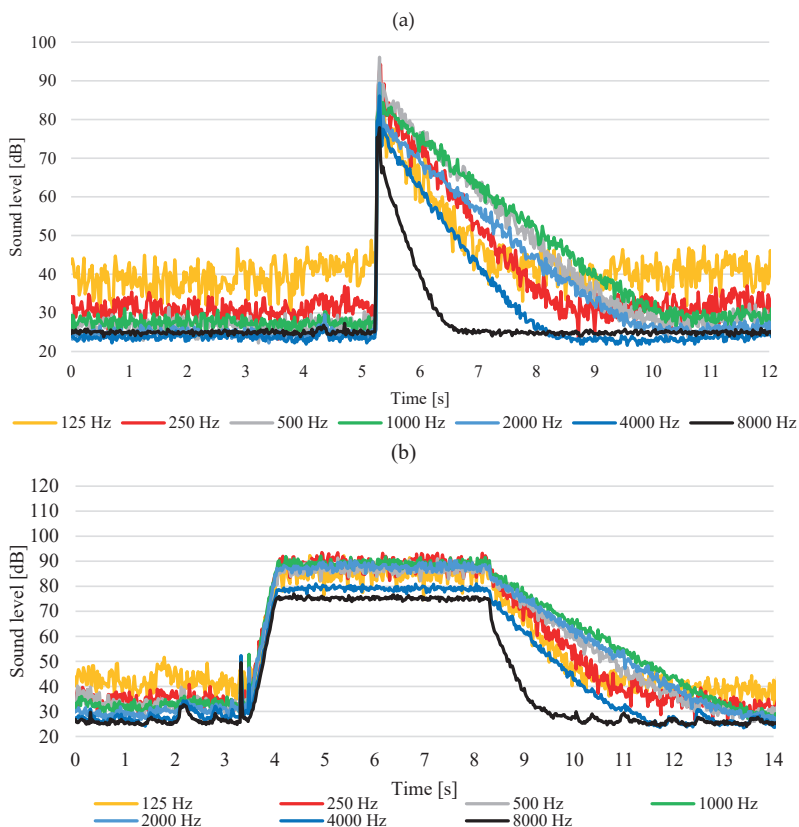
Fig. 5.   The graphs of sound levels using the pulse method (a) and interrupted noise method (b)

Both charts clearly show the background noise recorded in the first few seconds of the measurement. The acoustic background is at essentially the same levels, and slight discrepancies may result from a temporary change in the conditions inside the tested space or from the acoustic influence coming from the outside. The chart (a) clearly shows the moment of balloon explosion corresponding to an instantaneous spike in the sound pressure level. The chart (b) shows a gradual increase in the sound pressure level of the sound generated by the omnidirectional loudspeaker so that the maximum value is reached with a slight time shift. This difference results from the sound impulse generator used and the speed of the generated sound in the air. In both cases, the nature of the decrease in the sound pressure level over time is similar, which proves that the results are analogous and that the two methods used are equivalent. The descending trend of the chart is recorded until the pressure level value for the background noise is reached, of the value equal to the measurement before the sound impulse. The range of the drop in sound pressure level is the key section of the chart for the reverberation time study. Its slope is different for each frequency. The steepest pressure drop was recorded at 8,000 Hz. This is equivalent to the greatest slope of the line fitted to this chart. The smallest decrease was recorded for 1000 Hz.

Figure 6 shows an example of a drop in sound pressure for the frequency of 1000 Hz for the source 1. To compare the results with the interrupted noise method, the chart for the same grid point 12 in the loudspeaker test is presented.
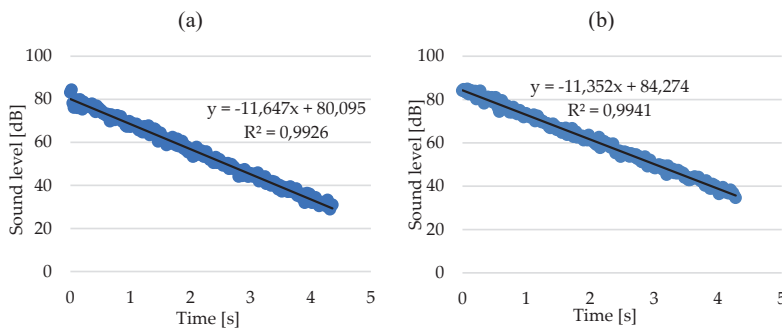
Fig. 6.   The graphs of the decrease in sound pressure levels for the frequency of 1000 Hz obtained by the impulse method (a) and interrupted noise method (b)

The coefficient of determination for the balloon is $R^2 = 0.993$, and for the loudspeaker, $R^2 = 0.994$. The obtained high values of the R^2 coefficient indicate a good fit of the data to the linear function. The trend line is very well adjusted to the results obtained. It is clearly noticeable that the nature of both charts is similar, as evidenced by the maximum and minimum sound pressure level for each chart, the range of arguments of the function, and, above all, the slope of the downward curve.

The obtained reverberation time values for all variants oscillate between $5.1 – 5.4$ seconds for each examined point of the temple, which is a difference of approx. 5.6%. This proves an even acoustic distribution in the church. It has also been shown that the location of the sound source in the presbytery or in the gallery does not affect the acoustic perception of sound.

The obtained results of the reverberation time can also be used to create a relationship presenting the characteristics of the tested building and to describe the method of changing

the reverberation time for individual measurement points in frequency bands. The chart in Fig. 7 shows the dependence of the reverberation time on frequency, where the individual points of the church measurement grid were marked with different colours.
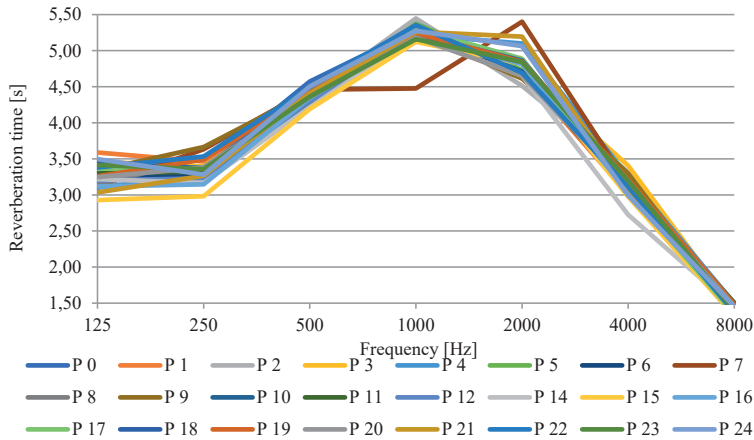
Fig. 7.   Reverberation time at various measuring points obtained by the impulse response method obtained for sound no 1 in Church

Because the temple is still unfinished, it was expected that the reverberation time at the low bands would give higher values. The low value of the reverberation time for higher frequencies results from high air absorption, while in the case of lower frequencies, it is the result of the presence of sound-absorbing objects in the space. Despite the fact that the church is uncompleted, the presbytery is panelled, and under the benches for the congregation, wooden boards are laid. These structures are most likely responsible for reducing the reverberation time in the temple. By comparing the reverberation times of the given frequencies at individual points (by the impulse response method), a chart illustrating the frequency bands for the building is obtained (Fig. 8). Lower values of the reverberation time for the frequencies of 125, 250 and 500 Hz were obtained by the researchers in church in Fatima [7].
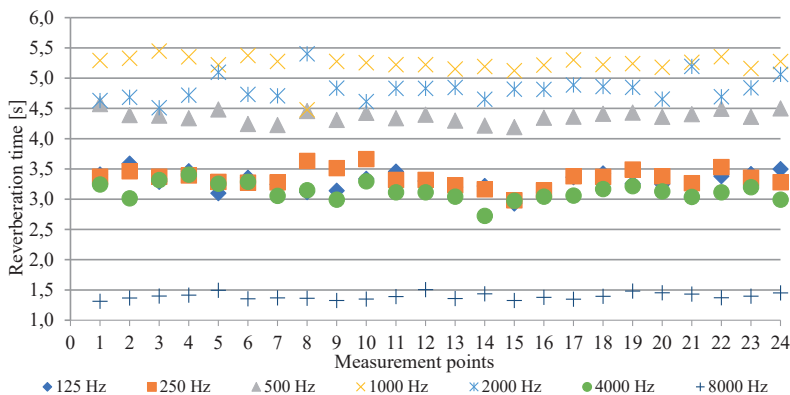
Fig. 8.   Reverberation time diagram in individual frequency bands at various measuring points

The absorption on the surface of the partitions also had an influence on the obtained reverberation times in accordance with the Sabine equation. Despite the unfinished condition of the church, its interior features well-absorbing elements such as pews, platforms and panelling. The interior of the church was not finished on the day of the examination. In the presbytery, only the wall cladding is 2.5–1.5 m high and the floor is made of wooden boards.

Due to the diversity of sacred buildings, there are no specific standard values for the reverberation time. In order to ascertain whether the acoustics of the examined churches is good, the obtained times were compared with the results of other churches described in the literature. Engel et al. have examined a number of places of worship in terms of various acoustic parameters [2]. One of the measured parameters was the reverberation time. The acoustics of the structures analysed in the publication are varied. Churches with large volume are characterized by long reverberation times, and thus, their acoustics is good for the performance of organ music but not so good for transmission and reception of speech. These phenomena can be observed, for example, in Saint Peter's Basilica in Rome. Among the mid-sized buildings, there are churches with poor acoustics – e.g. Charles' Church in Tallinn, whose interior is covered with flat, sound-reflecting surfaces – and buildings with good acoustics, such as St Mark's Church in Munich. This fact demonstrates is that the volume of the temple is not the only criterion for acoustic analysis, but the shape and finishing of the building determine the acoustics of a given interior as well. The authors describe St. Thomas Church in Leipzig as a structure with good interior acoustics. However, the lower reverberation times for the 125 and 250 Hz bands, resulting from wooden finishing of walls are an unfavourable phenomenon. Although lower frequency sounds are less audible, the room acoustics is good. The volume of the church examined in this study is 12258.75 m^3 and it is slightly smaller than the volume of St Thomas Church in Leipzig. The nature of these two objects is similar, but for the church in Szczecin, the tested reverberation time values are approx. 1 second longer. As it was already mentioned, the lower value of the reverberation time at low frequencies results from the finishing of the walls and wooden panelling. Both objects are similar in terms of the surface and the absorbing structures used, but the higher value of the reverberation time combined with a smaller volume of the church in Szczecin proves its worse acoustic conditions.

3.3. Sanctuary results

As it was in the case of the church, also for the sanctuary, the research methods used were compared first. In order to present a picture of the obtained values for the sanctuary, the representative point 8 was described and showed in Fig. 9.
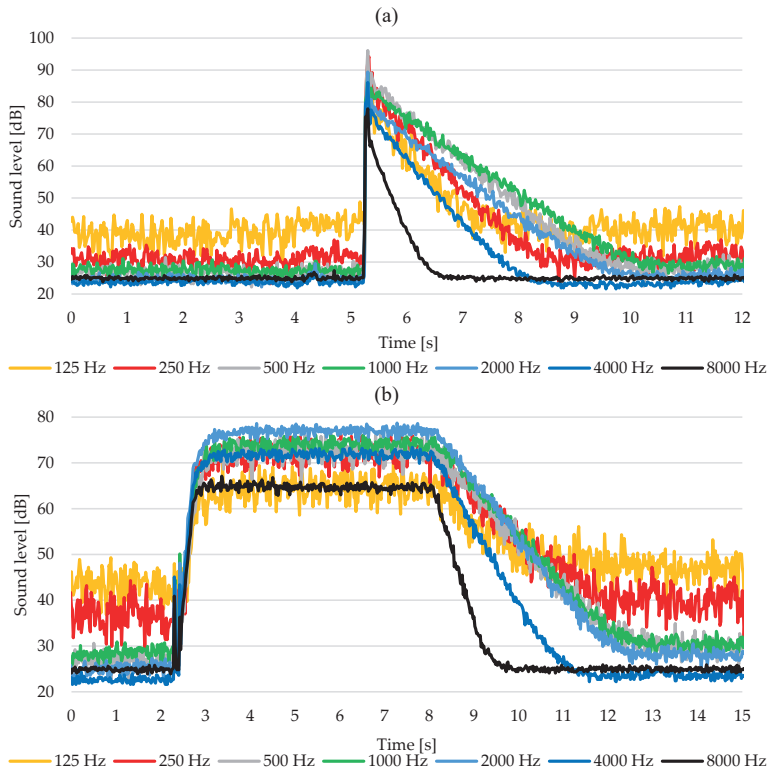
Fig. 9.　The graphs of sound levels using the impulse response method (a) and interrupted noise method (b)

Again, the background noise was recorded before and at the end of the test. The peak sound pressure level was obtained in a similar way, and its decrease was similar for both measurement variants. An example of the relationship for point 8 for 4000 Hz is presented below in Fig. 10.
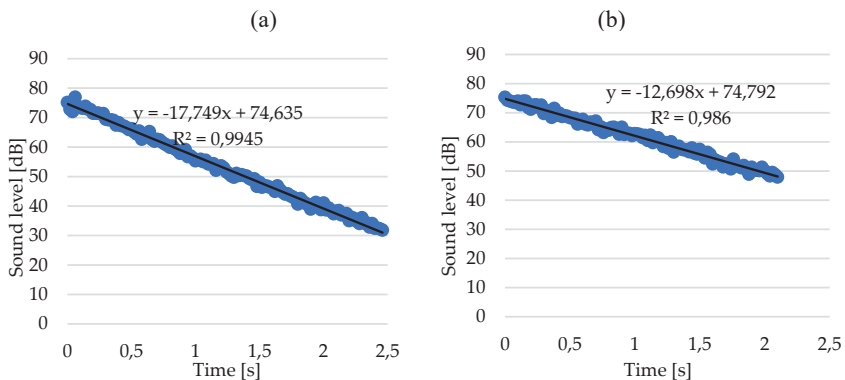
Fig. 10.　The graphs of the sound pressure drop for the frequency of 4000 Hz obtained by the impulse method (a) and interrupted noise method (b)

Despite the quite good fitting of the trend line to the measurement points and high values of the R^2 coefficient, the obtained slope factors of the straight lines differ significantly in both cases. For the balloon test, the sound pressure level drop was faster than for the loudspeaker noise measurement. A significant discrepancy in the directional coefficients of the fadeaway curves results in a significant difference in the obtained reverberation times for point 8 for the analysed measurement variants. Significant differences have been observed for the extreme bands, i.e. 125, 250, 4000 and 8000 Hz. In the case of the highest frequency, this discrepancy does not affect the reverberation time due to the fairly high slope of the trend line. The difference of 10.3% corresponds to only 0.2 second, which is not very significant with a reverberation time of 1.8 second. For the remaining cases, the differences show higher values. The largest of them is 25% at 125 Hz.

In order to evaluate the acoustics in the temple, the reverberation time values for the tested frequencies were analysed. It turned out that for the points located on the left side of the chapel and for the source located at point 17, the decrease in sound pressure was slower than for the points on the right side. In point 12, the decrease occurs much faster than for other variants. Despite the illustrated discrepancies, the characteristic of the building is practically constant for each measuring point, regardless of the location of the source and the measurement method used. This is best seen for the 1000 Hz band, where the difference in the reverberation time is only 1% for all the measurements made. Based on the data obtained, it can be concluded that the acoustic reception in the temple should be the same for all the members of the congregation gathered in it, and for people in the area of the presbytery.
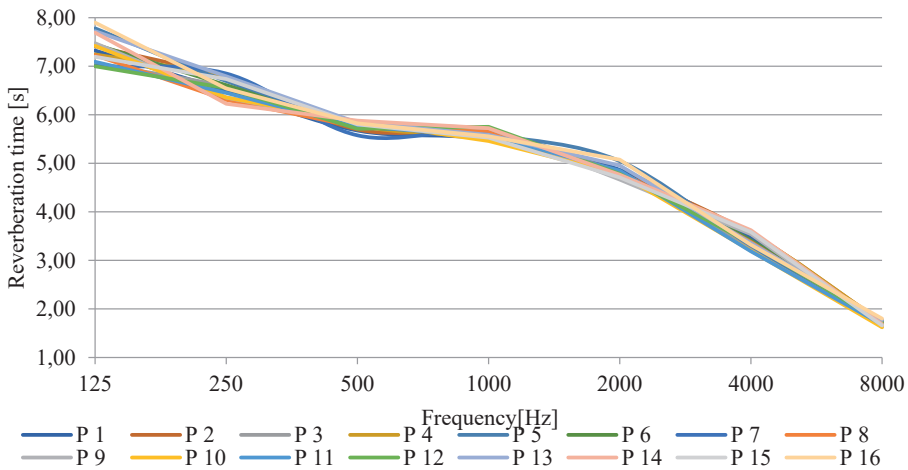
Fig. 11.   Reverberation time at various measuring points obtained by the impulse response method

The chart in Fig. 11 shows the dependence of the reverberation time on the frequency for the examined points (an exploding balloon as the sound source). The charts for all measurement points coincide with each other, creating a uniform scheme of the building acoustics. Only for the lowest frequency values, there are differences on the level of 4%. This, as explained previously, is caused by a poorer adjustment of the straight line to the results. For

the remaining frequencies, the difference in the obtained results is within 1%. Despite these facts, it can be noticed that the interior of the sanctuary largely differs from the interior of the church. In the case of the church, the sounds in the lowest frequency band have the longest reverberation time, up to 8 seconds, while for higher frequency values, the reverberation time decreases. The longest reverberation time for the church occurred in the 1000 Hz band and it was at the level of approx. 5.5 seconds. The smallest value, approx. 1.8 second, occurred at 8000 Hz, as it was for the chapel, where the reverberation time was approx. 1.5 second. For the obtained chart of the sanctuary profile, the longest reverberation time occurs for the lowest frequencies and decreases with increasing frequency. This is a typical characteristic of interiors that are not adapted. This is due to easier damping of shorter waves and the damping properties of the air itself.
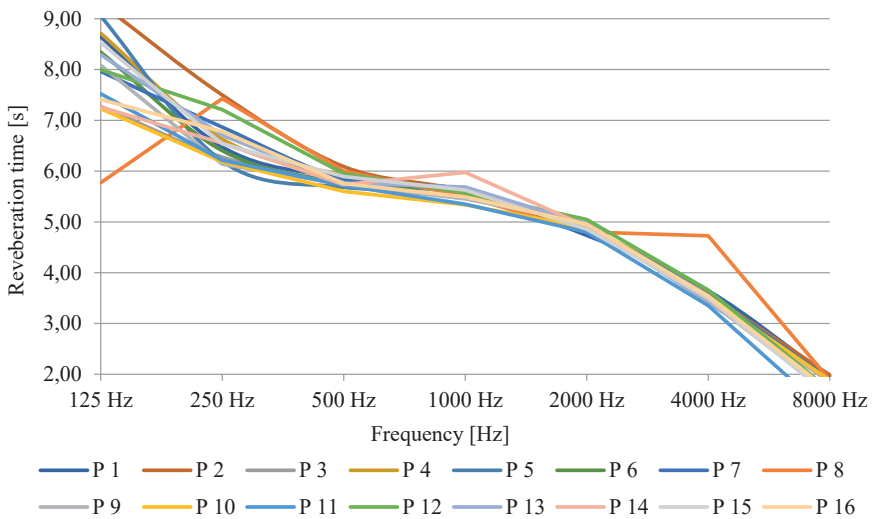
Fig. 12. Reverberation time at various measuring points obtained by the interrupted noise method

The chart of the facility profile was also prepared for the variant with a loudspeaker; it is presented below in Fig. 12. The chart for the variant with the loudspeaker and the source location in the presbytery does not present the uniform character of the interior. One point is most conspicuous here – its character is different from all others, and divergences in the 125 and 250 Hz bands can be noticed. For the lowest tested frequency, the reverberation time range, depending on the analysed point, is from 7 to 9 seconds, which is a difference of 27.5%. 2 second difference aggravates a listener's acoustic perception and may cause unfavoura- ble acoustic phenomena such as audible reverberation. The discrepancy of the results is also noticeable for 250 and 8000 Hz. However, it is best illustrated by the chart of reverberation time changes in frequency bands (Fig. 13).
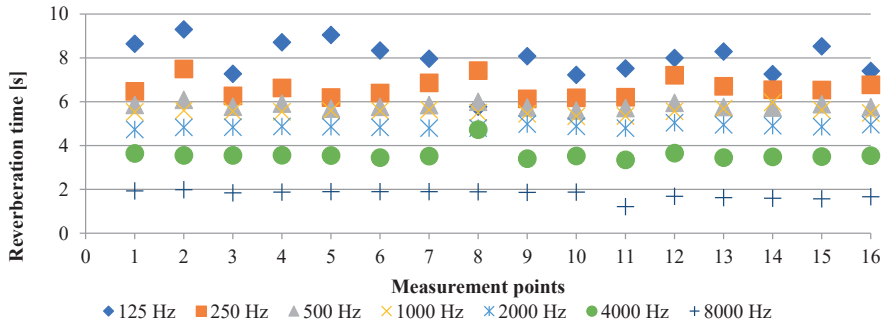
Fig. 13. Reverberation time graph in individual frequency bands at different measuring points

For 500, 1000 and 2000 Hz bands, the charts are constant with slight ripples. The more wavy the chart of a given frequency, the greater the number of reverberation time spikes at the points of the grid, which entails worsened acoustics of the room and differences in the perception of sounds by the audience. Inside the sanctuary, there are flat surfaces and not much decoration. The sanctuary is finished, but inside there are mostly sound-reflecting surfaces, and the vault is a dome. The floor is made of marble and a large part of the walls is covered with stained glass. These are surfaces that reflect sound well. The temple is crowned with a dome, which does not improve the acoustics of the interior either.

4. Discussion

The acoustics of the sanctuary in terms of the reverberation times obtained can be compared with St. Michael's Monastery in Kiev [2]. The volume of both temples is the same, and the acoustic profiles of the buildings are of the same shape. The reverberation time values given in [2] are practically the same as the average values obtained from the sanctuary studies. The discrepancy is only in the highest frequencies.

The problem of acoustics of domed structures intended for religious worship has been discussed previously [18]. The acoustic assessment of the interiors was performed on the basis of reverberation time measurement and the calculation of the speech transmission index. The obtained reverberation time values reached similar values as for the sanctuary. Acoustic conditions were defined as unfavourable for speech audibility and music perception. To adapt the interior to the needs of users, sprayed insulation material was used. After the acoustic adaptation, the reverberation time decreased significantly and the speech clarity improved at all measuring points. It follows that the conditions in the sanctuary are unfavourable. The reverberation time is too long due to the lack of sound-absorbing surfaces. It is necessary to carry out an acoustic adaptation of the interior in order to shorten the reverberation time.

4.1. Reverberation time

Tables 1 and 2 show the average reverberation times for the analysed temples in frequency bands. The average values are shown in Fig. 14.

Table 1. Average reverberation time in the church

Variant	125 Hz	250 Hz	500 Hz	1000 Hz	2000 Hz	4000 Hz	8000 Hz
K1 balloon	3.3	3.3	4.4	5.2	4.8	3.1	4.5
K2 balloon	3.5	3.4	4.4	5.3	4.8	3.1	4.6
K1 speaker	3.3	3.4	4.4	5.3	4.9	3.2	5.0
K2 speaker	3.5	3.4	4.4	5.4	5.1	3.3	5.2
Average value	3.4	3.4	4.4	5.3	4.9	3.2	4.8

Table 2. Average reverberation time in a sanctuary. *Source: own study*

Variant	125 Hz	250 Hz	500 Hz	1000 Hz	2000 Hz	4000 Hz	8000 Hz
S1 balloon	7.4	6.6	5.8	5.6	4.8	3.4	5.7
S1 speaker	7.9	6.6	5.8	5.6	4.9	3.6	5.4
S2 balloon	7.5	6.6	5.8	5.6	4.9	3.4	5.7
S2 speaker	7.9	6.7	5.8	5.6	4.9	3.6	5.7
S3 balloon	7.5	6.6	5.8	5.6	4.9	3.3	5.7
S3 speaker	7.7	6.7	5.9	5.6	4.9	3.6	5.7
Average value	7.7	6.6	5.8	5.6	4.9	3.5	5.6
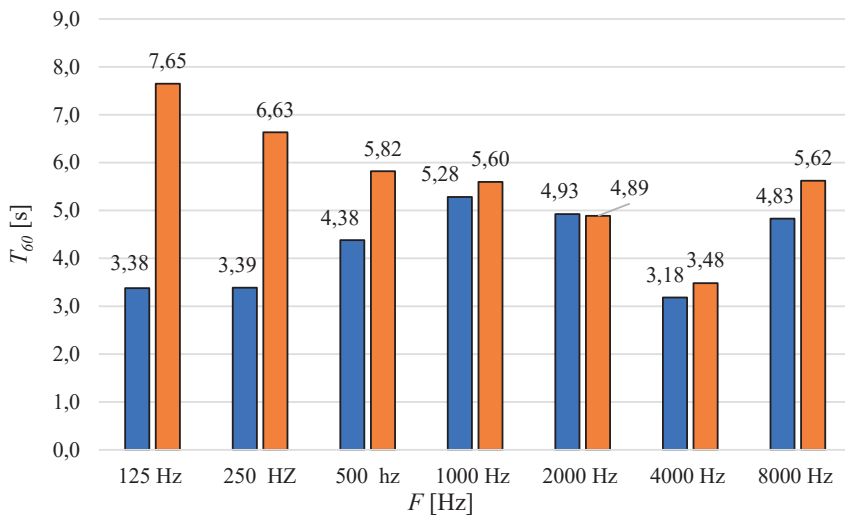
Fig. 14.   The average reverberation time in the Church and in the Sanctuary

Comparing of the obtained values for both temples reveals that the average reverberation times for the chapel and the church are comparable for frequencies from 1000 to 8000 Hz. On the other hand, for the lowest frequency bands, the average reverberation time is much longer for the sanctuary and is more than twice as long in the range of 125 Hz compared to the value obtained in the church. Taking into account the volume of these interiors, which is 2.5–3 times smaller in the sanctuary, the difference in the reverberation time indicates very poor acoustics of this building. For a church, the maximum value of the reverberation time occurs for 1000 Hz and reaches approx. 5.3 seconds. In the sanctuary, the reverberation

time decreases with increased sound frequency. The longest reverberation time occurs for 125 Hz band.

The acoustics of sacred spaces, due to the variety of forms, shapes, geometry, the surface of the building, or church equipment, is not shaped in the same way for every interior. Therefore, there is no standard range of reverberation time values that a temple should meet. Many scientists focused on the topic of the acoustics of sacred objects and, based on their own research, they have created dependencies regarding the optimal reverberation time. Günter Hartman [19] created a model for small and mid-sized churches in terms of the recommended reverberation time range. The volume of the sanctuary is 4681.5m^3, while the volume of the church is 12258.5m^3. Because the volume of the church is only slightly larger than the range for which the Hartman formula applies, the preferred reverberation time was calculated for those temples where T_{Hk} was the time for the church, and T_{HS} was the time for the sanctuary.

$$T_{HK} = 0.0598 \cdot 12258.5^{0.462} \pm 15\% = (3.94 - 5.32)\,\text{s} \tag{1}$$

$$T_{HS} = 0.0598 \cdot 4681.5^{0.462} \pm 15\% = (2.52 - 3.41)\,\text{s} \tag{2}$$

Average reverberation times for the temples obtained from the conducted research are: $T_k = 3.72$ s for the church, $T_S = 5.11$s for the sanctuary. The above dependencies show that the reverberation time for the church is too short, while for the sanctuary it is too long. Klepper [19] divided the temples into four groups and specified the preferred reverberation time values for them. According to this division, both analysed objects belong to the group of mid-sized churches, but neither of them has adequate acoustics according to Klepper's guidelines.

The values recommended by the literature differ. This is because the research relates to historical temples, where the acoustics were shaped along with the next epoch. It is, therefore, difficult to compare the reverberation of a contemporary church to the values recommended in the literature. Variations on other comparative theories and models for predicting energetic acoustic parameters in churches that differ in style, typology and location were discussed in the article [20].

4.1. Reverberation indicator

Due to the specific nature of sacred buildings, classic measurement methods for the acoustic assessment of these spaces do not provide a complete acoustic picture of the interior. Work was undertaken to standardize these methods and an index method for assessing the acoustic quality of sacred objects was developed. The method is based on the determination of one global index taking values from 0 to 1, where 0 means bad and 1 the most favourable reverberation conditions for the interior. This subject is discussed in the papers [2], [21], [22] such as reverberation time (RT. Literature provides a number of partial indices needed to calculate the final value. They include: reverberation index, internal noise index, music sound quality index, speech clarity index and sound uniformity index. To compare the obtained reverberation times with the analysed methods, this paper focuses solely on the reverberation indicator, which is the most important parameter in the index method. On the basis of the above-mentioned works, individual components and the final reverberation indicator for temples were calculated (Table 3).

Table 3. Reverberation factor for the temples

Temple	125 Hz	250 Hz	500 Hz	1000 Hz	2000 Hz	4000 Hz
The church	0.6	0.7	0.5	0.6	0.6	0.8
The sanctuary	0.1	0.1	0.3	0.4	0.5	0.6

The obtained values of the indicator for the church were in the range of 0.5–0.8, with the lowest indicator determined for the 500 Hz band, and the highest for 4000 Hz. The evaluation of the reverberation indicator can be made according to the scale for the global indicator presented in [2]. Therefore, it can be concluded that there is sufficient acoustic quality for the lower frequencies, while from 1000 Hz upwards, there is a good acoustic quality of the room in terms of reverberation time, for speech and organ music.

The reverberation indicator values obtained for the sanctuary, as for the church, reach their maximum values for the highest frequencies, but they are much lower. According to the scale presented in [2], poor acoustics of the sacred interior, and in this case, unfavourable reverberation time, occurs for a reverberation indicator of 0–0.6. This means that only for the frequency of 4000 Hz acoustic quality of the room is sufficient. Looking globally, the acoustics in the sanctuary is poor and the indicators for speech and the reverberation-volume index predominate. Quality of the interior is much better for organ music and if the reverberation indicator for organ music were considered separately [2], the temple would show good, and even very good acoustic conditions for playing the organ.

5. Conclusions

Churches have a variety of forms. They differ not only in shape, but also in the degree of interior development, depending on when the temple was built, and on the type of acoustic purpose, i.e. speech, singing, music. Depending on the religious denomination, different aspects are emphasized. All these features significantly affect the acoustic character of a sacred building.

In this paper, acoustic tests were carried out for two sacred buildings with different volume and shapes. The conducted analyses showed that the applied methods are consistent with each other and the results are comparable. Both for the chapel and for the church, the greatest discrepancies in the obtained reverberation times occurred for the 125 Hz band. This dependence is caused by a worse – in relation to other frequencies – adjustment of the trend line to the scattergram of the recorded sound pressure drop. The recorded values of the pressure level decreased abruptly with significant differences in subsequent time intervals. For the remaining frequencies this decrease was linear, which allowed for better matching of the lines to the obtained charts. Significant discrepancies in the reverberation time for individual measurement variants were observed in the case of the church for the frequencies of 500 and 2000 Hz, while in the case of the chapel, for frequencies of 250, 4000 and 8000 Hz. The highest convergence of test results in all variants was obtained for the frequency of 1000 Hz. Human hearing is most precise in the frequency range from 1000 Hz to 3000 Hz, so the obtained reverberation time values at the same level for different locations of the sound source and with the use of different sound generators prove the same acoustic perception in the whole room.

The analysis of the reverberation indicator shows that the average indicator for the church is 0.6, which corresponds to sufficient acoustics, and for the sanctuary, it is 0.3, which means poor acoustics. When analysing the components of the reverberation indicator, it was noticed

that poor acoustics in the sanctuary concerns speech, while interior acoustics is good for the reception of organ music.

In the church, the reception of liturgical music is also better than the reception of speech, but the differences between these values are small. The research carried out in this paper establishes the basis for further analysis of how to improve the acoustics in the studied temples. This analysis should be based on proposing systems allowing to improve the conditions of speech, singing and music perception. For a church, it may be a suitable interior finish with sound-absorbing materials. In the sanctuary, however, due to the very long reverberation time in the low frequency range, it will be necessary to use additional sound-absorbing systems.

Funding:

References

[1] Kulowski A., *Akustyka Sal.Zalecenia Projektowe Dla Architektów*. Gańsk: Wydawnictwo Politechniki Gdańskiej, 2011; ISBN 978-83-7348-364-4.

[2] Engel Z. et al., *Podstawy Akustyki Obiektów Sakralnych*. Kraków-Radom: ITE-PIB, 2007, ISBN 978-83-7204-622-2.

[3] Martellotta F. et al., "Guidelines for Acoustical Measurements in Churches DAU", *Applied Acoustics*, vol. 70, 2009, pp. 378–388. https://doi.org/10.1016/j.apacoust.2008.04.004

[4] Girón S., Álvarez-Morales L., Zamarreño T., "Church Acoustics: A State-of-the-Art Review after Several Decades of Research", *Journal of Sound and Vibration*, vol. 411, 2017, pp. 378–408. https://doi.org/10.1016/j.jsv.2017.09.015

[5] Carbonari A. et al., "Measuring Methods for the Acoustical Characterization of Churches", in International congress on acoustics Madrid, 2007.

[6] Carvalho A.P.O., "Objective Acoustical Analysis of Room Acoustic Measurements in Portuguese Catholic Churches", in Proceedings Noise-Con 94, Ft. Lauderdale, Florida, 1994.

[7] Carvalho A.P.O., Silva, P.M.A., "Sound, Noise and Speech at the 9000-Seat Holy Trinity Church in Fatima, Portugal", *Archives of Acoustics, vol. 35,* 2010, pp. 145–156.

[8] Plewa M., "Analysis of Sound Field in Dominicans' Church in Cracow", *Archives of Acoustics*, vol. 32, 2007, pp. 227–233.

[9] Małecki P., Wiciak J., Nowak D., "Acoustics of the Orthodox Churches in Poland", *Archives of Acoustics, vol. 42,* 2017, pp. 559–590. https://doi.org/10.1515/aoa-2017-0062

[10] Sygulska A., "The Study of the Influence of the Ceiling Structure on Acoustics in Contemporary Churches", *Archives of Acoustics,* vol. 44, 2019, pp. 169–184. https://doi.org/10.24425/aoa.2019.126363

[11] Tronchin L., Bevilacqua A., "Evaluation of Acoustic Similarities in Two Italian Churches Honored to S. Dominic", *Applied Sciences*, vol. 10, 2020, 7043. https://doi.org/10.3390/app10207043

[12] Merli F., Bevilacqua A., "Using a Church as a Temporary Auditorium. Acoustical Design of S. Domenico of Imola", *J. Phys.: Conf. Ser.*, vol. 1655, 2020, 012146. https://doi.org/10.1088/1742-6596/1655/1/012146

[13] PN-EN ISO 3382 – 2:2008 + AC:2009: Acoustics – Measurement of Room Acoustic Parameters – Part 2: Reverberation Time in Ordinary Rooms.

[14] Galindo M., Zamarreno T., Giron S., "Acoustic Analysis in Mudejar-Gothic Churches: Experimental Results", *J. Acoust. Soc. Am.*, vol. 117, 2005, pp. 2873–2888.

[15] Kandybowicz A., *Acoustic Research and Analysis of Selected Sacred Objects in Szczecin*. Master thesis, West Pomeranian University of Technology, Szczecin, Poland. 2020.

[16] Álvarez-Morales L. et al., "Methodology for the Study of the Acoustic Environment of Catholic Cathedrals: Application to the Cathedral of Malaga", *Building and Environment*, vol. 72, 2014, pp. 102–115. https://doi.org/10.1016/j.buildenv.2013.10.015

[17] Szłapa P. et al.,"Comparison of Handgun Shots, Balloon Bursts, and a Compressor Nozzle Hiss as Sound Sources for Reverberation Time Assessment", *Archives of Acoustics*, vol. 41, 2016, pp. 683–690. https://doi.org/10.1515/aoa-2016-0065

[18] Nowoświat A., Marcelina O., Marchacz M., "The effect of acoustical remedies changing the reverberation time for different frequencies in a dome used for worship: A case study", *Applied Acoustics,* vol. 160, 2020, 107143. https://doi.org/10.1016/j.apacoust.2019.107143

[19] Wróblewska D., Kulowski A., *Czynnik akustyki w architektonicznym projektowaniu kościołów.* Gdańsk: Wydawnictwo Politechniki Gdańskiej, 2007.

[20] Berardi U., Cirillo, E., Martellotta F.A., "Comparative Analysis of Acoustic Energy Models for Churches", *J Acoust Soc Am*, vol. 126, 2009, pp. 1838–1849. https://doi.org/10.1121/1.3205398

[21] Kosała K., Engel Z., "Assessing the Acoustic Properties of Roman Catholic Churches: A New Approach", *Applied Acoustics*, vol. 74, 2013,   pp. 1144–1152. http://doi.org/10.1016/j.apacoust.2013.03.013

[22] Kosała K., "A Single Number Index to Assess Selected Acoustic Parameters in Churches with Redundant Information", *Archives of Acoustics*, vol. 36, 2011, pp. 545-560. https://doi.org/10.2478/v10168-011-0039-3

Size effect at testing strength properties of concrete

Amanda Akram

Department of Structural Engineering; Faculty of Civil Engineering and Architecture;
Lublin University of Technology; 40 Nadbystrzycka St., 20-618 Lublin, Poland;
a.akram@pollub.pl (iD) *0000-0001-5619-2927*

Abstract: Various strength characteristics of concrete are considered as fracture parameters. The compressive strength of concrete is of paramount importance when designing concrete structures, whereas tensile strength of concrete is the basic property when estimating cracking resistance of a structure and analysing fracture processes in concrete. When testing the compressive strength of concrete, the results are dependent on the shape and dimensions of used specimens. Some findings reported in the literature suggest that size effect exists also when testing such fracture properties of concrete as tensile strength. Unfortunately this problem is much less recognized and described compared to size effect in compressive test results. In this paper, the experimental investigation is presented on how the length of cylindrical specimens influences the tensile splitting strength of concrete obtained by means of the Brazilian method. Additional variable parameters were: type of aggregate (natural gravel and crushed granite) and cement-water ratio (C/W = 1.8 and C/W = 2.6). In conducted laboratory experiments a higher splitting tensile strength of concrete was noted for all specimens with nominal dimensions of 150×150 mm, compared to specimens 150×300 mm in size, regardless of type of aggregate or cement-water ratio.

Keywords: concrete, size effect, tensile strength

1. Introduction

Concrete is a composite material which is produced by mixing cement, water, fine and coarse aggregates. Some additives, for example pozzolanas and superplasticizers can be added to improve the mechanical and physical properties of the concrete mixture as well as hardened concrete. The proportions of ingredients are calculated according to appropriate methods to obtain a required quality of hardened concrete, which is particularly important with regard to its compressive and tensile strength. When designing concrete structures, the compressive strength of concrete is of paramount importance, whereas when estimating cracking resistance of structure and analysing fracture processes the tensile strength of concrete is the basic

property. The tensile strength of concrete is much lower than its compressive strength and in normal strength concretes it reaches about 10% of compressive strength. Therefore, concrete is rated among quasi-brittle materials.

The bulk of concrete is made up of fine and coarse aggregates which should be of proper granulation. The type of aggregate is also crucial. Both crushed and gravel aggregates can be used as a coarse aggregate in concrete production. The internal structure of hardened concrete causes that concrete is an heterogeneous material and therefore its properties, especially the compressive and tensile strength, should be tested experimentally. Tests should be performed at standard conditions and using standardized specimens according to the code [1]. Concrete compressive strength should be tested in uniaxial compression test on cylindrical or cubic specimens according to the procedure given in the code [2]. To determine the tensile strength of concrete, indirect methods are usually applied due to the difficulty of performing the direct tensile test. As the standard method, the Brazilian splitting tensile test is recommended in the code [3]. The splitting test can be performed using both cylindrical and cubic specimens. Specimens which are admitted for testing, the compressive strength and the splitting tensile strength of concrete are presented in Fig. 1.
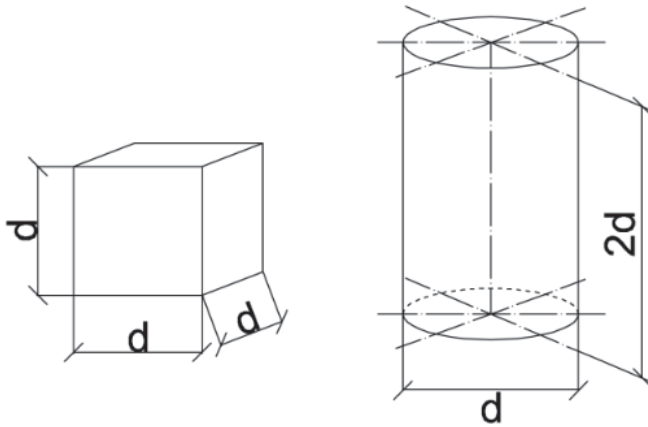
Fig. 1.   Admissible types of specimens for testing concrete compressive and tensile strength. Nominal dimensions for cubes: d = 100, 150, 200, 250, 300 mm, and for cylinders: d = 100, 113, 150, 200, 250, 300 mm, with acceptable dimension discrepancy ± 10%

When testing the strength properties of concrete, the shape and dimensions of tested specimens are crucially important. The influence of a specimen's size on concrete compressive strength has been described in depth ([4]-[7]). The specimens which are the most often used in testing compressive strength of concrete are 150 mm, 100 mm and 200 mm cubes, and cylinders 150 mm in diameter and 300 mm long. The relations among concrete compressive strengths tested on different specimens are presented below (Eq. 1).

$$f_{c,cube15} = 0.9 f_{c,cube10} = 1.05 f_{c,cube20} = 1.25 f_{c,cyl15/30} \tag{1}$$

where: $f_{c,cube15}$ – compressive strength tested on cubes 150 mm, $f_{c,cube10}$ – compressive strength tested on cubes 100 mm, $f_{c,cube20}$ – compressive strength tested on cubes 200 mm $f_{c,cyl15/30}$ – compressive strength tested on cylinders 150mm in diameter and 300 mm in length.

Some findings reported in the literature suggest that size effect also plays an important role when testing fracture properties of concrete such as tensile strength ([8]-[10])and fracture energy ([11]-[12]). Unfortunately, this problem is much less recognized and described. Furthermore, specimens of different shapes and dimensions are used when testing tensile strength of concrete. The schematic diagrams of examples of control specimens under loading for the measurement of tensile strength of concrete are shown in Fig. 2.
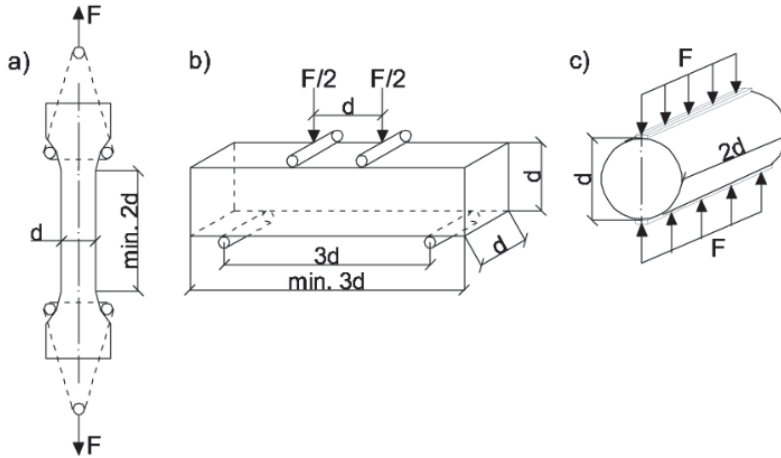
Fig. 2.   Test methods of tensile strength of concrete (with examples of admissible control specimens): a) uniaxial tensile test, b) flexural test, c) split cylinder test

The uniaxial tensile test is conducted on rectangular prisms of a cross section 100×100 mm or 150×150 mm and the length equals two times the specimen's width. The specimen is fixed in the load frame of the testing machine by wider ends of the specimens. In case of cylindrical specimens (which are also acceptable) grip handles or stiff plates glued to the face of the specimens are used for fixing. In the uniaxial test, the maximum axial load is measured when the failure of the specimen appears in the middle part of the specimen's length and the tensile strength is calculated from Eq. 2.

$$f_{ct,dir} = \frac{F}{A} \tag{2}$$

where: F – failure load, A – cross section area in a damaged place. When performing the flexural tensile test two static schemes are possible: a three point bending test and a four point bending test. As a standard method a simple plain concrete beam loaded at one-third span point is recommended. The span of the beam should be three times its depth. The typical arrangement for the test is presented in Fig. 2b. The flexural tensile strength is computed as a maximum tensile stress from the standard flexural formulas: Eq. 3 in case of two point loading and Eq. 4 in case of one point loading.

$$f_{ct,fl} = \frac{M}{W_c} = \frac{F \cdot l}{d_1 \cdot d_2^2} \tag{3}$$

$$f_{ct,fl} = \frac{M}{W_c} = \frac{3 \cdot F \cdot l}{2 \cdot d_1 \cdot d_2^2} \tag{4}$$

where: F – failure load, l –span of the beam, d_1 and d_2 – dimensions of beam's cross section.

It should be noted that a static scheme in flexural tensile test also influences the obtained results. Tensile strength is 13% higher when performing the test in three point bending compared to four point bending. Therefore, loading arrangement by two concentrated forces is recommended in the code [13].

During the splitting test, a specimen is placed in the compression testing machine (cylinders in a horizontal position) and the load is applied through plywood strips situated under and over the specimen in a central position. The specimen fails in tension into two halves (see Fig. 3). The concrete splitting tensile strength is calculated from Eq. 5.

$$f_{ct,sp} = \frac{2 \cdot F}{\pi \cdot L \cdot d}$$
(5)

where: F – failure load, L – specimen's length, d – dimension of a specimen's cross section.
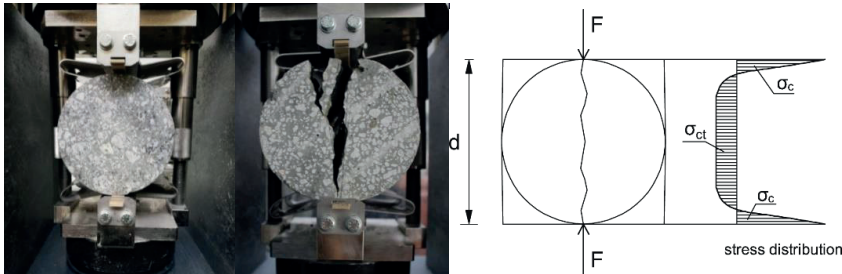
Fig. 3.   The Brazilian splitting test: specimen in the test stand before and after the failure (left); stress distribution in cross section σ_{ct} – tensile stress, σ_c – compressive stress (right)

It can be suspected that the shape and size of specimens have a certain influence on tensile concrete strength tested in the Brazilian test. In the code [3] we can find only a short comment on the shape and dimensions of specimens used during the splitting tensile concrete strength saying that the tensile strength tested on cubic specimens is approximately 10% higher than on cylindrical specimens, and that the higher tensile strength is obtained using smaller cubic specimens. There is no information on how the size of cylindrical specimens influence the tensile splitting strength of concrete.

In the paper the experimental investigation is presented on how the size of cylindrical specimens influences the tensile splitting strength of concrete.

2. Laboratory experiments

Experiments were performed to evaluate the impact of a cylinder's length on tensile concrete strength received in the Brazilian method. Cylindrical specimens with a diameter of 150 mm and varied length equalling to 300 mm and 150 mm respectively were used. Additionally, four different concrete mixtures were designed for forming the specimens. The variable experiment parameters were: two types of aggregate (natural gravel and crushed granite) and two cement-water ratios (C/W = 1.8 and C/W = 2.6). Each concrete mixture was based on the maximum aggregate size 16 mm.

The laboratory tests were performed in two stages. The first one included a pilot study involving fewer test specimens. The second one comprised of more specimens. During both stages the same conditions concerning the aggregate type and a C/W ratio were kept.

On this account it was possible to gather more results in a larger testing group and to carry out a statistical analysis in a wider spectrum. In the size effect analysis concerning the tensile splitting tests, the results from both stages were taken into account together, due to identical recipes for concrete mixtures and the same types of aggregates.

The composition of the aggregate grading curve played a significant role in the concrete mixture design. The proportion of aggregate granulation was very similar in concrete mixtures with gravel and granite aggregates. A second key point was to fit the grading curves in the recommended area [14], between the upper and lower limit curves (Fig. 4 and Fig. 5).
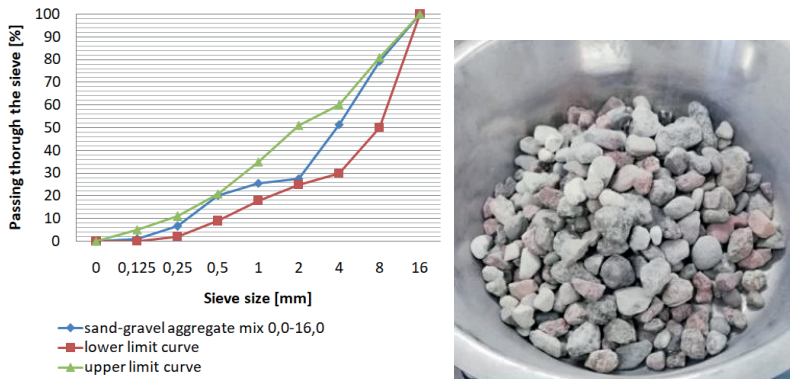
Fig. 4. Grading curve for sand and natural aggregate mixture (on the left); natural aggregate – fraction 8-16 (on the right)

Fig. 5. Grading curve for sand and crushed aggregate mixture (on the left); crushed aggregate – fraction 8-16 (on the right)

Two types of aggregates were used for preparing various concretes: one with a lower strength matrix (C/W = 1.8) and the other with a higher strength matrix (C/W = 2.6). Apart from the aggregate granulation, the cement matrix is one of the fundamental elements of the heterogenic structure of hardened concrete which influences the fracture processes ([15]-[19]). Therefore, the cement matrix was considered as an important strength parameter during laboratory investigations and it was tested in the flexural strength test of hardened cement mortar. The

tests were carried out in accordance with the code [20], on beams 40 mm × 40 mm × 160 mm in size, in a three-point bending test (Fig. 6). The proportions of water, cement and sand in the mortars were modified to obtain a proper consistency of the concrete mixtures comparing to requirements given the code PN-EN 196-1.
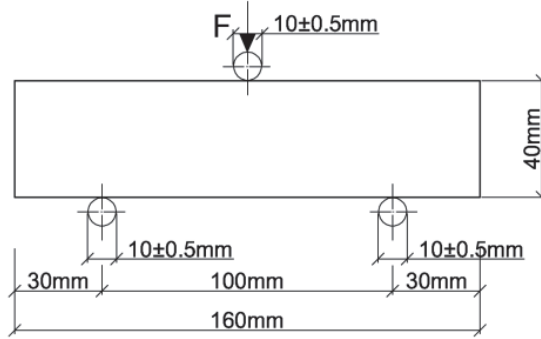
Fig. 6. A loading arrangement for testing flexural strength of cement mortar on a prism specimen according to PN-EN 196-1

Table 1. Composition of concrete mixtures

	Aggregate type	C/W	Cement [kg/m³]	Water [kg/m³]	Sand0.0-2.0 [kg/m³]	Coarse aggregate 2.0-16.0 [kg/m³]
1	Granite	1.8	375.6	206.6	481.0	1300.5
2	Granite	2.6	580.7	223.4	421.6	1140.0
3	Gravel	1.8	349.8	192.4	497.1	1344.0
4	Gravel	2.6	533.6	205.2	445.5	1204.5

The compositions of concrete mixtures are shown in Table 1. The flexural strength of the weaker cement matrix (C/W = 1.8) was 6.80 MPa and the flexural strength of the stronger matrix (C/W = 2.6) was 8.78 MPa.

Test results of tensile splitting strength are presented in Table 2.

Table 2. Test results

	Aggregate type	C/W	Cylinder's dimensions [mm]	Tensile strength – mean value [MPa]	Number of specimens [-]	Standard deviation, σ_s [MPa]	Coefficient of variation [%]
1	Granite	1.8	150x300	3.40	8	0.123	3.6
			150x150	3.49	8	0.295	8.5
2	Granite	2.6	150x300	3.78	8	0.415	11.0
			150x150	4.22	8	0.332	7.9
3	Gravel	1.8	150x300	2.68	8	0.227	8.5
			150x150	2.96	7	0.203	6.5
4	Gravel	2.6	150x300	3.54	8	0.197	5.6
			150x150	3.77	8	0.259	6.9

In the conducted laboratory experiments, a higher splitting tensile strength of concrete was noted for all specimens with nominal dimensions of 150×150 mm compared to specimens 150×300 mm in size. That tendency was observed in every series of tested cylinders, both for concrete containing natural gravel, and crushed granite. The increase of tensile strength was 6.6% for the gravel concrete with the ratio C/W = 2.6 (stronger concrete) and 15.9% for the gravel concrete with the ratio C/W = 1.8 (weaker concrete). In case of the granite concrete, the strength increase was 2.9% for the lower C/W and 11.7% for the higher C/W. However, this unique trend cannot be deduced from the obtained test results.

Fig. 7.   Examples of the specimens' failure after the tensile splitting test, concrete with natural gravel aggre-gate (from the left): cylinder 150x300, C/W = 1.8; cylinder 150x150, C/W = 1.8; cylinder 150×300, C/W = 2.6 and cylinder 150×150, C/W = 2.6

Fig. 8.   Examples of the specimens' failure after the tensile splitting test, concrete with crushed granite aggregate (from the left): cylinder 150×300, C/W = 1.8; cylinder 150x150, C/W=1.8; cylinder 150×300, C/W=2.6 and cylinder 150×150, C/W=2.6

The mode of failure for the tested specimens was similar and independent of aggregate type, cement water ratio C/W and the specimen's length.

The failure of cylinders in the performed splitting tensile tests resulted from cracking in the plane of load application, usually together with wedges chipping off from the bulk concrete (Fig. 7 and 8). The more intensive destructive cracks observed at the points of contact of the specimen with the testing machine were caused by concrete crushing as a result of compressive stresses due to the stress distribution in failure cross section (as it is presented in Fig. 3).

3. Conclusions

The main conclusion from the performed experimental research is that the length of cylindrical specimens influences the tensile concrete strength when performing the Brazilian splitting test. Lower test results were obtained when using a longer cylindrical specimen – 300 mm long compared with tensile strength on a shorter one – 150 mm long. However, due to a relatively big scatter of test results, it was not possible to draw conclusions about the

quantitative relations between tensile splitting test derived on cylinders 300 m long and cylinders 150 mm long. The type of aggregate, gravel or crushed granite, or the flexural strength of cement matrix did not affect the test results.

The observed size effect at testing tensile splitting strength of concrete requires further research on more samples. When planning the experimental investigation it would be valuable to differ the aggregate granulation, in particularly the maximum aggregate size.

References

[1]   *EN 12390-1:2013-03 – Testing hardened concrete – Part 1: Shape, dimensions and other requirements for specimens and moulds*, European Committee for Standardization, 2013.

[2]   *EN 12390-3:2019-07 – Testing hardened concrete – Part 3: Compressive strength of test specimen*, European Committee for Standardization, 2019.

[3]   *EN 12390-6:2011 – Testing hardened concrete – Part 6: Tensile splitting strength of test specimen*, European Committee for Standardization, 2011.

[4]   Aitcin P.C., Miao B., Cook W., Mitchell D., "Effects of size and curing on cylinder compressive strength of normal and high-strength concretes"*, ACI Materials Journal*, vol. 91(4), 1994, pp. 349-354.

[5]   Malaikah A., "Effect of Specimen Size and Shape on the Compressive Strength of High Strength Concrete", *Pertanika J Sci Technol*, 13(1), 2005, pp. 81-96.

[6]   Che Y. et al., "Effect of Specimen Shape and Size on Com-pressive Strength of Concrete", *Advanced Materials Research*, vol. 163-167, 2010, pp. 1375-1379. http://doi.org/10.4028/www.scientific.net/AMR.163-167.1375

[7]   Sudin M.A.S., Ramli M., "Effect of Specimen Shape and Size on the Compressive Strength of Foamed Concrete", *MATEC Web of Conferences*, vol. 10(1), 2014. https://doi.org/10.1051/matecconf/20141002003

[8]   Zhong W, Pan J, Wang J, Zhang C., "Size effect in dynamic splitting tensile strength of concrete: Experimental investigation", *Construction and Building Materials*, vol. 270(3), 2020. https://doi.org/10.1016/j.conbuildmat.2020.121449

[9]   Liu J, Wenxuan Y, Xiuli D, Wangxian Y., "Mesoscopic numerical simulation of dynamic size effect on the splitting-tensile strength of concrete", *Engineering Fracture Mechanics*, vol. 209, 2019, pp. 317-332. https://doi.org/10.1016/j.engfracmech.2019.01.035

[10] Suchorzewski J, Tejchman J, Nitka M., "Experimental and numerical investigations of concrete behaviour at meso-level during quasi-static splitting tension", *Theoretical and Applied Fracture Mechanics*, vol. 96, 2018, pp. 720-739. https://doi.org/10.1016/j.tafmec.2017.10.011

[11] Zhu R., "Scale and Aggregate Size Effects on Concrete Fracture: Experimental Investigation and Discrete Element Modelling", *Civil Engineering, Écolecentrale de Nantes*, 2018.

[12] Chandran K. S.R., Galyon Dorman S., "The nature of specimen-size-effect on fatigue crack growth and net-section fracture mechanics approach to extract the size-independent behavior", *International Journal of Fatigue*, vol. 145(2), 2021. https://doi.org/10.1016/j.ijfatigue.2020.106088

[13] *EN 12390-5:2019-08 – Testing hardened concrete: Flexural strength of test specimens*, European Committee for Standardization, 2019.

[14] *PN-B-06250 – Beton zwykły* (Eng. Plain concrete), Polski Komitet Normalizacyjny Miar i Jakości, 1988.

[15] Benkemoun N., Khazraji H.A., Poullain P., Choinska M., Khelidj A., "3-D mesoscale simulation of crack-permeability coupling in the Brazilian splitting test", *International Journal for Numerical and Analytical Methods in Geomechanics*, vol. 42(1), 2017, pp. 1-20. https://doi.org/10.1002/nag.2749

[16] Słowik M., Stroeven P., Akram A., "Crack mechanisms in concrete – from micro to macro scale", *Budownictwo i Architektura*, 19(4), 2020, pp. 55-65. http://doi.org/10.35784/bud-arch.2147

[17] Karamloo M., Mazloom M., Payganeh G., "Influences of water to cement ratio on brittleness and fracture parameters of self-compacting lightweight concrete", *Engineering Fracture Mechanics*, 168(A), 2016, pp. 227-241. http://doi.org/10.1016%2Fj.engfracmech.2016.09.011

[18] Nitka M., Tejchman J., "Meso-mechanical modelling of damage in concrete using discrete element method with porous ITZs of defined width around aggregates", *Engineering Fracture Mechanics*, 231, 2020, https://doi.org/10.1016/j.engfracmech.2020.107029.

[19] Sadrmomtazi A., Lotfi-Omran O., Nikbin I.M., "Influence of cement content and maximum aggregate size on the fracture parameters of magnetite concrete using WFM, SEM and BEM", *Theoretical and Applied Fracture Mechanics*, 107, 2020, https://doi.org/10.1016/j.tafmec.2020.102482.

[20] *EN 196-1:2016-07 – Methods of testing cement – Part 1: Determination of strength*, European Committee for Standardization, 2016.

The functio-spatial structure of airport surroundings: the case of Kraków Airport

Tomasz Bajwoluk

Chair of Spatial Planning, Urban and Rural Design; Faculty of Architecture;
Cracow University of Technology; Warszawska 24, 31-155 Kraków, Poland;
tomasz.bajwoluk@pk.edu.pl iD *0000-0002-3017-9326*

Abstract: The area around Krakow airport is an attractive developmental urban area. The concentration of passenger traffic and the flow of goods is conducive to new development projects. These projects are associated with the operation of airports, as well as new uses which see the proximity of an airport as an additional asset in operating a business based on access to a form of high-speed transport. This paper presents the findings of research concerning the existing spatial structure, transport accessibility and compositional determinants within an area around Krakow Airport, which can be used to assess the phenomena present and formulate principles and trajectories of shaping them in the future. The study was based on an analysis of selected elements of the existing functio-spatial structure, as well as available materials and subject-specific planning documents. Due to the specificity of areas around airports, which undergo dynamic change, it appears key to determine the individual form of development and land cover, that skilfully combines modernity and comfort of use with meshing with the local landscape, featuring a network of linkages and the character of suburban space. The issues present in this area are distinctive of many cities and require coherent land development proposals.

Keywords: airport city, sustainable development, functio-spatial structure, airport, urban planning

1. Introduction

In recent years, areas around airports in Poland were found to be undergoing major spatial changes. This was a result of aerial passenger and cargo transport becoming widespread and well-developed. Airports, by providing a network of local, regional, national and international connections, act as concentrators of major traffic flows that require a wide range of services. These contemporary circulation nodes became attractive spaces for many forms of economic activities, attracting investors interested in the location, providing services to the airport and the clearly highlighted accessibility of these regions. In Poland, the number of passengers using air transport grew significantly over the past several years, which was accompanied by

this mode of transport becoming increasingly widespread, as demonstrated in table 1. One consequence of this was that the number of air transport connections grew and it became necessary to extend airport infrastructure [1] (pp.4-9).

Despite expected changes and the necessity to adapt to the development of the aerial transport industry, activity in areas around airports was initially associated with the extension of terminals and passenger and cargo transport infrastructure, and over time became linked with the concept of planning the areas around airports. This development was affected by the scope of safety zones, as noted by Di Mascio et.al. [2].

This zone stems from the assessment of aviation incident risk. These are areas around runways, where constraints on development are placed. Its reach is defined individually for every airport and depends on site-specific conditions.

The objective of this paper is to present the findings of an investigation of the existing spatial structure, transport accessibility and compositional determinants in the immediate area surrounding Kraków Airport in Poland, which can be used to assess the existing phenomena and formulate principles and trajectories for shaping them in the future.

The investigation began due to the dynamism of the transformation of suburban areas, as airports and the areas around them are highly specific and integral elements of such spaces [3].

Investigation in this area allows the assessment of the current development, available planning materials, and to formulate principles for shaping the functio-spatial structure in the future, as it should form a coherent and attractive fabric at the point of contact between the city, its suburban municipalities and the airport grounds. Defining land development principles can contribute to sustainable development.

Krakow Airport was selected as a case because, at the time of performing research, it was the second-largest airport in Poland. The number of passengers passing through the airport has been increasing dynamically for several years (Table 1), and in the period under study amounted to 68.91%.

Table 1.   Yearly number of passengers for Kraków Airport in the years 2016–2019, source: www.ulc.gov.pl

Airport	Number of passengers			
	2016	2017	2018	2019
Kraków airport	4,974,676	5,829,190	6,759,683	8,402,859

In recent years, the suburban zone of Krakow saw structural transformations associated with the development of settlement, which contributes to the necessity to define the form of development of areas around airports. The case of Kraków Airport is distinctive of numerous airports in Poland and Europe in terms of the transformation of the development of areas around them and how their connections with their respective cities are planned. It can also be referenced to spatial analyses of areas around other airports of similar size and degree of development, especially in Poland.

The scope of this study covers the area in close proximity to Kraków Airport, Poland, which is located in the administrative limits of three neighbouring municipalities: Kraków, Zabierzów and Liszki, and is accessible from major transport arterials (Fig. 1).

The study is based on original analyses of the existing functio-spatial structure, compositional determinants and transport accessibility.

It also analysed selected planning documents that had been drafted for this region and the relevant literature.

The airport can be said to affect the development of areas around airports, just as they affect their surroundings. In many cases, their forms can be considered hallmarks of their respective cities and affect their visual reception. Therefore, areas around airports require individualised approaches and a rational form of development. The study of these areas can be seen as relevant and essential, due to:

- The dynamic development of suburban zones in recent years, including that of the area within the airport's area of influence,
- Concentrations of a diverse range of economic activity in these areas,
- Functional and compositional relations forming in emergent development structures,
- The current transformation trajectory of areas around airports.

The area under analysis within the vicinity of Kraków Airport is a local case of structure shaping, yet the tendencies discussed are global and are parts of processes that take place elsewhere around the world. They include, among other things, landscape and environmental changes that happen as a result of the urbanisation of new areas [4], [5]. They are diverse in terms of scale and transformation dynamics, but are perceived as interesting areas that can act as starting points for structures with an urban character that are built in connection to a transport node [6] (pp.395-414), [7].

European municipal decision-makers have long since acknowledged the potential of such zones and make attempts to comprehensively plan them, especially in how they form relations with cities proper [8] (pp.100-111). An interesting solution was used in Luxembourg, Copenhagen and Amsterdam, by creating new attractive development structures that were functionally and compositionally linked with these cities.

Referencing selected models of planning these areas featured in the literature, such as the Airport City, Aerotropolis or airport corridor as defined by J.D. Kasarda [9], [10] (pp.1-22), can allow us to investigate an optimal form of planning areas around airports, adapted to the case of Kraków Airport, and a form that is more adapted to local determinants instead of building a new, separate form of city around an airport, specifically in the context of a city of high historical value.
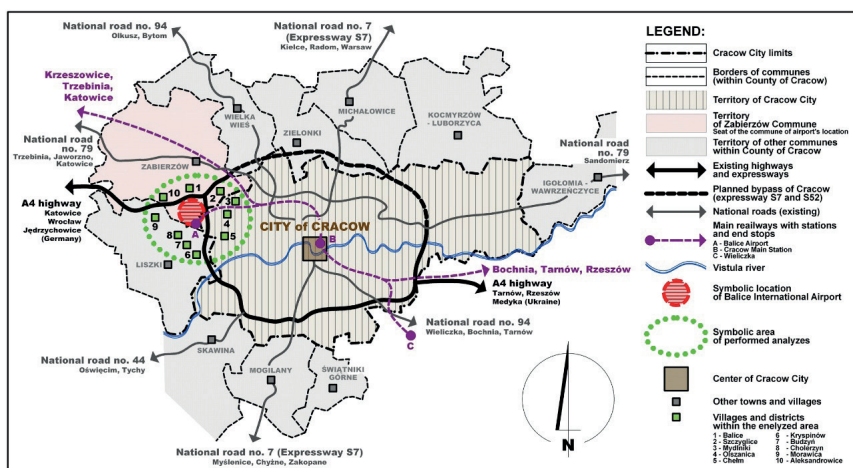

Fig. 1. Diagram showing the location of the airport and the area under analysis within Krakow and its neighbouring municipalities, original work, 2021

1.1. Selected models of planning areas around airports

Planning areas around airports is a process which involves accounting for an airport's impact as a transport node that combines the function of passenger and goods transport. Increasing passenger traffic flows require comprehensive operations, as well as providing a service zone with the maximum possible amount of comfort, thus enhancing the quality of this operation. Hence, in the case of many airports, the terminals themselves and their immediate vicinity become the sites of a wide array of ancillary services and act as elaborate transfer nodes integrally linked with public transport access [11]. At present, airports are transport nodes, but also distinctive structure-genic elements, in most cases located in suburban areas [12], [13]. J.D. Kasarda presented an interesting model of development of both airports and their adjacent areas [14]. The globalisation of airline connection and goods exchange is becoming the reason behind adopting a much broader perspective on the shape of space that surrounds airports, especially in the twenty-first century. The Airport City and the Aerotropolis are distinctive spatial forms of urban structures, defined and proposed by J.D. Kasarda. They are associated with airports, but affect the development of the space of the contemporary city. They combine the dense development of the centre in the immediate proximity of terminals (Airport City) with gradually impacting the space and its functional structure along transport corridors that extend from it. They form the entirety of new type of urban fabric called the Aerotropolis, which consists of mixed-use developments associated with aviation, as well as ancillary functions that utilise well-presented and attractive distant surroundings with good transport connections (Fig. 2). The author of these models noted that, in the twenty-first century, airports could become elements with a major impact on urban development, similarly to the role that had been played by the railway in the nineteenth century and highways in the twentieth century.

The development of areas around airports forms integral and independent structures in space, which are linked with the core city, and sometimes blend into its tissue. The model of planning areas around airports described by J.D. Kasarda develops individually in areas that accompany airports, adapting to local conditions and development potential. We were able to observe a dynamic development of such areas in Asian cities in recent years.

One interesting case is the zone around Changi Airport in Singapore, which develops around an airport that was used by 55.4 million passengers in 2015, and 65.6 million in 2018, which is an increase by 18.41% [15]. It is an example of model based on the development of its adjacent area long a transport corridor that connects the airport with the city, in this case placed parallel to the airport's runways and that ends at passenger terminals which house elaborate service functions, providing passengers with a wide spectrum of attractions and ways of spending free time. These include a cinema, a swimming pool, shopping galleries, playgrounds and gardens with tropical greenery for rest and recreation. Due to the scale of the project, the terminals are connected by rail and two indoor moving walkways that provide freedom of movement between them. This model, which J.D. Kasarda described as an airport corridor, is also referenced by many areas around European cities. They include the airports of Amsterdam, Luxembourg, Frankfurt or Copenhagen, which form new, intensely developed office, service and housing districts, connected both with the city and the airport via transport linkages [7]. Of course, when it comes to detailed solutions, these projects vary, but they are linked by a shared idea of intense use of the area around the airport, specifically around the primary arterial that connects the airport and the city, and is often supplemented by a high-speed railway line. When analysing the spatial models of areas around airports, we should emphasise

the local determinants of every case, especially those that stem from the competitiveness of a given airport within the system of airports of a given region [16]. It arises from, among other things, an airport's strategic location, the size of the city and its economic significance. These qualities affect air traffic volume, including the transport of goods.

This is why the selected models presented(Airport City, Aerotropolis, Airport corridor), although repetitive by assumption, take on varying sizes, scales and forms when implemented. However, they appear to be an interesting and proper reference for the analysis of the area around Kraków Airport, which recently became an area subjected to transformation and the siting of new functions.
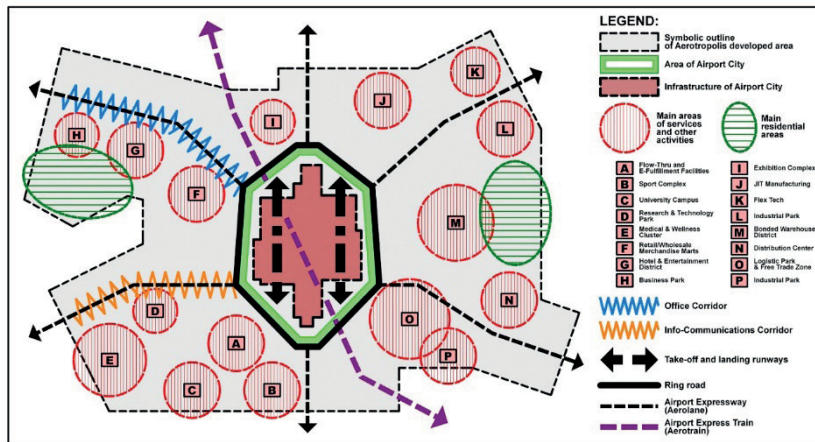
Fig. 2.   Diagram of models of developing the area around an airport. *Source: own study based on [9], [10], [14], 2021*

2. Research scope and methods

This study of the area around Kraków Airport in Kraków, Poland, is based on an analysis of selected elements of its existing functio-spatial structure. The investigation covered past suburban villages, new single-family, office, storage and manufacturing and services buildings, as well as forested, agricultural and recreational areas and natural greenery (Fig. 3).

Other elements that were analysed included compositional determinants and transport accessibility in this area, which accounted for elevated points, visual axes in the area as identified in the compositional section, forest complexes surrounding the area and providing a vista background. In the section concerning transport accessibility, primary transport arterials, railway lines and stops, and car parks (Fig. 4).

The study analysed selected planning materials drafted for this area in terms of land use regulations and planned transport solutions, as well as the relevant literature.

Based on the analyses, an estimate listing of area assigned for selected functional areas as encountered at the time of writing, and in its planned state (resulting from an analysis of selected planning documents) (Tables 2, 3).

The area under study covered Kraków Airport, the area in its immediate vicinity as outlined in the IA General Development Plan (Plan Generalny Rozwoju MPL), and a buffer zone within around 3 km of the airport, which included a part of the territory of Kraków within

urban unit 39 from the Spatial Development Conditions and Directions Study [17] of the city and the former villages of Olszanica, Chełm and Mydlniki, parts of the Zabierzów and Liszki municipalities covered by the Study [18], [19], along with the former areas of Aleksandrowice, Balice, Szczyglice, Morawica, Cholerzyn, Budzyń and Kryspinów villages.

An analysis of the functio-spatial structure in the immediate vicinity of the airport was performed, which also covered the terminal locations, single-family development and services (including car parks, manufacturing and storage) (Fig. 5) and an analysis of how the area evolved between 2003 and 2020 (Fig. 6).
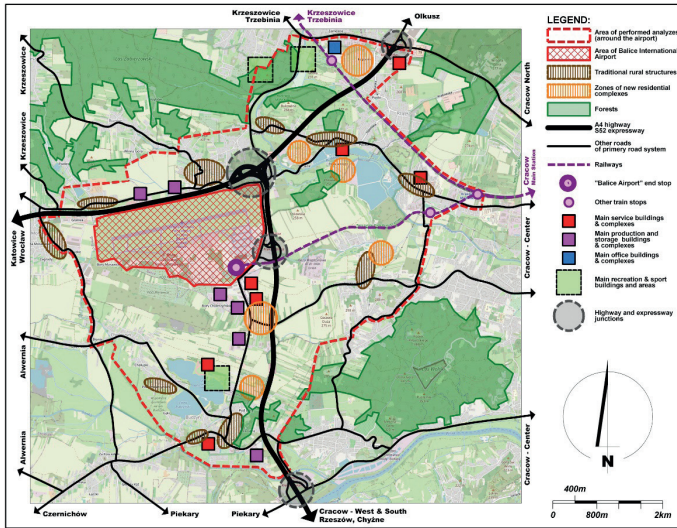
Fig. 3.   Analysis of selected elements of the existing functio-spatial structure of the area around Kraków Airport. *Source: own study, 2021*
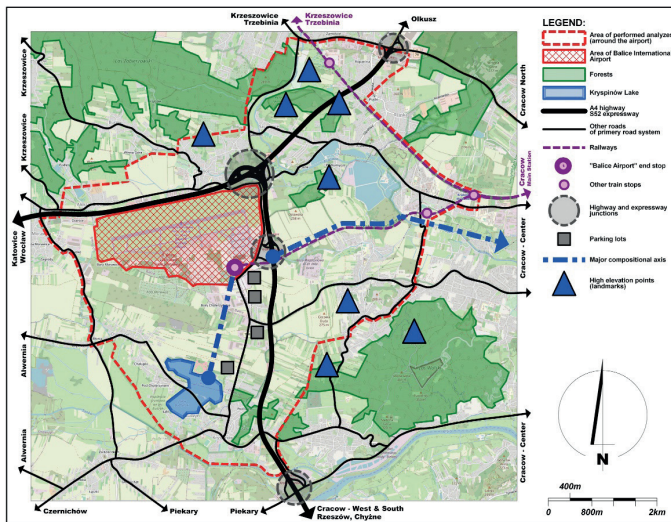
Fig. 4.   Analysis of compositional determinants and transport accessibility within the area around Kraków Airport. *Source: own study, 2021*

3. Results

3.1. Overview of local determinants affecting the settlement network

The area under study is located within the administrative limits of three municipalities: Kraków, Liszki and Zabierzów. The airport proper is located in the municipality of Zabierzów. This area is a part of Kraków's suburban area and its settlement layout consists of former villages which have changed in character over the past twenty years and gradually changed their functio-spatial structures. They transitioned from agriculture, previously featuring typically agrarian development, into a more suburban format, with a predominance of single-family housing, services and fragmentary industrial and storage buildings. The former villages were found to have retained their urban layouts, based primarily on development organised along a main transport route. New development that supplements the structure or forms new enclaves was observed to be accessible via their respective and steadily extended transport layouts. This largely the result of continuing existing transport routes rather than forming new, integrating linkages within the area (Fig. 3).

In the section that belongs to Kraków, the former villages that were studied were Olszanica, Mydlniki and Chełm, in Zabierzów they were Szczyglice, Aleksandrowice and Balice, and in the municipality of Liszki they were Kryspinów, Morawica, Cholerzyn and Budzyń. All of them are located within 3 km of the airport. Their predominant function is housing, but sizeable portions of their territory are occupied by greenery and agricultural use, which is a result of the past character of the area. Developed areas comprise 31.2% of the area under analysis (Table 2).

Table 2. Listing of selected existing elements of function-spatial structure elements within the area around Kraków Airport under analysis. *Source: own study, 2021*

Land use	Area under analysis
Airport	12.4%
Housing	15.4%
Services	1.6%
Offices	0.5%
Industry and storage	1.3%
Forests	4.2%
Natural greenery and water bodies	13.5%
Others (including agriculture)	51.1%

3.2. Development structure – architectural and urban form

At the time of performing the analysis, the development structure of the area around the airport was highly diverse. The area immediately adjoining the airport featured a complex of buildings that were handling international and domestic passenger and cargo traffic. They included the main terminal, a multi-level car park and a section that handled cargo transport [20]. This urban form references the Airport City model, yet the continuation and linkages with further areas do not form a legible composition within space.

To the south, in the direction of Kryspinów, there was a developing services, industry and storage complex. Plant-type buildings with 1 to 2 storeys and located on separate plots predominated, which was found to hinder the emergence of an integrated urban complex

(Fig. 5). Airport car parks also occupy a significant portion of this area. The spatial transformation of this area in the years 2003 and 2020 indicate the presence of development pressure and a mixing of single-family buildings with service and manufacturing buildings (Fig. 6).

The remaining buildings, mostly housing office or service spaces, in addition to manufacturing, formed small complexes within Zabierzów, Kryspinów, Balice and Mydlniki, which can be seen as a sign of interest in the area among developers, yet it can also be argued that it is not solely a result of proximity to the airport, but also of access to the A4 highway and providing services to Kraków's growing suburban zone.
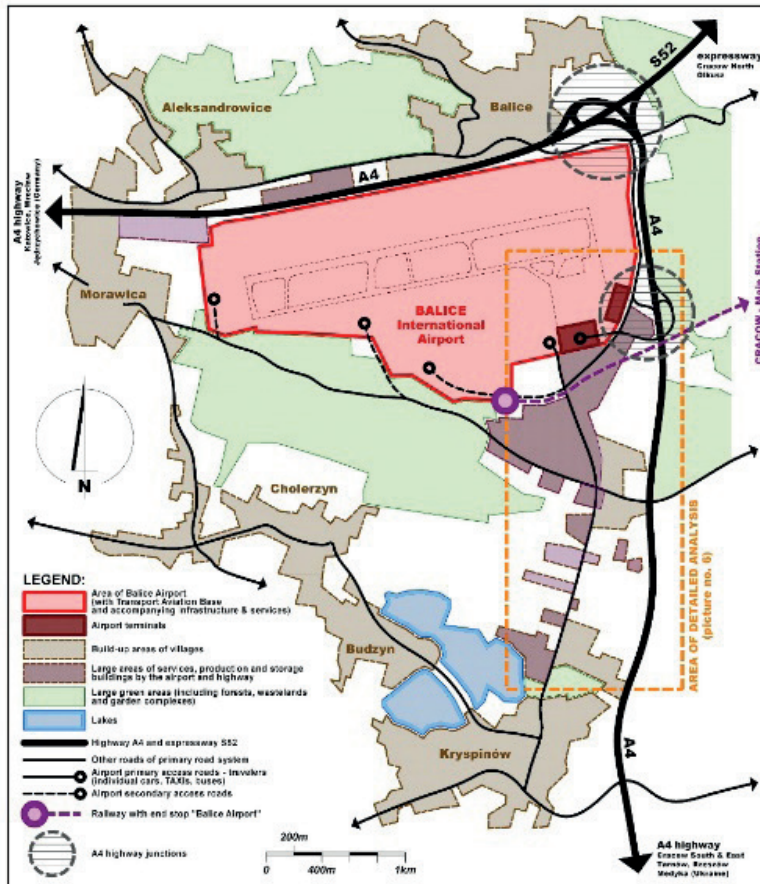
Fig. 5.   Analysis of selected elements of the functio-spatial structure in the immediate vicinity of Krakow Airport. *Source: own study, 2021*

Fig. 6.   Analysis of the transformation of selected elements of the functio-spatial structure in the immediate proximity of Krakow Airport in the years 2003 and 2020. *Source: own study, 2021*

3.3. Transport linkages

The area under analysis was observed to have access to the A4 highway, which acts as Kraków's beltway. The A4 connects to the local road network via the Balice and Modlniczka intersections. The local transport layouts provides linkages with Kraków via four arterials from the east, and with the existing settlement layout. The area is connected to Katowice, a nearby major agglomeration, via road through Zabierzów and the A4 highway, and with Oświęcim via a road through Liszki. Internal transport layouts which handle traffic inside the settlement layout and the former villages themselves were found to be illegible, and the immediate surroundings of the airport along the road towards Kryspinów was observed to have become a site with multiple large car parks. They are a predominant and unattractive form of land use, but that was nevertheless preferred in this area (Fig. 4). A railway line with a stop near the passenger terminal provided a connection with the city. The role of this line was confined to handling traffic from the airport and partly the former village of Mydlniki. This railway line connected with a metropolitan railway system and its stops.

3.4. Compositional and functional determinants with the immediate area

The findings of compositional analyses point to two attractive directions formed by new areas in the development of the zone along which the building structure can grow (Fig. 4). In Figure 4, these are compositional axes.

The eastern direction that connects the airport with Kraków appears to be strategically significant. Supplemented by a railway line, a network of stops and, as included in the plans analysed, a new arterial and development that can become an attractive transport route linked with the city centre.

The southern direction that connects the airport with recreational areas near a lake in Kryspinów defines a space that integrates development in the vicinity of the airport with the existing functio-spatial structure and green areas in a more local manner. At present, this area features point-like instances of service and manufacturing buildings, which considerably limits the identification of this compositional axis in space. The planning documents analysed appeared not to make use of it.

The area north and east of the airport had development of varying height. Major elevation points in this area and its immediate vicinity were measured to range between 255 m above sea level to 384 m above sea level. Together with forest complexes, they form a visual background in the area.

It appears that pursuing compositional relations can contribute to creating attractive fragments in areas around airports, in which newly emergent urban structures, located in the open landscape, could utilise distinctive visual axis directions so as to integrate the space around the airport.

4. Applicable planning documents

Kraków Airport is subjected to the provisions of planning documents drafted for its territory. One of these is Kraków Airport General Plan [21] for the years 2016–2036, approved on 26.11.2018 by the Minister of Infrastructure, which is required as stipulated in the Aviation Law Act. It was subjected to consultation with municipalities covered by the plan and which are affected by the airport's operations and air traffic itself. Among other things, it defines the scope of the airport's impact, as well as planned buildings and elements of airport development associated with its operation and the immediate vicinity. The Plan defines areas for infrastructure associated with handling passenger and cargo traffic, and areas assigned for projects in the pre-existing military section located from the south-west. In the zone of direct passenger processing, located from the south, there is the terminal, a hotel, a train stop and a multi-level car park, surface parking lots, as well as a section with administrative spaces, and cargo handling and technical facilities.

The placement of these buildings from the south-eastern side of the runway, near its start, affected the spatial solutions and urban layout of the complex that provides circulation, but does not create a compositionally legible link with the zone of new development projects located in the south. The existing transport and circulation layout is the result of old linkages with Zabierzów and Liszki, and despite several modernisation projects in the immediate vicinity of the terminals, it does not provide safe relations with the railway. Due to the siting of the airport in a location that belongs to three municipalities, planning documents that concern this zone are not often up-to-date to the same degree. The eastern part that belongs to Kraków was,

at the time of writing of this paper, in the design phase and was to be ultimately divided into five local spatial development plans: Balice I, Balice II, Podkamyk, Olszanica and Zakamycze.

Fragments of these plans shall affect the planning of the area around the airport in its eastern section. At this stage, it was possible to reference the current Spatial Development Conditions and Directions Study [17] of the city of Kraków. Within the 'Olszanica' structural unit, this document assumed a new transport link with the airport in the form of an extension of Armii Krajowej Street. This arterial can become the main road to connect the city centre with the airport, introducing a legible direction and possibility of creating an attractive functio-spatial structure. Around the airport itself, the Study assumed the placement of service buildings, including exposition, office and commercial spaces, which can be seen as a form of recognising the potential of the airport's vicinity in terms of new functions that enhance its competitiveness on the scale of the city and the wider region. The plan also assumed the relocation of the highway intersection in the area of the airport, and as such a modernisation of the transport layout, the airport's accessibility and its infrastructure. The provisions of Kraków's Study in this area preserved the settlement layout within the former villages of Mydlniki and Olszanica, to be dominated by existing and future single-family housing. The area of the airport and its vicinity in the area under study is also subjected to the Study of the municipalities of Zabierzów and Liszki [18], [19]. In the Zabierzów municipality, the territory of the airport and the highway from the north was assigned for concentrating services. The villages of Aleksandrowice, Balice and Szczyglice are primarily areas occupied by single-family housing. The municipality of Liszki covers territory from the south-western part of the airport and that of the old villages of Morawica, Cholerzyn, Budzyń and Kryspinów, which were assigned for the development of single-family housing, and in close proximity to the airport—for commercial areas. The Study of the municipality of Liszki also assumed the development of recreational areas around the water reservoirs of Kryspinów and an extension of the transport layout for this area.

An analysis of land use provisions in the studies of Kraków, Liszki and Zabierzów for the area under analysis demonstrates an increase of areas assigned for development. In the territory of the Kraków municipality, this is 46.4%, in Liszki it is 39.2%, and in Zabierzów it is 27.4% (Table 3). This specifically applies areas for single-family development, which is to focus around the existing settlement network, primarily tied with historical suburban villages, but at present it is tied with growing suburban development. The documents were found to feature concentrations of commercial uses in close proximity to the airport, from the east and south, yet apart from a new link with Kraków, they were not found to introduce new, integrating solutions.

Table 3.   Listing of specific land uses as featured in the Spatial Development Conditions and Directions Studies of the municipalities of Kraków, Liszki and Zabierzów for the area under study. Kraków Airport, source: SUiKZP. *Source: own study, 2021*

Land use stipulated in the SUiKZP	Municipality		
	Kraków	Liszki	Zabierzów
Housing	19.8%	25.4%	16.1%
Services	23.2%	5.5%	9.8%
Industrial plants and storage	3.4%	8.3%	1.5%
Greenery	36.2%	21.9%	18.6%
Other	17.4%	38.9%	54.0% (including the airport)

6. Discussion

General development plans of areas around airports are essential elements of planning them [22]. Such documents were highlighted by, among others, J.D. Kasarda and I.M.H. Canon [23] (pp.29-31), who noted its complexity. Economically, it is intended to attract domestic and foreign capital into the area, providing opportunities for profit. The proximity of an airport is rated as a development opportunity as it provides access to global markets via aerial transport and high traffic concentrations. Controlling the attraction of new investors and developers via attractive architectural and urban form, and the zoning of individual functions, can contribute to the development of such areas and establishing a space for economic activity that can compete with other areas of a city. As noted by these authors, it is a long-term process that requires numerous experts and coordination of efforts by decision-makers In the process of carrying out such a project, especially in the initial phase, in close proximity to an airport, and over time, in its extended zone of influence.

Airport-focused urban development is an essential trajectory that economically activates contemporary cities. However, it should also be synchronised with spatial planning of significance to the city and its region [24] (pp. 800-811). Scholars from these fields note the conflicts between spatial planning in these areas, which are under the purview of local governments, and the development pressure of large corporations who focus more on matters of project profitability rather than the form of developing the functio-spatial structure [25] (pp.914-921).

Does the Spatial Development Conditions and Directions Study for Kraków reference these models by Kasarda? It appears to do so partially, in the area linked with the airport itself, on a local scale and form, subjected to handling aerial traffic. In more distant areas, it showed characteristics of concentrating activities, but this concerned singular buildings and urban complexes that did not form a cohesive urban space that could define new development trajectories.

This general aspect was noted by L. Krier [26], who stressed that many urban planning solutions do not automatically create an atmosphere of the city. It appears that, in the case under analysis, one of the causes behind this could be the administrative division of the territory around the airport and as such its character as a point of contact between three municipalities with differing potential and character. The area around the airport is crucial to each of them, but it is not their sole developmental area.

The planning documents presented were not found to define innovative development trajectories for this zone, apart from the siting of service uses in the immediate vicinity of the airport, in the area around the terminals from the east and south. In addition, transport linkages were likewise within the standards of accessibility and did not create well-defined directions, axes or public spaces.

The general plan of the airport's development, in terms of scope, was found to be confined to the airport's immediate vicinity, and did not affect the development of the more distant part of the zone. The various commercial and office complexes formed singular enclaves and the areas assigned for housing projects, mostly single-family units, were slowly filling the space around the airport, creating an impression of randomness and being scattered.

The model of building a city around an airport (airport city, aerotropolis), in the case of the Kraków Airport, was found to appear to be limited, and any attempts at realising it through planning document provisions of each municipality, concern its immediate vicinity, and any pursuits of turning it into an aerotropolis appear to be largely aimless. The reason for

this is the transformation of the suburban zone in this area rather than the dominant impact of the airport itself. Accommodations, parking spaces and catering services offered around the airport stem largely from providing services to passengers, and their placement does not form a coherent space, merely answering the basic needs of the place.

It appears that the form and manner of public space design in these areas is crucial, as in the case of areas around airports, such spaces integrate them both overall and in their individual fragments.

The role and significance of these types of elements in the city and the specificity of their design and reception was discussed by M. Carmona [27] (pp.374–405) [28], [29] (pp. 241–259). Providing sustainable environmental development, including transport-related development, is another essential aspect, which appears to come with additional challenges in areas around airports [30] (pp.61-73), [31]. Changes in land use around airports and in suburban zones. the role of spatial planning in these urban and rural areas, specifically with the intent to preserve the value and quality of the environment, were noted by K. Swangjang [32] and Z. Pucherowa et.al. [33]. This can be seen as a sign that scholars recognise spatial transformations and their impact on the environment, which significantly affects the shaping of areas around airports.

7. Conclusions

My analyses of the area around Kraków Airport in Poland point to its current transformation trajectory as being within the confines of building singular infrastructural buildings associated directly with the airport, and building service and manufacturing buildings in the areas around the airport. This scheme of action treats the space around the airport as being attractive to new projects, yet without clear characteristics of creating a coherent airport city space. It is instead a form intended to handle passenger and cargo air traffic, and is not seen producing a new and attractive form of development that could truly begin the creation of the area. The transformation of the area around the airport is considerably affected by growing development pressure in Kraków's suburban area. This is also indicated by the development of housing areas based on old suburban villages located around the airport, Zabierzów, Aleksandrowice, Balice, Kryspinów, Morawica, Cholerzyn and Budzyń, as well as areas of Kraków's former suburban hamlets: Mydlniki and Olszanica, which are currently within the city's administrative limits.

It appears that the further intensification of settlement in these regions, especially in the form of housing, could constrain the airport's development and degrade it to the role of an element of functio-spatial structure and not an attractive place that could become a starting point for a new space that could integrate various forms of development, specifically in the vicinity of the function that is to provide access to global markets and linkages. In the area under analysis, the airport occupied a sizeable territory with restricted access, including runways and their accompanying infrastructure, which is why it is also a functional barrier, as is the highway from the north and east.

However, this does not predefine the potential for shaping the area around the airport, especially along the southern and eastern direction. It appears that the most compositionally and functionally attractive direction is the one towards the city. My analysis of existing development showed that the greatest potential and opportunity for creating a new structure lied with a planned transport corridor that would link the airport with the city. This requires a skilful balancing of development scale and form in the area, ensuring interesting compositional relations and making use of environmental assets (the Rudawa River Valley, the former bed

of the historical Młynówka Królewska Creek near Mydlniki, which dates back to the fourteenth century). It also appears essential to connect with existing housing areas in Olszanica, Mydlniki and Wola Justowska.

This study can be used to formulate the following general conclusions concerning areas located around airports:

- New development structures should specifically adapt to the character of suburban areas, with a preference for solutions aimed at the sustainable development of these areas and the preservation of green areas, including agricultural ones, as well as cultural continuity.
- We should pursue extending the scope of general airport development plans to include plans of the development of the areas around them, defining major development trajectories, the preferred development structure, and create a space that integrates the area and that is linked with the nearby suburban fabric.
- Delineating major development trajectories should be done by utilising local determinants, e.g. in terms of composition. Greenery in the form of landscaped areas that supplement the development structure, provide insulation from nuisance-causing uses and act as a foreground for areas of intense development, should be an essential element of the area.
- Service concentrations should form spatially cohesive zones which provide links with the city, and come equipped with housing, properly insulated from nuisance-causing uses.
- The main road link with the city should be an element that increases the airport's accessibility and a compositionally and functionally attractive transport and circulation route that defines the entrance zone to the city. Continuing development along such an arterial could become a starting point for a mixed-use airport–city transport corridor.
- Creating a new functio-spatial structure around airports and the zones in their immediate proximity should provide a safe and attractive public space that affects the integration network of the new urban fabric.
- Spatial planning and urban design that accounts for local determinants is the only proper tool for the sustainable planning of areas around airports and providing the structures that emerge in such areas with spatial cohesion.

Detailed conclusions concerning the principles of shaping the area around Kraków Airport:

- The link with the city along the eastward compositional axis and the potential for southward development should be taken advantage of.
- Forming development structure should be based on a new transport layout
- The intensification of development along compositional axis should feature public space that create attractive and integrating linkages with the airport.
- Urban sprawl should be prevented, and leisure areas adjoining the Kryspinów reservoir should be protected.

References

[1]   Huderek-Glapska S., „Co oznacza sukces portu lotniczego i kiedy ma wpływ na gospodarkę miasta i regionu?", *Przegląd Komunikacyjny*, 2017, vol. 11, pp. 4-9. https://doi.org/10.35117/A_ENG_17_11_01

[2] Di Mascio P., Perta G. Cantisani G., Loprencipe G., "The Public Safety Zones around Small and Medium Airports", *Aerospace,* 2018, *5*, 46. https://doi.org/10.3390/aerospace5020046

[3] Bajwoluk T., *Przestrzeń podmiejska. Wybrane zagadnienia struktury funkcjonalno-przestrzennej.* Kraków: Wydawnictwo Politechnik Krakowskiej, 2020.

[4] Thornbush M. J., Allen C.D., *Urban Geomorphology. Landforms and Processes in Cities*. Elsevier, 2018.

[5] Tzu-Ping Lin, *Urban Microclimate*. Elsevier, 2021.

[6] Wang Y., Chou Ch., Yeo G., "Criteria for Evaluating Aerotropolis Service Quality"*, The Asian Journal of Shipping and Logistics*, 2013, 29, 3, pp.395-414.

[7] Conventz S., Thierstein A., "The knowledge economy, hub airports and accessibility. A location based perspective", in *The Case of Amsterdam-Schiphol, European Regional Science Association (ERSA) Conference*, Barcelona, Spain, 2011.

[8] Zak D., Getzner M., "Economic Effects of Airports in Central Europe: A Critical Review of Empirical Studies and Their Methodological Assumptions, Horizon Research Publishing", *Advances in Economics and Business*, vol. 2(2), 2014, pp.100-111, https://doi.org/10.13189/aeb.2014.020206

[9] Kasarda J. D., "The Evolution of Airport Cities and the Aerotropolis", in *Airport Cities: The Evolution*, ch.1, London: Insight Media, 2008.

[10] Kasarda J. D., "Aerotropolis: Business Mobility and Urban Competitiveness in the 21st Century", in *Culture and Mobility*, ch. 1, Heidelberg: Heidelberg University Press, 2013, pp.1-22.

[11] Stangel M., *Airport City. Strefa okołolotniskowa jako zagadnienie urbanistyczne*. Gliwice: Helion, 2014.

[12] Schlaack J., "Defining the Airea: Evaluating Urban Output and Forms of Interaction Between Airport and Region", in *Airports in Cities and Regions: Research and Practise*, eds. Knippenberger U. and Wall A., 113–26. Karlsruhe: KIT Scientific Publishing.

[13] Schlaack J., *Flughafen und Airea, Impulsgeber fur Stadtregionen*. Berlin: DOM Publishers, 2015.

[14] Kasarda J.D, "Aerotropolis", in *The Wiley-Blackwell Encyclopedia of Urban and Regional Studies*; Orum A.M. Ed.; Hoboken: John Wiley&Sons, 2019.

[15] Changai Airport, https://www.changiairport.com [Accessed: 12 Jan 2021]

[16] Source: https://static.fraport.de/ONLINE/zdf/zadafa_e_2015/mobile/index.html#p=14 [Accessed:12 May 2021]

[17] SUiKZP miasta Krakowa uchwała nr CXII/1700/14 Rady Miasta Krakowa z dnia 9 lipca 2014, https://www.bip.krakow.pl [Accessed: 25 Jan 2021]

[18] SUiKZP gminy Zabierzów Uchwała Rady Gminy Zabierzów z 16.07.2010 nr L/488/10 https://www.sip.gison.pl/zabierzow [Accessed: 25 Jan 2021]

[19] SUiKZP gminy Liszki Uchwała Rady Gminy Liszki z 23.03.2011 nr VI/36/2011 https://www.liszki.pl [Accessed: 12 Feb 2021]

[20] Wróbel P., "Kraków Airport – studium przypadku. Przekształcenia architektoniczno-urbanistyczne", *Builder* 01(270)*,* 2020. https://doi.org/10.5604/01.3001.0013.6476

[21] Plan Generalny Lotniska Kraków–Balice (2018) https://www.krakowairport.pl [Accessed: 18 Jan 2021]

[22] Bradley A.L.W., *The Independent Airport Planning Manual*, Woodhead Publishing, UK, 2010.

[23] Kasarda J.D., Canon I.M.H., "Creating an Effective Aerotropolis Master Plan", *Regional Economic Review*, 2016, vol. 5, pp.29-31.

[24] Boloukian R., Siegmann J., "Urban Logistics; a Key for the Airport-Centric Development – a Review on Development Approaches and the Role of Urban Logistics in Comprehensive Airport-Centric Planning", *Transportation Research Procedia*, 2016, vol.12, pp. 800-811. https://doi.org/10.1016/j.trpro.2016.02.033

[25] Ventura P., Zazzi M., Rossetti S., Carra M., "Urban Development and Airports in Northern and Central Italy: Main Trends and Focus on Parma Giuseppe Verdi Case Study", *Transportation Research Procedia,* 2020, vol.45, pp.914-921. http://doi.org/10.1016/j.trpro.2020.02.076

[26] Krier L., *Architektura wspólnoty*. Gdańsk: Słowo/Obraz Terytoria, 2011.

[27] Carmona M., "Re-theorising Contemporary Public Space: A New Narrative and a New Normative", *Journal of Urbanism,* vol. 8(4), 2015, pp.374–405. https://doi.org/10.1080/17549175.2014.909518

[28] Carmona M., "Principles for public space design, planning to do better", *Urban Des Int*, 2019, 24, 47-59. https://doi.org/10.1057/s41289-018-0070-3

[29] Carmona, M., Hanssen, G.S., Lamm, B. *et al.,* "Public space in an age of austerity", *Urban Des Int,* 2019*,* 24, pp. 241–259 . https://doi.org/10.1057/s41289-019-00082-w

[30] Russo F., Comi A., "City characteristics and urban goods movements: A way to environmental transportation system in a sustainable city", *Procedia Social and Behavioral Sciences*, 2012, vol. 39, pp.61-73.

[31] Verma P., Singh P., Singh R., Raghubanshi A., *Urban Ecology. Emerging Patterns and Social-Ecological Systems*. Elsevier, 2020.

[32] Swangjang K., Iamaram V., "Change of Land Use Patterns in the Areas Close to the Airport Development Area and Some Implicating Factors", *Sustainability*, 2011*,* 3*,* 1517-1530. https://doi.org/10.3390/su3091517

[33] Pucherová Z., Mišovičová R., Bugár G., Grežo H., "Changes in Landscape Structure in the Municipalities of the Nitra District (Slovak Republic) Due to Expanding Suburbanization", *Sustainability*, 2021, 13, 1205. https://doi.org/10.3390/su13031205

Crossref
Similarity Check
Powered by iThenticate

Orginal Article

The acoustic climate of spaces located under overpasses in the context of adapting them for outdoor public events – a pilot case study

Elżbieta Komarzyńska-Świeściak[1], Piotr Z. Kozłowski[2]

[1] *Department of Public Architecture, Basics of Design, and Environmental Development; Faculty of Architecture; Wrocław University of Science & Technology; 53/55 Prusa, 50-317 Wrocław, Poland; elzbieta.komarzynska-swiesciak@pwr.edu.pl* (iD) *0000-0002-2688-4073*
[2] *Department of Acoustics, Multimedia and Signal Processing; Faculty of Electronics, Photonics and Microsystems; Wroclaw University of Science & Technology; Wybrzeże Wyspiańskiego 27, 50-370 Wrocław, Poland; piotr.kozlowski@pwr.edu.pl* (iD) *0000-0002-3122-6606*

Abstract: Due to the current shortage of traditional public space because of its privatization, commercialization, and securitization, there is an urgent need to reclaim areas affected by motorized traffic in the urbanized areas. On the other hand, the process of adapting them for new purposes should be carefully carried out, addressing several issues, among them environmental acoustics. This study is meant to contribute to our understanding of acoustic conditions of a general model of the bridge underspace. Therefore, the aim of the research was to examine the existing acoustic climate by measuring noise levels and comparing them with equivalent acceptable noise levels for the expected type of space development and Noise Rating curves. In this research, a pilot case study approach was used, as measurements were taken for a chosen space located under an elevated road that represents certain criteria set by the researchers. The results allowed us to: (1) verify the relationship between the geometry of the bridge underspace and the noise levels, (2) assess the initial acoustic conditions in terms of possibilities of acoustic adaptation of the examined space for outdoor public events, and (3) formulate hypotheses and preliminary assumptions for the planned further and broader studies of the issues raised in this article. The presented results and their analysis show that it is possible to bring the acoustic conditions in the studied space to the state required for public or cultural meeting spaces. In comparison with earlier findings, the research undertaken appears to be pioneering and the results can be used as valuable input for further research on this topic.

Keywords: architectural and acoustical design, public space, bridge underspace, environmental acoustics, urban acoustics

1. Introduction

The authors of this article are currently involved in an interdisciplinary research project focusing on examining to what extent existing space under bridge-like facilities (flyovers, viaducts, bridges) can be adapted for high-quality public space, dedicated especially for outdoor events, such as recreation and sport events, concerts, film screenings, lectures, etc. This research addresses several issues from various scientific disciplines such as, for example, urban planning, structural design, environmental engineering, and acoustics (Figure 1). The research undertaken appears to be pioneering and the results can be used as valuable input for further research on this topic, which has wide possibilities of use. Although the last decade has witnessed an increase in research interest in utilization of the bridge underspace, previous studies have failed to conduct in-depth analysis of its environmental conditions, especially in terms of possibilities of acoustic adaptation of this space for outdoor public events.
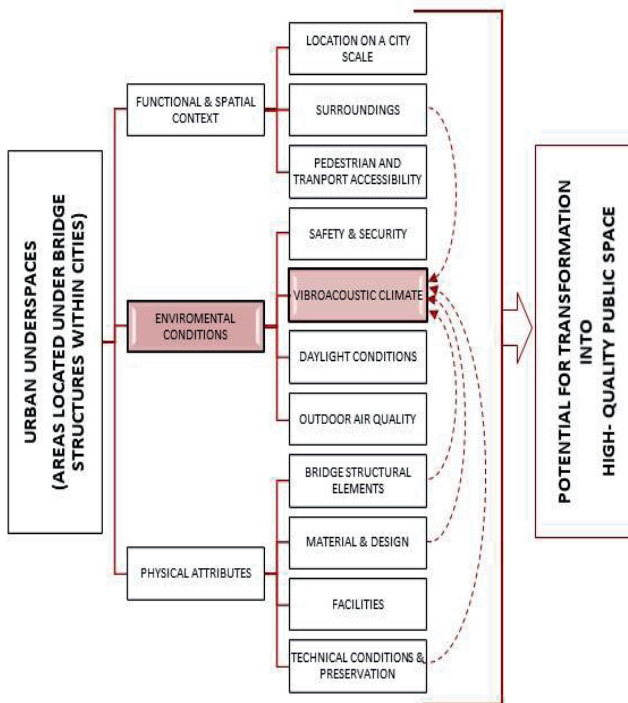
Fig. 1.   Scheme of the interdisciplinary research project focusing on examining to what extent an existing space under flyovers, viaducts, and bridges can be transformed into high-quality public space. Colour indicates the focus of the analysis presented in the article. *Source: authors' own elaboration*

The article presents a selected case study that represents the starting point for the wider research on the acoustic climate within urban areas located under bridges, viaducts, and flyovers. The presented study is to contribute to our general understanding of acoustic conditions of a general model of the bridge underspace. Therefore, the authors started the research by describing the model scheme of the propagation of sound waves and vibrations under elevated infrastructure. In further stages, data were collected by measuring noise levels and comparing

them with equivalent acceptable noise levels for the expected type of space development and Noise Rating curves. This allowed us to verify the relationship between the geometry of the bridge underspace and the noise levels, and assess the initial acoustic conditions in terms of possibilities of acoustic adaptation of the examined space for outdoor public events. The outcome of the presented research are also managerial recommendations in the form of hypotheses and preliminary assumptions for the planned further and broader studies of the issues raised in this article.

2. Background of the study

Nowadays there is a need to reclaim public space caused by the most contested issues in the contemporary transformation of public space: privatization, commercialization, and securitization [1]–[3]. Therefore, it is necessary to reclaim areas affected by motorized traffic (streets, rail and post-rail areas, transport nodes) located within the urbanized area and thus having high investment potential [4]–[7]. On the other hand, a possible resistance to use of spaces under a bridge for urban functions can be confronted with other current trends: the growing need for compact and sustainable cities [8] and urban regeneration of *terrain vague* areas where enclaves for social activities are increasingly created [9]. These types of urban transformations, also carried out in areas located under elevated transport routes, such as bridges, viaducts, and flyovers, can be a response to the deficit of social areas and the current crisis of traditional public space (Figure 2 and Figure 3). In this context, the hypothesis put forward by Komarzyńska-Świeściak [4] becomes even more valid, indicating an even greater need for interdisciplinary research on the adaptability of areas of transport conduits. *In urbanized areas of European cities, bridge underspace located under elevated transit infrastructure is subject to functional and spatial transformations that can contribute to the regeneration of these public spaces and boost their attractiveness*.

Fig. 2.   Manifesto Market Florence – temporary industrial-chic dining & drinking hub with more than 20 container stalls located under and nearby Wilsonova Flyover in Nové Město borough in Prague, 08.09.2019. *Source: author's Elżbieta Komarzyńska-Świeściak own photo archive*

Fig. 3.   Polish Bike Polo Championship organized within Temporary City Sports Centre – a recreation space arranged as a bottom-up initiative called #Project103 under the flyover of Turowicza Street in Kraków. The Centre is planned to be built in 2022 in the same location thanks to financing gained from the civic budget of the City of Kraków [10]. *Source: S. Barański*

Ensuring a sense of safety and physical and psychological well-being for users of the bridge underspace, as with any other public space, is an essential condition for its proper utilization. On the other hand, some of characteristics of this space may not only enhance or reduce the impact of negative factors such as crime or traffic noise, but also affect the personal feelings of the person under the overhead traffic route. These areas have important constraints in this regard, for instance, they are usually poorly connected with urban tissue and are located near traffic routes. At the same time, studies of the literature show the rich collection of the examples of use of spaces located under elevated transit infrastructure, and architects and urban designers consider these spaces to have the potential to transform into pleasant and lively urban areas. Furthermore, the topicality of the research problem is confirmed by the results of literature analysis and field studies on 60 cases of European implementations of bridge underspace conducted by Komarzyńska-Świeściak in 2009-2017 [4], [10]. These examples show that proper retrofitting reduces their frightening, cold, and dark image and allow people to use them. Therefore, there is a need for research focusing on the baseline environmental conditions of the bridge underspace and the available solutions available minimizing the negative effects of environmental factors on the health and well-being of their users.

3. The literature review

Although the last decade has witnessed an increase in research interest in the use of the bridge underspace, previous studies have failed to address in-depth studies of its environmental characteristics in light of its adaptive potential. The research shows that most of the literature has studied the transformation and utilization of the leftover space of overpasses from the perspective of an architect and urban planner, thus focusing mainly on land use and spatial forms. Moreover, these scientific works usually concern the analysis of the transformation of bridge underspace in certain geographical and cultural locations, e.g. Tokyo city [12]–[14] and Kuala Lumpur [15] or by limiting the analysis to a historical context [16]–[18]. The areas located under elevated transit infrastructure are also analyzed in publications on the interface between public spaces and transport routes [5], [19], [20] and on informal and bottom-up annexation of the city by local communities [21]. Furthermore, there are publications on the development of spaces under a bridge for green areas and landscape [22], [23]. However, most of the above-mentioned studies have overlooked environmental characteristics of the bridge underspace (e.g., acoustic climate, air quality, daylight access, health and safety issues) and their dependence from its unique spatial features, thus investigating whether they have potential to become safe and high-quality public spaces.

The study of the available literature shows that no comprehensive research has been conducted so far on the use of bridge underspace in the context of acoustics. Literature analysis shows that the published results of research on the vibroacoustic climate in such areas are very limited. There are publications devoted to the analysis of traffic noise at the level of the communication route [24], [25], [26], [27] but not of the areas below it (with the exception of cases where the route passes under a flyover, for example, [28]). On the other hand, there are studies on the noise generated by open-air concerts and events [29], [30], but there are no clear guidelines on the optimal vibration climate for such open-air activities. Furthermore, the available data on the acoustic maps are inaccurate in the context of the presented study, as the measurements of the acoustic maps are carried out at the level of the elevated transport route, not below it [31], [32]. For a newly-designed urban space, to the knowledge of the authors, there are currently no binding legal acts or recommendations, even in the form of standards or recommendations, which would explicitly specify criteria to assess the baseline situation regarding noise and vibration level in underspaces. Some issues related to noise protection are regulated in Directive 2002/49/EC [33], which specifies the allowable noise limit values in the environment. The areas for which the said acts set allowable noise limits include those intended for very vaguely defined recreational purposes. The authors of the article failed to find any publications in the literature review which would verify the acoustic climate in the bridge underspace exposed to the noise generated by the road traffic on a flyover. In the context of analyzing the usefulness of bridge underspace for creating recreational areas, the research presented below appears to be pioneering. Literature analysis, therefore, confirms that the issue is up-to-date and relevant and that attempts at finding solutions are needed.

Fig. 4.   Under The Bridge Music Festival organized annually under Ring 3 road flyover in the district Nydalen in the Nordre Aker borough in northern Oslo, 2019. *Source: Thomas Refvik / Very Agency*

Fig. 5.   A temporary cinema arranged for the community-engaging arts and culture event called Folly for a Flyover held in 2011 under the A12 flyover in the Hackney Wick area of London. *Source: Assemble Studio*

On the other hand, during research the authors noticed an increasing number of cases of use of bridge underspace for open-air concerts (e.g., 'Under The Bridge Music Festival'

annually organized at several locations: New York, London, and Oslo (Figure 4), an international project 'Play Me, I'm yours' realized under the Westway flyover in London, a series of trumpet concerts by Piotr Damasiewicz performed under various bridges in Wrocław (Figure 8), theatre performances (e.g. the musical of Daniel Ottsa "Paulinenbrücke" presented under the road flyover in Stuttgart, performances of the 'Cirque du Soleil' group under the highway flyover in Québec and cinemas (e.g., 'Folly for a Flyover' festival in Hackney Wick in the area of London (Figure 5), KinoMost Czerniakowski Cape under Łazienkowski Bridge in Warsaw). The organizers of these events often justify their choice of this particular location by the unique acoustic conditions created by the structural elements of the flyovers (bridge slab, pillars) and water surface [34], although this has not been confirmed by any professional acoustic measurements.

4. Materials and methods

In the current research, a pilot case study approach was used as the measurements were taken for a chosen space located under an elevated road representing certain criteria set by the researchers. The presented small-scale preliminary study was conducted to formulate hypotheses about acoustic climate of bridge underspace and to evaluate feasibility and improve the study design prior to implementation of a full-scale research project. As the well-known research of Hartley [35] and Yin [36], the purpose of a case study is not to bring about generalizable findings, but to add to the field by providing a comprehensive understanding of the studied phenomenon (see [37]). In this respect, though the small sample and the context-dependent nature (see [38] on case studies) of this research prevent generalization, it does contribute significantly to the creation of new knowledge on the acoustic climate of areas located under elevated roads in the context of adapting them for public space. The presented case can be also used as valuable input for further research on this topic. That is why, the study's context and sample, and data sources and analyses are discussed more in-depth.

The obtained noise levels measurements in selected points of the examined bridge underspace were compared with equivalent acceptable noise levels ($L_{A, eq}$) for the expected type of space development as defined in:

- WHO recommendations [39],
- regulations applicable in Poland [40].

The measurement results were also compared with NR (Noise Rating) curves, which define the maximum acceptable noise level in the given space. The family of NR curves was originally defined in ISO/R 1996:1971 [41] as the international standard for indicating acceptable sound levels within a space. NR curves are used in Europe, while the Noise Criterion (NC) family is more popular in the United States. Both curve families are used similarly and can be regarded as an interchangeable way of defining acceptable noise levels.

Interpretation of the results obtained at particular measurement points allowed us to verify the relationship between the geometry of the urban space under analysis (in particular: the location of the flyover deck in relation to the terrain and supporting elements) and the noise level. The obtained data allowed for assessing the initial acoustic conditions of a given space in terms of possibilities of acoustic adaptation of the examined space to serve selected functions. The analysis of the results also made it possible to determine the aims and scope of further research enabling detailed exploration of the issues raised in this article.

4.1. Noise level requirements

The negative context associated with spaces in the immediate vicinity of elevated transport routes includes traffic-related noise and the vibrations of a bridge. The awareness of their negative impact on human health (both physiological and mental), makes urban planners avoid constructing of residential buildings, especially for long-term stay, as well as public spaces in the immediate vicinity of traffic routes. Traffic noise, in the form of sounds of air of excessive intensity caused by the major routes crossing central urban areas, is emitted by many individual sources, and thus depends on several factors: traffic volumes, the share of noisy vehicles (rail vehicles, lorries, buses, motorcycles) and vehicles in poor technical condition, traffic smoothness, condition of the road surface and roadways. Noise in the form of material sounds moves directly from the route structure to the ground and structurally connected buildings, if adequate road insulation is not provided.

For the following discussion, it should be noted that in accordance with the applicable regulations and guidelines, noise levels in public recreational areas should be minimized.

According to the regulations in force in Poland [40], the permissible level of noise caused by the roads for recreational areas for a reference time interval of 8 hours equal to the least favourable hours on consecutive days, $L_{A,eq\,D}$, is 55 dB A.

The WHO recommendations [39] clearly indicate that in open spaces used by people, $L_{A,eq}$ noise level should not exceed 55 dB A, and it is recommended that the optimum noise limit is 50 dB. Detailed WHO recommendations state as follows:

1. The recommendations in Chapter 4.3.1 Dwellings [39] are as follows: "To protect the majority of people from being seriously annoyed during the daytime, the sound pressure level on balconies, terraces, and outdoor living areas should not exceed 55 dB $L_{A,eq}$ for a steady, continuous noise. To protect the majority of people from being moderately annoyed during the daytime, the outdoor sound pressure level should not exceed 50 dB $L_{A,eq}$". These values are based on annoyance studies, but most countries in Europe have adopted 40 dB $L_{A,eq}$ as the maximum allowable level for new developments [42]. Indeed, the lower value should be considered the maximum allowable sound pressure level for all new developments whenever feasible".

2. The recommendations in Chapter 4.3.2 Schools and preschools [39] are as follows: "For outdoor playgrounds (at schools and preschools – added by the authors), the sound pressure level of the noise from external sources should not exceed 55 dB $L_{A,eq}$, the same value given for outdoor residential areas in the daytime".

The literature broadly discusses the expectations concerning permissible noise levels for architectural indoor spaces intended for the organization of concerts and lectures. The requirements for such spaces are based on the use of the so-called Noise Rating curves (NR) which determine the maximum acceptable noise level in a given space. These curves are commonly used by event venue designers to set requirements for concert, theatre, studio spaces in Europe, e.g. [43]. For outdoor public spaces, noise requirements are determined by means of single figure coefficients such as $L_{A,eq}$. There are no guidelines for determining permissible noise by using noise curves in urban interiors. For this work, we used analogies with the requirements available in the specialist literature on event venues. The following recommendations can be found in these sources:

- indoor stadiums and gyms – NC/NR curve 40-55 [44],
- corridors, gyms NC/NR curve 35-45 – equivalent 45-55 dB A [45],
- swimming pools, sports arenas NC/NR curve 40-50 – equivalent 50-60 dB A [45].

Based on the above analysis of the cited literature, we assumed that for the purpose of adaptation to public recreational spaces, the following noise requirements should be met:

- noise level $L_{A,eq} \leq 55$ dB A,
- noise spectrum $\leq$ NR45.

4.2. Scheme of the survey site

To analyse the vibroacoustic climate of the theoretical bridge underspace model, the authors described and illustrated the sources of noise and traffic vibrations, as well as the propagation of acoustic waves under an elevated route (Figure 6) for an urban, bilaterally enclosed interior (the upper cover being a bridge and the lower being area beneath it). Such an interior cannot be completely isolated from the external environment, and the sound waves present there are subject to reflection, absorption, deflection, and interference. Common sources of interference associated with traffic noise and vibrations (identified by symbols $Z_1 - Z_3$) generate air and shock (so-called material) sounds together with vibrations that reach an area located below the elevated road, respectively, in the form of the following waves:

- direct airborne noise wave (Wda), caused by traffic on a bridge (Z_1 and Z_2 on Figure 6) or a road in the bridge underspace (Z_3 on Figure 6).
- reflected airborne noise wave (Wra), associated with a change of the direction of wave propagation, e.g., at the border with neighbouring buildings or structural elements (e.g., dilatation gaps in prefabricated constructions).
- partially absorbed airborne noise wave (Wpaa), for example thanks to green areas next to the road.
- direct structure-borne noise wave (Wd-sb), associated with structural vibrations caused by traffic on a bridge (Z_1 and Z_2 in Figure 6) (the so-called audible material sounds).
- direct vibration wave (Wdv), linked to vibrations from road traffic (especially due to heavy and rail vehicles) and causing vibrations directly in the structural elements of a bridge.
- lateral transmission of vibration wave (Wltv), linked to the spread of the above-mentioned vibrations and so-called lateral transmission to subsequent interconnected elements, e.g., supports, ground, and construction facilities set there.
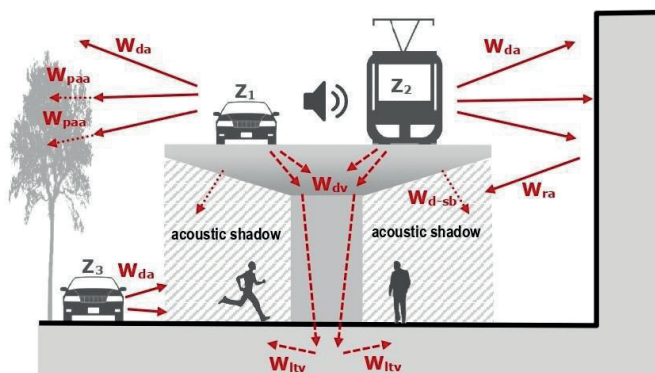

Fig. 6.   Model scheme of the propagation of sound waves and vibrations under elevated infrastructure, e.g. flyover (individual symbols explained in the text). *Source: authors' own elaboration*

In the presented diagram of sound wave and vibration propagation, it is a bridge plate that is of particular importance. Located between the source and receiver of the noise, it acts as a horizontal sound-reflecting screen, possibly partially absorbing air noise from road and rail traffic on a bridge (from source Z_1 and Z_2). This does not apply to shock sounds connected with vibrations generated directly in bridge structural components. In this case, the location under a bridge plate is a disadvantage because the vibration noise comes from the large effective radiation surface, which is bridge underside. In addition, as shown in [28], bridge underside greatly amplifies the noise due to reflection of the acoustic waves generated below the bridge underside. The reflection of the acoustic wave on the steel or concrete bridge underside not covered with any sound-absorbing materials can result in amplification of noise from side sources (Z3 in Figure 6) by up to 8 dB.

The theoretical bridge underspace model shows that the given starting conditions depend not only on the characteristics and location of the source of sound and vibrations but also on the environment and the urban and architectural elements. Therefore, when analyzing the bridge underspace for new investment in the existing condition, a detailed analysis seems desirable. Such an analysis was performed for a selected bridge underspace.

4.3. Survey site

For case analysis, we selected a bridge underspace with a high potential for adaptation for recreational purposes, i.e. one that:

- has no major traffic route in its vicinity (in order to avoid a reflection of sound from the bridge underside [28]),
- in its neighbourhood there are some recreational (the Odra River, HotSpot city beach, walking, and cycling areas), residential (Port Popowice estate), as well as non-invasive services (indoor Orbita – WCT Spartan skating ring and the Orbita three-star hotel), which all indicate high investment potential of the plot,
- has a continuous/solid (without holes) bridge plate – shielding is provided,
- the existing land use under the bridge is not in the conflict with potential adaptation, and the land topography is even favourable to adaptation to, for example, the audience area (sloping ground),
- the geometry and size of the analyzed area allow for potential adaptation.
- the space has been already used for various outdoor social activities, e.g. movie making (Figure 7) and concerts (trumpet player Piotr Damasiewicz recorded a jazz song under Milenijny Bridge among many others Wrocław bridges, Figure 8).

Fig. 7.   Movie makers working on a video clip in the surroundings of the flyover construction elements in the area of the study. Milenijny Bridge (left-bank flyover) – span № 8, between 8th axis and Odra river bank, 20.11.2020. *Source: author's Elżbieta Komarzyńska-Świeściak own photo archive*

Fig. 8.   The Sound of Wrocław Bridges – one of the trumpet concerts of Piotr Damasiewicz recorded on 25th of February 2021 under Rędziński Bridge. *Source: Adam Skórzewski and Tomasz Parużyński Musiał*

The authors examined a stretch of about 25 m and about 90 m located under the left bank overpass of the Milenijny bridge (2 pylons in total) (Figure 9, Figure 10). The bridge structure is a reinforced concrete plate based on pairs of reinforced concrete pillars. The bridge has a bar support system and is placed on supports. The support on the pillars uses bearings and vibration isolators to prevent the transmission of vibrations to the pillars. On the 25.12 m wide bridge, there are two carriageways (with the width of 7 m each), two bicycle paths (with the width of 1.5 m each), and two pedestrian sidewalks (with the width of 2 m each) [46] (Figure 11).

Fig. 9.   Photos of the examined area. Milenijny Bridge (left-bank flyover) – crossing over the Odra River with access roads as part of the city-centre bypass, the section from Legnicka Street to Osobowicka Street, Wroclaw – span № 7, between 7th and 8th axis – measurement axis #2. *Source: author's Elżbieta Komarzyńska-Świeściak own photo archive*

Fig. 10.   Photos of the examined area. Milenijny Bridge (left-bank flyover) – crossing over the Odra River with access roads as part of the city-centre bypass, the section from Legnicka Streer to Osobowicka Street, Wroclaw – span № 6, between 6th and 7th axis – measurement axis #1. *Source: author's Elżbieta Komarzyńska-Świeściak own photo archive*

Fig. 11.   The examined area – bird's eye view. Milenijny Bridge (left-bank flyover) – crossing over the Odra River with access roads as part of the city-centre bypass. Section from Legnicka Street to Osobowicka Street, Wroclaw. *Source: authors' own elaboration*

4.4. Research description

The following schedule has been adopted for this research:

1. Specification of the selection criteria and selection of test facility.

2. Analysis of the design documentation of the selected test facility.

3. A preparatory session, during which test measurements were performed to determine the research plan.

4. A proper measurement session, the results of which are given in the text below.

Specialized vibration isolation solutions such as bearings, vibration pads, etc. are used for the flyover located over the analyzed area [46]. During the preparatory session, the authors confirmed that vibration insulation of the flyover structure works as intended so that no noticeable vibration of the flyover poles up to 2 m from the ground level was detected. Based on this preliminary test, the authors decided not to carry out vibration tests for the test facility, because they were virtually absent there.

During the measurements, sound levels were measured as broadband and for terce bands (1/3 of an octave). In all the cases, equivalent values measured for 10 minutes are given. The measurements taken during the preparation session confirmed that an increase in the measurement time of more than 10 minutes does not result in noticeable changes in the results obtained.

During the preparatory session, the authors noted that the predominant noise component in the examined space under the flyover is the noise caused by road traffic on four lanes on the flyover. The effect on the results of minor traffic on local roads located on the ground near measuring axis #1 is negligible. However, the authors noted that intensification of noisy works in the nearby residential construction site resulted in an increase in noise measured in the examined space under the flyover. Even though there is a greater distance from the test area to the construction site than to the carriageways, where the dominant component noise component was generated, the incidental noise from the construction site was clearly perceived. This is because of reflection of sound waves on the underside of the flyover; a similar situation was described by Chi-Chwen et al. [28]. During the proper measurement session, the authors avoided taking measurements during the incidental increase in noise levels from the site. Thus, the presented results can be considered as relating mainly to noise caused by road traffic on the flyover.

There are no elements on the bridge that could absorb noise; for example, green belts. The analyzed area under the flyover is partially green and partially paved. On the sides of the flyover, there are some individual trees in a number and distance virtually excluding their influence on the acoustic environment beneath the flyover. There are no buildings in the vicinity of the test areas which should be considered as elements that reflect the acoustic waves generated on the flyover. After considering the structure and surroundings of the analyzed facility, the authors were able to adopt a simplified model for the propagation of noise in the bridge underspace shown in Figure 12.
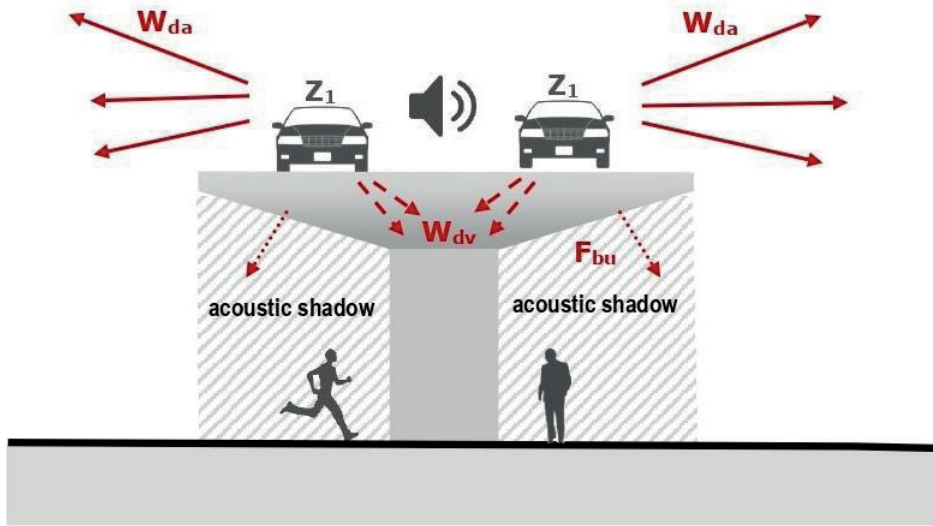
Fig. 12. Model scheme of the propagation of sound waves and vibrations in the area of the study – Milenijny Bridge (left-bank flyover) – crossing over the Odra River with access roads as part of the city-centre bypass, the section from Legnicka Street to Osobowicka Street, Wroclaw. *Source: authors' own elaboration*

In the test area shown in Figure 11, four measuring axes (#1 – #4) with four measurement points each were selected. The location of the axes and the individual measurement points are shown in the projection presented in Figure 13.

For axes #1 – #3, the location of the individual measurement points is determined as in the following diagram, where * is the axis number:

- points with an R*.1 index were on the axis of the entire flyover,
- points R*.2 were located under the carriageway axis,
- points R*.3 were located under the flyover edge,
- points R*.4 were located outside the flyover at a distance from the R*.3 point (flyover edge) equal to the distance between the R*.1 points (flyover axis) – R*.3 (flyover edge).

This arrangement scheme was chosen to check the effect of shielding traffic noise by the flyover. A comparison of the measurement results for individual points within a single axis provides an answer to the question whether the location of new functions of the bridge underspace is sensible from the point of view of protection from the road noise point resulting from the traffic on the flyover.
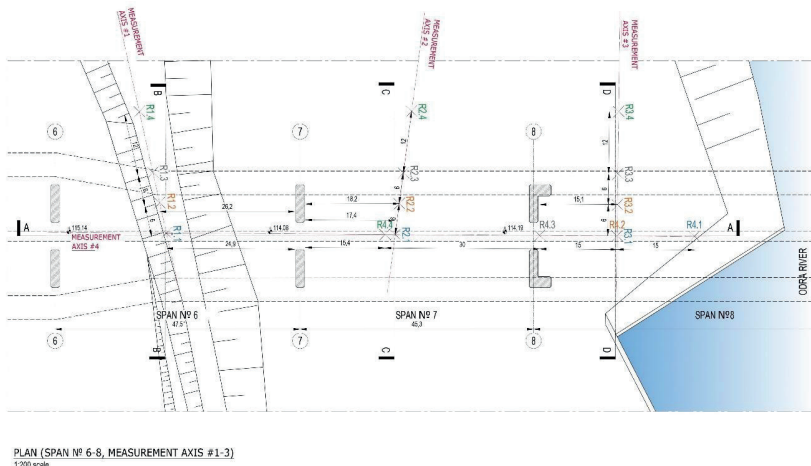
Fig. 13. The area of the study – plan. Milenijny Bridge (left-bank flyover) – crossing over the Odra River with access roads as a part of the city-centre bypass. Section from Legnicka Street to Osobowicka Street, Wroclaw. *Source: authors' own elaboration, based on* [46]

The measurement axis #1 was drawn along a paved walking/cycling path passing almost perpendicular to the flyover axis (Figure 14). In this case, from all the measurements made the flyover underside was closest to the measuring microphones. For the R1.1 and R1.3 points, the flyover underside was 5.8 m above the path, whereas for the R1.2 point, it was 3.5 m above the path. This means that the measuring points were placed 4.3 m and 2 m under the flyover respectively.

The measurement axis #2 has been positioned between the successive flyover supports on unpaved ground (Figure 15). In this axis, the flyover was higher over the ground than in the case with measurement axis #1. The distance between the ground and the concrete flyover underside was 8.5 m for points R2.1 and R2.3 and 6.2 m for point R2.2, which yields the distance of the measuring microphones from the flyover underside of respectively 7 m and 4.7 m.

The measurement axis #3 was placed between the river banks and the subsequent flyover supports (Figure 16). In this place, the ground is paved with concrete slabs typical for construction sites. For this axis, the distance from the flyover underside to the ground was the largest of all the measurement axes and it was 9 m. This means that the distance from the flyover underside to the measuring microphones was 7.5 m.

The differences in location of measurement axes #1 – #3 were intended to verify the effect of the distance between the ground and the flyover underside on the resultant noise level. In addition, with such an arrangement of measurement axes, it was possible to determine whether, for the examined flyover, the noise level depends on the ground material (the cobbled pavement near the lawn and cobbled parking lot, unpaved ground, extensive ground paved with concrete slabs in the vicinity of the river).

The measurement axis #4 is located below the flyover central line (Figure 17). The R4.1 point was located near the edge, 30 m from the nearest pylon. The R4.3 point was in the immediate vicinity of the flyover supports. The R4.4 point was in two-thirds of the distance between successive supports, i.e. 30 m from one support and 15 m from

the next one. The location of the measurement points on axis #4 was intended to check whether for the tested flyover the noise level or its spectrum differs as a function of distance from the river and coming closer to the structural supports. For axis #4, for the individual measurement points the distance from the flyover bottom to the ground in the case of axis #4 was as follows: R4.1 – 9.1 m, R4.2 – 9 m, R4.3 – 9.1 m, R4.4 – 8.7 m; thus, the distance between the flyover bottom and microphones was 7.6 m, 7.5 m, 7.6 m and 7.2 m respectively.

Fig. 14. Axis #1 was placed along the pavement located on the slope in the area of the paved parking area and the lawn located below. *Source: author's Piotr Kozłowski own photo archive*

Fig. 15. Axis #2 was placed on unpaved ground (below the slope). *Source: author's Piotr Kozłowski own photo archive*

Fig. 16.   Axis #3 was placed near the river bank on the area paved with concrete slabs (below the slope). *Source: author's Piotr Kozłowski own photo archive*

Fig. 17.   Axis #4 was placed along the flyover partly on unpaved ground and on ground paved with concrete slabs. *Source: author's Piotr Kozłowski own photo archive*

The Svan971, Svan945A, and Svan979 sound meters were used for the tests. All meters were calibrated using the factory calibrators included in each of the measurement sets. The

calibration was made before and directly after completing the measurements. Calibration corrections are included in the presented results. The meters have been placed on independent tripods in such a way that the measuring microphones were 150 cm above the ground, which means that the measurement situation corresponded to a standing eye level. All meters were battery-powered. The distances between the measurement points and the flyover elements were measured using a laser distance meter and measuring tape.

The tests were conducted during the morning rush hours on a working day to verify the acoustic conditions of the chosen location in the worst possible conditions when the highest possible noise levels may occur. Measurements started at 07:00 a.m. Measurement series for measurement axis #1 was performed first. Then, the authors proceeded to the series of measurements for axis #2, #3, and #4. After that, a second series of measurements for all axes #1 – #4 were performed. Finally, the third series of measurements was performed for all axes #1 – #4. This test schedule allowed for even allocation of top traffic intensity periods, i.e. just after 7 a.m., and lower traffic intensity periods, i.e. time before 11 a.m., among the measurement axes.

5. Results

The maximum difference in the equivalent $L_{A, eq}$ values measured in successive series at the same measurement points do not exceed 3 dB. This means for the test area under the flyover of the city bypass that stable noise conditions occur from morning to noon. Due to small differences observed between the results obtained in each measurement series, the authors decided not to include all the partial results for each series separately here, but to use the final results, which are the averages of all series. The values shown in the diagrams below were obtained by averaging the measurement results for each measuring point and each terce band independently. The equivalent broadband sound levels $L_{A, eq}$ presented here are also the result of energy averaging of the values indicated by the sound meters in subsequent measurement series.

As already mentioned earlier on the basis of literature studies, the authors assumed that the maximum permissible noise in the test space, after adaptation for public recreational purposes, expressed as a single-figure factor should not exceed $L_{A,eq} = 55$ dB a, while the determined noise curve should meet the NR45 criterion.

Figure 18 and Figure 19 present sectional views of measurement axes #1 – #4 with the $L_{A, eq}$ values at individual measurement points. This visualization allows us to easily link the results obtained to the location of the measured noise levels.

Analysis of the results presented in Figure 18 and Figure 19 shows that no significant increase in noise levels was observed at measurement points extended under the flyover. This proves that the phenomenon of wave deflection at the flyover edge is not strong enough to limit new functions of the tested bridge underspace only to the surface located directly under the bridges. Moreover, no clear differences of the noise levels measured were found in the test areas under the central line of the flyover and those clearly extending under the flyover. Only for axis #3 the authors noticed an increase of 4 dB of noise for the measurement point located outside the direct flyover underspace. For axis #3, it is rather the effect of lack of noise attenuation by the ground due to large surface paved with concrete plates and the greatest distance from the measurement points to the flyover underside.

For axis #1, the differences in noise levels measured at each point do not exceed 1 dB, which is the greatest level of noise alignment in these measurements. This may be because the #1 axis has the smallest distance between the measurement microphones and the flyover underside.

Analysis of the graphs shown in Figure 18 and Figure 19 indicates that measured $L_{A, eq}$ values range from 62 to 69 dB A, which means that noise in the test space exceeds recommendations and requirements by 7 to 14 dB in a broadband.

It is worth mentioning that the highest levels were recorded in two cases:

- when point R3.4 was above the ground paved with concrete plates at the greatest distance from the bridge plate,
- when point R4.3 was very close to the concrete pillars reflecting acoustic waves.

In Figure 26 it can be seen that point R4.3 is characterized by a clear increase in noise level at frequencies above 2 kHz.

In other words, local increase of noise level is expected in areas in vicinity of large reflective concrete surfaces. This, in turn, confirms the justness of the following actions:

- assembly of broadband sound-absorbing systems on sound-reflecting components such as pillars and flyover underside,
- avoiding, as much as possible, ground pavement in areas where this is not necessary due to functional requirements.
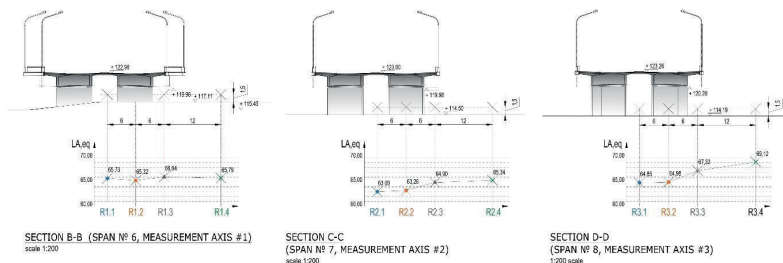
Fig. 18. Cross-sections compiled with graphs illustrating the $L_{A,eq}$ parameter (equivalent SPL A-weighted) obtained at each measurement point: A. Cross-section B-B compiled with averaged results of three measurement sessions on axis #1. B. Cross-section C-C compared with averaged results of three measurement sessions on axis #2. C. Cross-section D-D illustrated with averaged results of three sessions on axis #3. *Source: authors' own elaboration based on* [46]
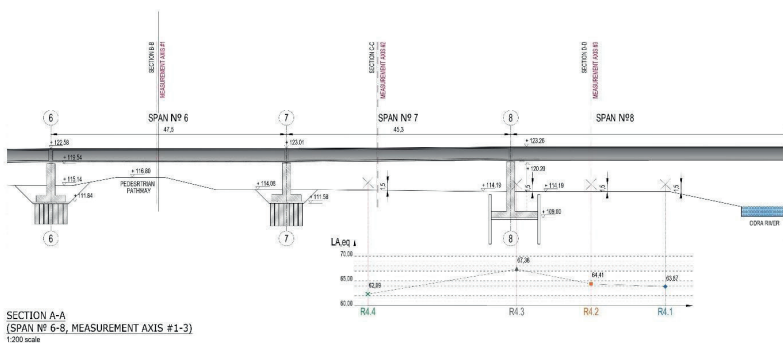

Fig. 19. Longitudinal section A-A compiled with a graph illustrating the $L_{A,eq}$ parameter (equivalent SPL A-weighted) obtained as an averaging of the values measured in the three sessions at individual measurement points R4.1-R4.4. *Source: authors' own elaboration based on* [46]

Figure 20, Figure 22, Figure 24 and Figure 26 present noise spectra for all the Rx.1 – Rx.4 measurement points on the individual #1 – #4 measurement axes. Such presentation of the results makes it possible to check which spectral differences occurred between the individual measurement points.

The graphs shown in Figure 21, Figure 23, Figure 25, and Figure 27 presenting the averaged characteristics of frequency for all the four points of a given measurement axis compared with the lowest NR noise curve met by the background noise determined in this way and the NR45 curve. Such presentation of data allows for clear visualization of what noise conditions expressed by NR curves can be currently found in the test location and what noise reduction measures should be taken to meet the requirement defined in NR45.

Fig. 20.   Results of measurements taken at every measurement point (R1.1 – R1.4) at axis #1. Equivalent value (10 minutes) of SPL A-weighted $L_{A, eq}$ in the function of frequency f. *Source: authors' own elaboration*

For axis #1, not only the single-figure $L_{A, eq}$ levels but also the noise spectrum proved to be very similar for all the measurement points (R1.1 – R1.4). Figure 11 indicates that the noise level for this axis is exceeded by 11 dB A. Figure 21 shows that the limit values are exceeded for octave bands over 125 Hz. Relatively smallest exceedance of noise limits occurs for frequency band 1/1 octave, 8 kHz. Significant noise exceedances were recorded for the 250 Hz to 4 kHz bands, with a maximum of 1 kHz octave, resulting in the noise on the #1 axis being finally described by the NR56 curve, which is 11 dB higher than the allowable limit.

Fig. 21.   Mean value SPL A weighted $L_{A,eq}$ at axis #1 in the function of frequency vs NR56 and NR45 curves. *Source: authors' own elaboration*
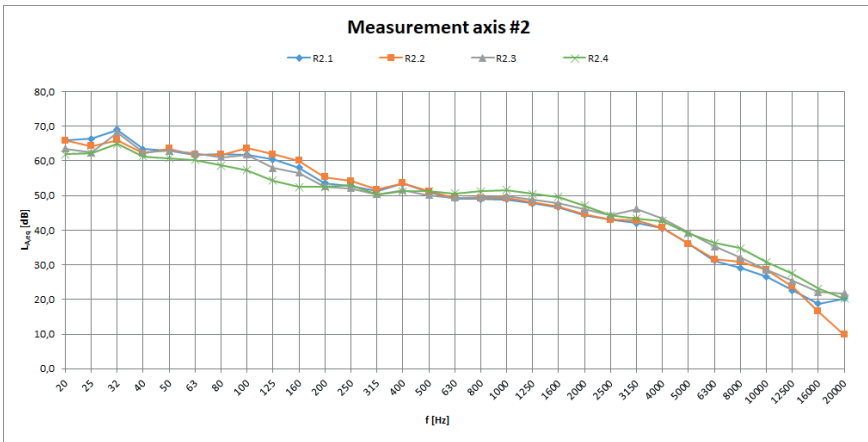
Fig. 22.   Results of measurements done at every measurement point (R2.1 – R2.4) at axis #2. Equivalent value (10 minutes) of SPL A weighted $L_{A,eq}$ in the function of frequency f. *Source: authors' own elaboration*

For the #2 axis, the difference between the single-digit noise level values $L_{A,eq}$ (Fig. 11) for individual points does not exceed 2.5 dB A. This is mainly due to differences in medium and high frequencies (Figure 22). The exceedance of the permissible level the single-digit $L_{A,eq}$ value is 10 dB A. The noise measured in this axis does not exceed the NR 55 curve. No exceedances were observed for octaves 31, 63, and 8 000 Hz.

Fig. 23.   Mean value SPL A weighted $L_{A, eq}$ at axis #2 in the function of frequency vs NR55 and NR45 curves. *Source: authors' own elaboration*
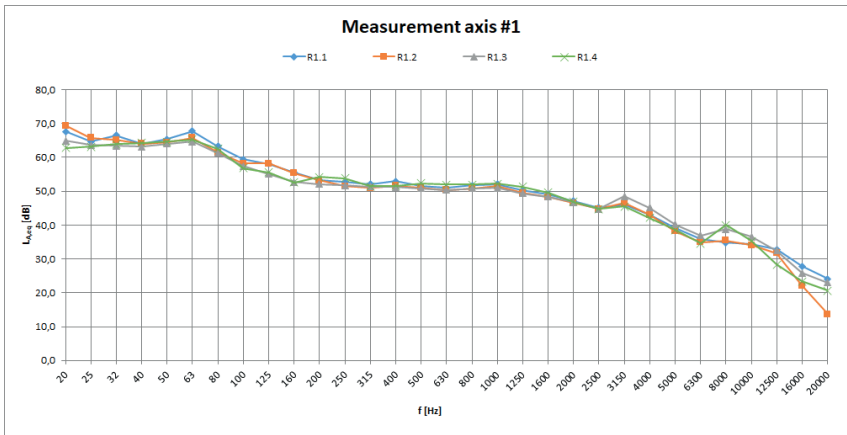

Fig. 24.   Results of measurements done at every measurement point (R3.1 – R3.4) at axis #3. Equivalent value (10 minutes) of SPL A weighted $L_{A, eq}$ in the function of frequency f. *Source: authors' own elaboration*

As already stated above, for the measurement axis #3 top noise level of $L_{A, eq}$=69.12 dB A was recorded for point R3.4, which, as shown in Figure 24, results from higher levels for medium and high frequencies. Finally, this also results in the highest NR57 noise curve in the whole research. If for the axis #3, the authors limit the analysis exclusively to the points under the flyover of its edge, then the single-digit $L_{A, eq}$ limit value would be exceeded by 12.32 dB but the averaged noise measured in three points on the R3.1 to R3.3 axes would still be described by the NR57 noise curve. Thus, for this axis, the noise requirements are exceeded by 12 dB A.
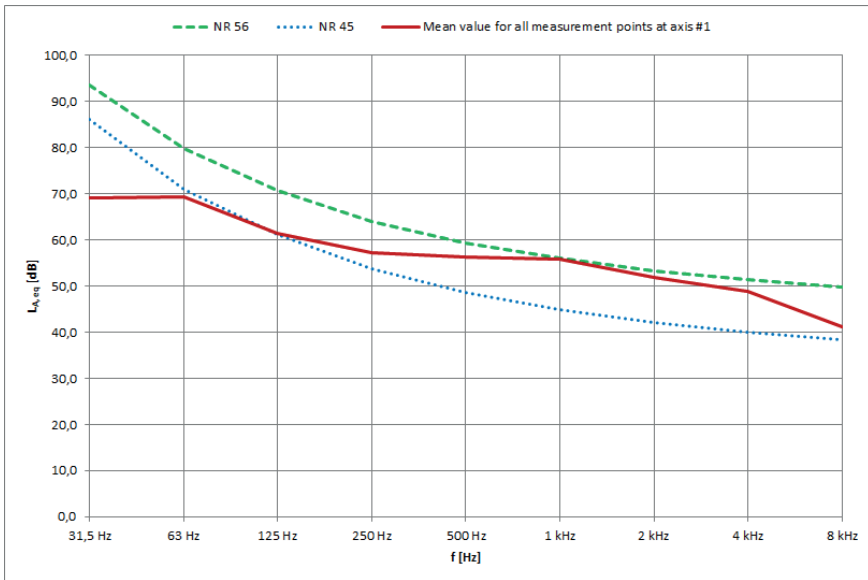
Fig. 25. Mean value SPL A-weighted $L_{A,\,eq}$ at axis #3 in the function of frequency vs NR57 and NR45 curves. *Source: authors' own elaboration*

As already noted, when analyzing Figure 19, for point R4.3 the noise level was much higher than for the other measurement points on this axis. The noise frequency characteristics presented in Figure 26 indicate that noise levels mainly increased in the high-frequency range. This is due to the proximity of large concrete pillars, which reflect sound waves, as already mentioned. The average noise spectrum on the #4 axis did not exceed the NR54 noise curve (Figure 27). The NR45 curve was exceeded for the octave bands from 125 Hz to 8 kHz.

Fig. 26. Results of measurements taken at every measurement point (R4.1 – R4.4) at axis #4. Equivalent value (10 minutes) of SPL A weighted $L_{A,\,eq}$ in the function of frequency f. *Source: authors' own elaboration*
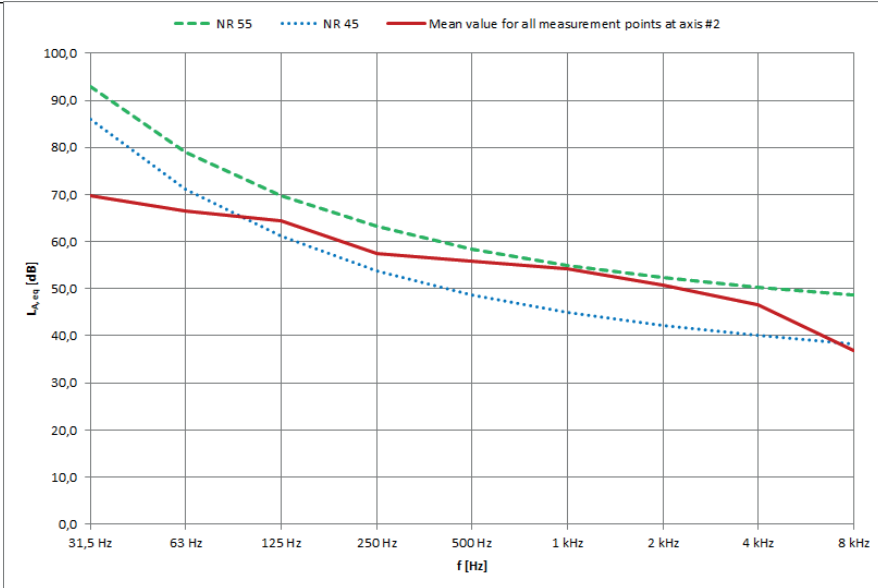
Fig. 27.   Mean value SPL A weighted $L_{A, eq}$ at axis #4 in the function of frequency vs NR54 and NR45 curves.
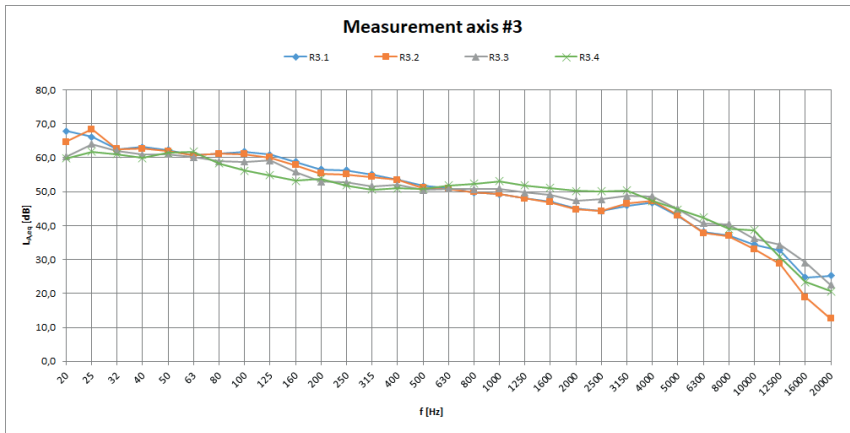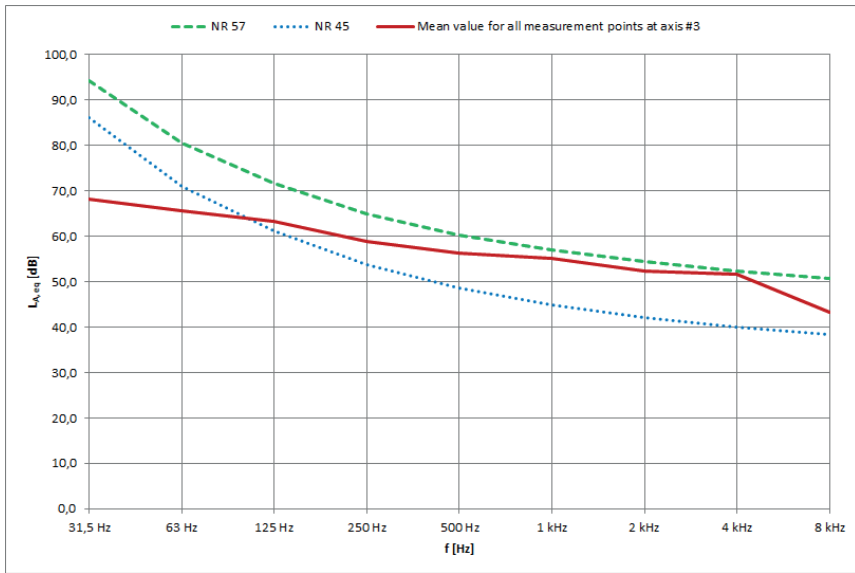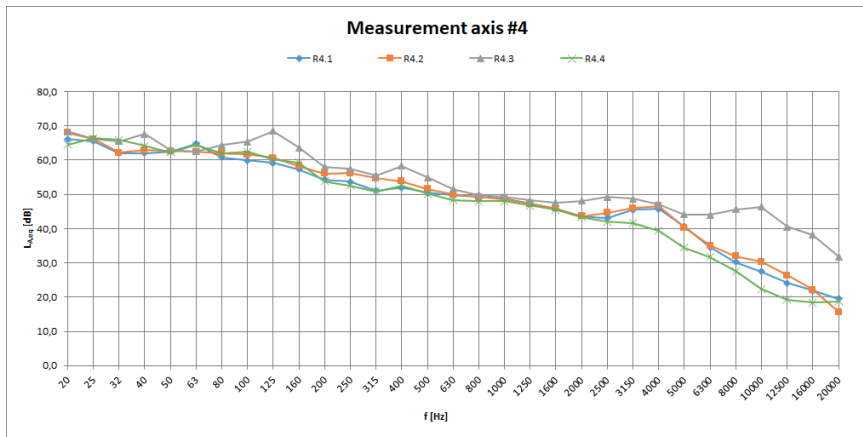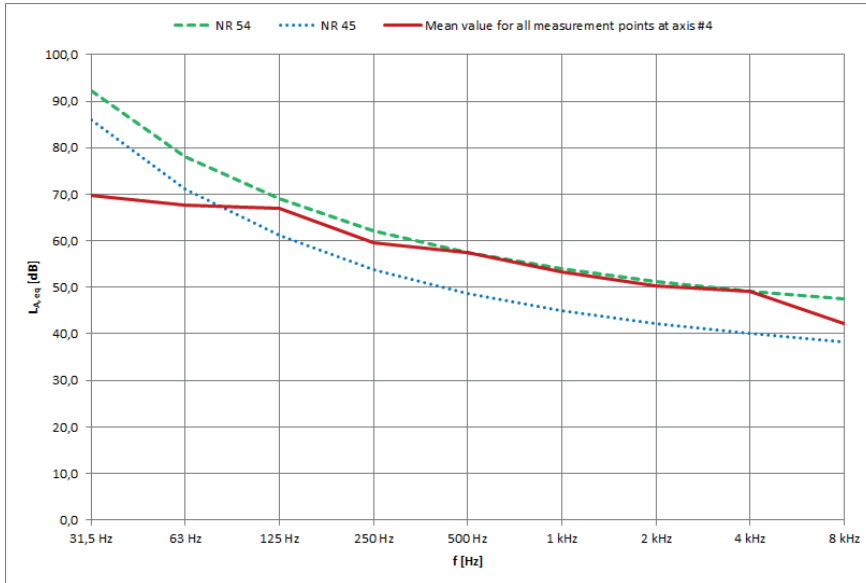*Source: authors' own elaboration*

6. Discussion

The presented research differs significantly from previous studies on the use of bridge underspace as it is a multidisciplinary approach that brings together the research and design experience of acousticians and architects. Most researchers examining the utilization of the leftover spaces of overpasses focus mainly on land use and spatial forms [12] – [23]. None of them address the initial acoustic conditions of a given space in terms of possibilities of acoustic adaptation for outdoor public events. Therefore, this study appears to be the first to conduct research on the use of bridge underspace in the context of acoustics. The presented findings add substantially to our understanding of initial acoustic conditions of a general model of the bridge underspace, e.g. relationship between the geometry of the urban bridge underspace and the noise levels. The situation widely regulated and analysed is the case of traffic noise generated at the level of a communication route [24] – [27] and [31], [32]. However, this work offers one of the first investigations devoted to analyzing the impact of traffic noise on an overpass on the areas below it. Thus, the authors had to come up with their own method of assessment of the acoustic conditions of the examined bridge underspace as there are currently no binding legal acts or recommendations, which would explicitly specify criteria to assess the baseline situation regarding noise levels within it. For this reason, both equivalent acceptable noise levels (defined for recreational spaces in WHO recommendations [39] and Polish regulations [40]), as well as the family of NR (defined in ISO/R 1996:1971 [41]) were compared with noise levels measured at selected points of the examined bridge underspace.

As discussed in the Literature Review chapter, it was discovered that the only study focusing on acoustic climate of bridge underspace is the research reported by Chi-Chwen et al. [28]. However, it has totally different assumptions. While Chi-Chwen et al. examine only the effects of noise coming from the nearby major traffic route reflected on the overpass underside, our aim was to examine general acoustic climate of the space located under an overpass in

order to assess the possibility of adapting them for outdoor public events. In order to avoid a reflection of traffic noise on the overpass underside and at the same time to distinguish the study from the one mentioned above [28] the chosen site for the study didn't have major traffic route in its vicinity, except the one located on the flyover.

Given these points, comparing to earlier findings, this research appears to be pioneering and the results can be used as valuable input for further studies on this topic.

6.1. Managerial recommendations

Summing up, the results allow to make the following preliminary assumptions for the planned further studies on the revitalization possibilities of bridge underspaces:

1. Noise limit values are generally not exceeded for low-frequency ranges, which makes the expected noise reduction achievable.

2. In the medium to high-frequency range noise limits are mostly exceeded in the 125 Hz to 4 kHz band.

3. The vertical and horizontal reflecting surfaces should be covered with materials with possibly high sound absorption coefficient for medium and high frequencies. Ideally, these should be solutions in the acoustic absorption class A.

4. In the research area, noise limit values were not exceeded by more than 12 dB A. This allows us to assume that it is possible to reduce noise levels as much as to meet the requirements for recreational and sports spaces.

5. It is advisable to minimize the number of paved surfaces and thus maximize the amount of unpaved and maximally green surfaces.

6. Areas for which the distance between the flyover underside and the ground is smaller are likely to exhibit lower noise levels than those spaces where this distance is greater, provided that the volume of traffic, and thus the source of noise is the same and the spatial conditions on the flyover sides are also the same.

In subsequent research the authors plan to verify the following solutions and hypotheses:

7. Creation of vertical screens for noise reduction that would cut off the space beneath the flyover to improve the acoustic conditions of such enclosed bridge subspaces, in particular:

   a. Reduction of noise levels to the required values.

   b. Reduction of reverberation time.

   c. Increase in the speech intelligibility factor.

8. Verification of the relationship between noise reduction efficiency in the bridge underspace as a result of introducing acoustic noise barriers compared to introducing noise-absorbing elements.

9. Verification of the conclusions presented above with other bridge underspaces.

The analysis of acoustic climate in bridge underspaces shows that the given starting conditions depend not only on the characteristics and location of the source of sound and vibrations, but also on the environment and the urban and architectural elements. Therefore, when analyzing the bridge underspace for a new investment in the existing condition, a detailed analysis seems desirable. It may include the following elements:

- field measurements of the so-called background noise to identify the physical acoustic properties of a given area,
- checking the location of noise sources in a given area, for example by using an acoustic camera,
- field measurements of ground vibrations at a planned investment site (especially in the vicinity of rail routes) using an accelerometer (acceleration/vibration sensor); the so-called vibration diagnostics,
- analysis of the results obtained.

From the acoustic point of view, bridge underspace would be analyzed differently, depending on the intended use; whether it will be developed or used as open space. Due to the acoustic characteristics, the bridge underspace not limited by any barrier is a limited built urban space (with the upper limit being the bridge and the lower limit being surface area beneath it), whereas in design practice (excluding the very peculiar case of an outdoor theatre) the sole aim is to reduce noise and vibration levels. Such an interior should not be completely isolated from the environment. However, when designing entirely enclosed spaces, the researchers are dealing with an architectural and construction interior; therefore, they should seek to achieve specific vibro-acoustic conditions by isolating it from ambient noise and vibrations, as well as appropriate interior acoustics parameters resulting mostly from the interior shape, dimensions, and finish. Both the presented variants of the acoustic modernization and spatial transformation of the bridge underspace will be subject to further research.

7. Conclusions

The research resulted in gathering unique data from the pilot case study examining the noise conditions under the flyover resulting from road traffic taking place on chosen flyover of Milenijny Bridge crossing over the Odra River in Wrocław. Taken together, these findings are basis for formulating hypotheses and preliminary assumptions for the planned further and broader studies on the revitalization possibilities of bridge underspaces. The conclusions that could have been drawn from the analysis of these results allow us to make more detailed assumptions for creating public spaces in bridge underspace that meet noise requirements for recreational and sports venues, or a local agora. The results of this study already show that on the basis of the presented measurement data, it is possible to assess the plausibility of such kind of investment and to select an optimal location for them and a form and functional program of the planned facility, and to propose optimal noise and anti-vibration safeguards.

References

[1]   Bibri S.E., Krogstie J., Kärrholm M., "Compact city planning and development: Emerging practices and strategies for achieving the goals of sustainability", *Developments in the Built Environment*, vol. 4, 100021, 2020. https://doi.org/10.1016/j.dibe.2020.100021

[2]   Bodnar J., "Reclaiming public space", *Urban Studies*, vol. 52(12), 2015, pp. 2090-2104. https://doi.org/10.1177%2F0042098015583626

[3]   Barron P. and Mariani M., *Terrain Vague: Interstices at the Edge of the Pale*. London: Routledge, 2013.

[4]   Komarzyńska-Świeściak E., *Conditions and forms of activation of spaces located under elevated transport routes at the turn of the 20th and 21st centuries*. Wrocław: Oficyna Wydawnicza Politechniki Wrocławskiej, typescript, in press.

[5]   Bauer C. et al., *Under the elevated.* New York: Design Trust for Public Space, 2015.

[6]   Chohan A.H., "Infrastructure Development and Implication of Negative Spaces in City Centers", GSTF Journal of Engineering Technology, 3: (1), 2014, pp. 53-60. http:// doi. org/10.5176/2251-3701_3.1.110

[7]   Duarte, G. "Infrascapes: Interstitial Enclaves of the Unplanned", in *306090 09: regarding public space*, eds. Lyster C. et al.., New York: Princeton Architectural Press, 2006, pp. 72-79.

[8]   Saaty T.L., De Paola P., "Rethinking Design and Urban Planning for the Cities of the Future", *Buildings*, 2017, vol. 7, 76. https://doi.org/10.3390/buildings7030076

[9]   Barron P., Mariani, M., *Terrain Vague: Interstices at the Edge of the Pale*. London: Routledge, 2013.

[10] Barański S., „Projekt 103", photography. Availble: https://www.facebook.com/projekt103/photos/ pcb.1826727410805002/1826727207471689/ [Accessed: 30 Oct 2021]

[11] Komarzyńska-Świeściak E., Kirschke P., "The issue of integration of elevated transport routes in the areas of historic polish cities. Example of the modernization of a cross-city railway line in the Śródmieście district of Kraków", *Technical Transactions,* 2019, vol. 10, pp. 35-58. https://doi.org/ 10.4467/2353737xct.19.106.11030

[12] Sheng J., Xu H., Zheng J., Luo M.,Zhou X., "Commercial Value Assessment of "Grey Space" under Overpasses: Analytic Hierarchy Process", *Advances in Civil Engineering*, vol. 2018, Article ID 4970697, 2018. https://doi.org/10.1155/2018/4970697

[13] Weize X., "The Bottom Space Usage Model And Characteristic Of Tokyo's Viaduct", *Planners*, vol. 33, 2017, pp. 101-105.

[14] Snapir A., *A research on the inhabited viaduct architecture in Tokio. Focusing on its contribution to the vitality of the city centre*. Tokyo: University of Tokyo, 2012.

[15] Qamaruz-Zaman, N., Samadi Z. and Azhari N. Opportunity in Leftover Spaces: Activities Under the Flyovers of Kuala Lumpur. *Procedia – Social and Behavioral Sciences*. 68. pp. 451–463. 10.1016/j.sbspro.2012.12.241. 2012.

[16] Murray P. and Stevens M., *Living bridges: Inhabited Bridge – Past, Present and Future*. Londyn: Prestel, 1996.

[17] Piekarski J., *Living Bridges.* Warszawa: Związek Mostowców Rzeczypospolitej Polskiej, 2007.

[18] Wesołowski J., *Railway in the urban space – problems of integration*. Gliwice: Silesian University of Technology, 1997.

[19] Hauck Th., Keller R., Kleinekort V. (eds.), *Infrastructural Urbanism. Addressing the In-between*. Berlin: DOM publishers, 2011, pp. 93-108.

[20] Crisman P., "Interstices: Appropriation of Transportation Infrastructure in the Post-Industrial City", in *Heteropolis: Immigration, Ethnicity and the American City*, ed. Wells-Bowie L., Washington: ACSA Press, 2000, pp. 74-80.

[21] Duarte G., "Infrascapes: Interstitial Enclaves of the Unplanned", in *Tom 306090 09: regarding public space*, eds. Benites C. et al., New York: Princeton Architectural Press, 2005, pp. 72-79.

[22] Buchner A., *Bridge routes in the cityscape*. Warsaw-Łódź: Wydawnictwo Naukowe PWN, 1982.

[23] Łapko A., "Functional transformation of bridges and other engineering structures", *Technical Transactions,* vol. 15, 2010, pp. 235.

[24] Jagniatinskis A. et al., "Annual Assessment of Noise Generated by Road Traffic using Measurements", *Procedia Engineering*, vol. 187, 2017, pp. 614-619. https://doi.org/10.1016/j. proeng.2017.04.421

[25] Bohatkiewicz J., "Protection against traffic noise in urban areas in relation to noise control plans", *Budownictwo i Architektura*, vol. 13(4), 2014, pp. 075-082. https://doi.org/10.35784/ bud-arch.1708

[26] Motylewicz, M. and Gardziejczyk, W. (2014) "Road traffic noise in areas surrounding intersections", *Budownictwo i Architektura*, vol. 13(1), 2014, pp. 137-147. https://doi.org/10.35784/bud-arch.1934

[27] Nurzyński J., "Acoustical assessment of urban residential environment", *Budownictwo i Architektura*, vol. 13(4), 2014, pp. 033-040. https://doi.org/10.35784/bud-arch.1690

[28] Lin C-C. et al., "Impact and Control of Reflected Noise from an Overpass Bottom", *Applied Sciences*, 2018, vol. 8(10):1908. https://doi.org/10.3390/app8101908

[29] Wai Ming T., Chung A.W.L., Schulte-Fortkamp B., "Soundscape design of an open-air concert venue using virtual reality technologies", in *Proceedings of meetings on acoustics Acoustical Society of America,* 2017, 30. 040013. https://doi.org/10.1121/2.0000829

[30] Minell G. et al., "Prediction of off-site noise levels reduction in open-air music events within densely populated urban areas", in *INTER-NOISE and NOISE-CON Congress and Conference Proceedings*, vol. 259 (5), 2019, pp. 4450-4459.

[31] Benocci R. et al., "Accuracy of the Dynamic Acoustic Map in a Large City Generated by Fixed Monitoring Units", *Sensors*, 2020, vol. 20, 412. https://doi.org/10.3390/s20020412

[32] Do Nascimento E.O. et al., "Noise prediction based on acoustic maps and vehicle fleet composition", *Applied Acoustics,* 2021, vol. 174, 107803. https://doi.org/10.1016/j.apacoust.2020.107803

[33] Directive 2002/49/EC of the European Parliament and of the Council of 25 June 2002 relating to the assessment and management of environmental noise, Official Journal L 189, 2002, P.0012-0025.

[34] Wysocki T., *An unusual project by a jazzman: concerts under Wrocław's bridges.* Available: https://www.wroclaw.pl/extra/niezwykly-projekt-jazzmana-koncerty-pod-wroclawskimi-mostami [Accessed: 30 Oct 2021]

[35] Hartley J., "Case study research", in E*ssential Guide to Qualitative Methods in Organizational Research*, eds. Cassell C., Gillian, S., London: Sage Publications Ltd, 2004, pp. 323–333.

[36] Yin R.K., *Case Study Research: Design and Methods*, Thousand Oaks: Sage Publications, 1994.

[37] Harrison H. et al., "Case Study Research: Foundations and Methodological Orientations", *Forum Qual. Soc. Res*., 2017, 18. https://doi.org/10.17169/fqs-18.1.2655

[38] Flyvbjerg B., *Case Study. In The Sage Handbook of Qualitative Research*. 4th ed., eds. Denzin, N.K., Lincoln, Y.S., Thousand Oaks: Sage:, 2011, pp. 301–316.

[39] Berglund B., Lindvall, Th., Schwela, D.H. Occupational and Environmental Health Team. Guidelines for community noise, https://apps.who.int/iris/handle/10665/66217, 1999 (accessed on 6 July 2021).

[40] Decree of Minister of Environment of 15 October 2013 on publishing the consolidated text of the Regulation of the Minister of the Environment on permissible levels of noise in the environment, Journal of Laws, No 120, item 826. Warsaw, 2014.

[41] ISO 1996-2:2017 Recommendation. Acoustics — Description, measurement and assessment of environmental noise — Part 2: Determination of sound pressure levels.

[42] Gottlob D., "Regulations for community noise", *Noise/News International*, December 1995, pp.223-236.

[43] Kozłowski P. Z., "Acoustics and Stage Technology Solutions at New Home for Polish National Radio Symphony Orchestra in Katowice", in *Progress of acoustics,* ed. Bismor D., Gliwice: Polish Acoustical Society 2017, pp. 277-288.

[44] Mehta M.M., Johnson J., Rocafort J., *Architectural Acoustics Principles and Design*. New Jersey: Prentice Hall, 1998.

[45] Mapp P., *Audio System Designer. Technical Reference*. Kiddermnister: Klark-Teknik, 1985.

[46] Biprogeo-Projekt LLC, Kieleckie przedsiębiorstwo Robót Mostowych Skanska joint-stock company. Crossing of the Oder River with access roads within the inner ring road from Legnicka Street to Osobowicka Street in Wroclaw, Wrocław 2002 [Building Permit Documentation] (in Polish).

Simplified analytical method for the robustness assessment of precast reinforced concrete structural systems

Viktar Tur[1], Andrei Tur[2], Aliaksandr Lizahub[3]

[1] Department of Building Structures; Faculty of Civil Engineering;
Bialystok University of Technology; 45E Wiejska Street, 15-034 Bialystok, Poland;
profturvic@gmail.com 0000-0001-6046-1974
[2] Department of Building Structures; Faculty of Civil Engineering; Brest State Technical University;
267 Moskovskaya, 224017 Brest, Belarus;
aturphd@gmail.com 0000-0002-9744-9044
[3] Department of Building Structures; Faculty of Civil Engineering; Brest State Technical University;
267 Moskovskaya, 224017 Brest, Belarus;
p_332_14lizogub@mail.ru 0000-0002-8896-0246

Abstract: The article presents the simplified implementation of alternative load path method based on the energy balance approach. This method should be used to check the global resistance of a damaged structural system after the occurrence of an accidental event. Basic assumptions of simplified analytical models for modelling resistance of horizontal ties in a damaged structural system, taking into account the membrane (chain) effects, were presented. An approach to modelling the dynamic resistance of a damaged structural system based on the energy balance method is described. Calculated dependencies for checking the robustness of a prefabricated multi-storey building with hollow-core slabs after the loss of the central column are proposed and considered using an example. On the considered example, a comparison of the required tie sections area with the dynamic resistance designed using the energy balance method (EBM) and according to the current standards, and a statistical assessment of the reliability of the load-bearing capacity models are carried out. In the end, a brief algorithm for the simplified calculation of the dynamic resistance of a damaged structural system is proposed.

Keywords: alternative path method, simplified analytical model, robustness, ties, energy balance method, membrane effect

1. Introduction

Resonant building disasters over the last century [1], [2] have shown that checking the robustness of damaged systems in accidental design situations should be considered as one of the most important stages of the design and detailing of the building structural elements .

A structural system should fulfil the requirements regarding robustness at the stage of conceptual design, taking into account the use of various strategies for protection against progressive collapse.

It should be noted that in scientific and technical literature definitions of the term "*robustness*" are widely presented [1]–[6]. For example, *fib* Bulletin 43 [7] guidelines define *structural robustness as the insensitivity of a structural system to local failure*. In this context, insensitivity is understood as the state of a modified structural system, when damage to individual elements (the so-called key elements with respect to the system as a whole) causes only insignificant changes in its structural behaviour (its response). The ability of the system to redistribute additional action effects that appear after damaging the structure under the accidental actions is achieved. In this case, we expect to observe a ductile (not brittle) behaviour of structural components without global collapse mode in the structural system.

In the current standards [8]–[13], the requirement for robustness checking is implicit where an accidental situation is caused by events such as fires, explosions, impacts of vehicles on parts of the building, consequences of human errors made at various lifetime stages of the structure.

It should be noted that almost all known definitions of the term "robustness" [2] are based mainly on the phenomenon of disproportionate collapse, and only a few, for example [5], consider robustness as an aspect of the safety of a structural system. According to [13] *"robustness is a specific aspect of structural safety that refers to the ability of system subject to accidental of exceptional loadings (such as fire, explosions, impact or consequences of human error) to sustain local damage to some structural components without experiencing a disproportionate degree of overall distress or collapse"*.

The draft new *fib* MC2020 develops provisions related to the assessment of the robustness of structural systems, which are based on the risk assessment format as presented in ISO 2394:2015 [14]. According to *fib* MC2020, structural robustness checks should include the following basic steps: (1) identification of the intended hazard (H) or the list of hazards to which the structural system is likely to be exposed during a lifetime. At the same time, it should be taken into account that we may not identify some hazards at the designing stage (for example, terrorist and/or criminal attacks); (2) determination of the local resistance of an individual key element (D); (3) determination of subsequent indirect damage to the system (S) following direct local failure, also described as progressive collapse; (4) quantifying the values of direct C_{dir} and indirect C_{ind} consequences, including economic, social, environmental losses, as well as the cost of human life losses (human victims) in monetary terms according to ISO 2394:2015. Direct costs (damage) are usually localized because of the damage to individual structural components, while indirect losses are associated with the system functionality loss because of the implementation of direct losses. The total risk R_{tot} associated with a system failure in an accidental design situation is calculated according to ISO 2394:2015.

The main strategies for the protection of structural systems from progressive collapse and the requirements for the robustness assessment of reinforced concrete structural systems are detailed in [1], [10], [12], [15]–[18]. In this article, we will consider only the alternative load path strategy (ALP) in more detail.

The combination of horizontal (internal and perimetric) and vertical ties placed in floor elements, columns and walls ensures the integrity of the structural system. In an accidental

design situation, the system of ties is considered as the "*second line of defence*" of the structural system after the exhaustion of the flexural resistance of its elements.

When the internal support is removed in the floor elements, the arched effect, bending (beam) and membrane (chain) effects can be realized in succession (depending on the vertical displacement development for the different boundary conditions). If the slab deflection exceeds the critical value and the ties collapse or lose anchorage in adjacent spans, this will indicate that the limit state has been exceeded.

Compared to monolithic reinforced concrete structural systems, precast RC buildings are more sensitive to the effects of accidental actions. This is due to the presence of different types of butt joints that ensure integrity of the structural system and continuity of alternative load paths. At the same time, prefabricated systems distinguish between joints working in tension, compression, bending, torsion, and shear. When designing precast buildings, all requirements are taken into account, both the strategies for protection against progressive collapse and the checks of the structural system robustness .

In traditional prefabricated reinforced concrete systems, friction forces on the contact of elements, restraining deformations on supports (arch effect) and welded joints of embedded parts slightly increase the resistance of the system under the action of vertical (gravity) loads. However, this is not enough to ensure sufficient resistance of the structural system in accidental design situations. In this way, in the original precast RC-structural system, it is necessary to reserve enough ties that have the required continuity and ductility to ensure the integrity of the damaged system. The continuity of the tie elements provides resistance to an accidental combination of actions by mobilizing alternative load paths after the support has been removed. Ductility is the ability to obtain significant plastic bond elongation before rupture. Such property is important for redistributing forces and obtaining large deflections necessary for the realization of the chain (membrane) effect, as well as a measure that provides energy absorption (damping) during ?dynamic application of an accidental action after the vertical support loss.

In structural systems made of prefabricated reinforced concrete elements, all key elements whose failure can lead to the disproportionate collapse of the complete system should be identified at the stage of conceptual design. Therefore, at the first stage, it is recommended to analyse the local resistance of key elements, as it is performed, for example, in case of the panel buildings designing.

In a two-stage design, a structural system robustness check using non-linear static (NLS) or dynamic (NLD) models that consider the spatial work (3D) of the structural system is performed. Adequate modelling of ties is important when using computer software and it should be based on fairly simple and reasonable relationships. ("*Make everything as simple as possible, but not simpler*" – Albert Einstein).

The article presents simplified analytical solutions for the design of horizontal ties in precast hollow-core slabs floor which are obtained on the basis of the provisions of the energy balance approach [16]–[19]. Using the example of a real prefabricated floor, we compared the calculation results of the required parameters of horizontal ties designed according to the proposed method and calculation models included in the structural codes of various countries [8]–[13], [20]. It has been established that the ductility of ties is one of the basic parameters that should be controlled when calculating ties.

2. Analytical models for horizontal ties resistance

2.1. Membrane (chain) effects in a damaged structural system

As shown above, redundancy of alternative load paths is considered as the main strategy for the protection of the structural system from progressive collapse. Alternative load paths in a damaged structural system are realized through "chain" (or "membrane") effects for floor slabs, cantilever and beam effects for precast walls, vertical suspension of walls and columns, diaphragm effect in the floor plane. When the chain (membrane) of the mechanism in the damaged structural system is implemented, all gravitational loading is detected due to reactions in the tensioned horizontal ties.

As follows from [2], until now there has been no consensus on the magnitude of the vertical deflection, after the exceeding of which chain effects are accounted for in the structural system resistance. It is generally accepted that this is a state when compressive axial forces become tensile, or a state in which the tie elements begin to actively detect tensile forces.

In RC frames, the beam-end-moment effect is initially implemented. Flexural plastic hinges are formed in the near support sections. After the exhaustion of their bending resistance at large deflections, chain (membrane) resistance mechanisms come into operation.

In accordance with the requirements of the standards [8], [10]–[13], [20], calculation of chain (membrane) forces in a deformed structural system is performed, as a rule, separately, without taking into account its bending behaviour during the formation of plastic hinges.

Chain (membrane) effects should be considered as the "second line of defence" of the structural system against progressive collapse if the damaged structural system is capable of mobilizing alternative loading paths.

2.2. Basic assumptions of simplified analytical models

For damaged structural systems, the resistance will depend on the dynamic effects during the transition to a deformed shape under an accidental action combination, as well as on the nonlinear behaviour of the connections. In the design, we should consider these effects in the calculation model. Bulletin 43 [7] proposed a simplified approach for such an analysis. The basic provisions of a simplified model for calculating modified systems with alternative load paths based on the application of the energy approach were developed in [16]–[19]. We apply the considered model for simplified analysis of the damaged load-bearing structural systems for which the global resistance depends on the resistance of the horizontal ties loaded by tension. However, the basic principles adopted in the described model are valid also for the analysis of another type of the collapse mechanism, where the plastic displacements are localized in connections. Considering the collapse mechanisms of the structural system, the development of analytical resistance models of horizontal tensile ties was carried out basing on the following assumptions:

1) we assume the key element to be removed from the structural system suddenly after the accidental action has been applied;

2) we assume that gravity force only loads the damaged system with the removed element. The accidental combination includes the characteristic value of the dead load and the quasi-permanent value of the imposed load. Basic rules for accidental load combinations when checking damaged structural systems are discussed in detail in [21], [22];

3) prefabricated elements under displacement of the system are assumed to be perfectly rigid bodies connected by deformable ties;

4) the global resistance of the damaged structure depends only on the resistance of some critical ties. During the development of the deflection in the damaged structural system, maximum forces arise in the ties;

5) at the stage when the support has suddenly been removed, these connections providing alternative load paths are assumed to be unstrained.

The gravity forces acting on the system are modelled by the resultant $Q = mg$ applied at the centre of gravity of the prefabricated elements. The actual position of the damaged system is determined by the generalized displacement a_q at the centre of gravity and a rotation θ (here, in the general case, a_{qz} is the vertical component of displacement). It is possible to establish simple geometric relationships between the vertical deflection of the system a_{qz} and the linear elongation w_i of the ductile joints following assumptions (2) and (4). The load-displacement relationship "N-w_i" should describe the nonlinear behaviour for each tie connection i (see section 2.2).

2.3. Modelling the dynamic resistance of a structural system based on energy balance: design equations

According to assumption 5, immediately after the support is removed, the vertical displacements of the structural system are practically not limited because the ductile joints are unloaded. The system, when moving down, is under acceleration. The resultant tie forces in the damaged system can be taken as the system resistance R, which balances the gravity force acting in its centre of gravity. We can define resistance as static (quasi-static) or dynamic. According to the energy approach [16]–[19], the static resistance varies depending on the value of displacement and can be expressed by the resistance function $R_{stat}(a_{qz})$ associated with the "N-w" relationship for ductile ties in the joints of precast elements [7].

In the general case, the energy balance equation for the vertical displacement a_q and rotation θ of the moving system (see Fig. 1) can be written in the traditional form as:

$$\frac{m}{2} \cdot \left(\frac{da_q}{dt}\right)^2 + \frac{I_m}{2} \cdot \left(\frac{d\theta}{dt}\right)^2 = m \cdot g \cdot a_{qz} - \sum_{i=1}^{n} \int_{0}^{w_{i,max}} N_i(w_i)\,dw_i \tag{1}$$

where I_m is the mass moment of inertia.

The first term on the right-hand side of equation (1) describes the potential energy, and the last term is the absorbed strain energy of the tie. The two terms on the left-hand side of this equation describe the kinetic energy because of the displacement and rotation, respectively. To obtain a deformed state of equilibrium, the motion of the system must stop. At the downward position, the kinetic energy of the structural system has the value $W_k = 0$. In this case, we assume that the maximum vertical deflection $a_{qz,max}$ of the gravity centre of the damaged part in the structural system and of the tie linear displacements w_i is reached. The equilibrium equation for the deformed state of a system with single-degree-of-freedom (SDOF) in the first half-period of oscillations can be written in the traditional way (Eq. 2):

$$Q \cdot a_{qz,max} = \sum_{i=1}^{n} \int_{0}^{w_{i,max}} N_i(w_i)\,dw_i \tag{2}$$

where $a_{qz,max}$ is the maximum vertical deflection in the point, where the driving force Q is applied, when the downward motion stops; $w_{i,max}$ is the horizontal displacement of the i-th connections.

According to [7], the strain energy capacity of the tie can be obtained from the relationship *"N-w"* as follows:

$$\xi(w) = \frac{W_{\text{int}}(w)}{N_u \cdot w} = \frac{\int_0^w N(w)dw}{N_u \cdot w} \tag{3}$$

Therefore, Eq. 2 expressing the energy balance of the deformed system can be written as:

$$Q \cdot a_{qz,\max} = \sum_{i=1}^{n} \xi_i(w_{i,\max}) \cdot N_{i,u} \cdot w_{i,\max} \tag{4}$$

At the stage when the motion stops at the downward position, the system is not necessarily in equilibrium. Therefore, besides Eq. 4, the following inequality should be met:

$$R_{stat}(a_{qz,\max}) \geq m \cdot g \tag{5}$$

If inequality (5) is not met, the accepted value of $a_{qz,\max}$ is not correct, since before it is reached, the tie elements are broken. The process of successive destruction of the tie elements with an increasing displacement of the modified system is called the zipper-type mode.

The conditions of the equilibrium of forces in the deformed state for the proposed collapse mechanism are checked using Eq. 4 and Eq. 5. The dynamic resistance of the damaged system is based on the resistance of horizontal ties to the maximum driving force $Q = mg$ after a sudden removal of the column.

As follows from Eq. 4, the dynamic resistance $R_{\text{dyn}}(a_{qz,\max})$ depends on the maximum vertical deflection $a_{qz,\max}$, which is chosen to consider 1) the availability of free space for the downward movement of the system (for example, according to [7] and [11], it is the distance to the underlying floor) and 2) the ductility of the ties.

A quantitative assessment of the uncertainties of the proposed simplified method based on energy balance, in comparison with the direct nonlinear dynamic analysis, is considered in [16]–[19], in particular in the most recent of them [23]. In [23], it was noted that instead of the cumbersome nonlinear dynamic analysis (NLD), which contains a number of uncertainties (for example load history, damping coefficient, etc.), the method based on energy balance (EBM) is a promising approach for determining the maximum dynamic response of the structure. Despite some errors adopted in the estimation, authors [23] show that the method based on the energy balance is quite accurate and effective both 1) in implementing the bending mechanism (the formation of plastic hinges at small deformations), and 2) at the stage of the membrane (chain) effect implementation in ties that detect tension (the stage of large displacements). Studies [23] show that the model describing the uncertainty (modelling error) of the energy balance method (EBM) compared to nonlinear dynamic analysis (NLD) describes it well using a lognormal distribution with the following statistical parameters LN (0.95; 0.20). (*It should be noted that there is a certain amount of slyness here: the finite element model should be tested basing on classical laws, and not vice versa*).

3. Prefabricated building with hollow-core slabs

3.1. Static and dynamic resistance

As shown above (see Eqs. 2-4), the resistance of a damaged system with alternative loading paths almost directly depends on the ductility of the tie connections.

Let us consider a prefabricated floor with hollow-core slabs of equal spans. The internal support of the continuous girder is removed under accidental action. When the support is removed, a longitudinal strip of the prefabricated floor together with the ties forms an alternative load-bearing bridging system. In accordance with the formulated assumptions (see Section 2.2), in the ultimate state prefabricated floor elements are considered as rigid bodies connected by ductile ties.

After the sudden removal of the mid-column of the continuous girder, the prefabricated slabs rotate at the adjacent supports and move in the horizontal direction.

As follows from [2] and [7], the resistance model considers a longitudinal strip of prefabricated floor elements (for example, hollow-core slabs). In this simplified model, the resistance in the transverse direction, arch, and beam effects in the longitudinal direction are neglected and are not taken into account.

We assume that the horizontal ties of the system have the same mechanical characteristics; therefore, for any state of deflection, the three ties have the same tensile force and the same elongations, because the characteristic load-deflection N-w relationships for each tie are the same. For each precast floor element, the resultant Q, which is assumed to be placed in the gravity centre of the element, represents the self-weight and other permanent loads. The deformed state is described using the deflection a_{qz} of the driving force [7] (see Fig. 1).
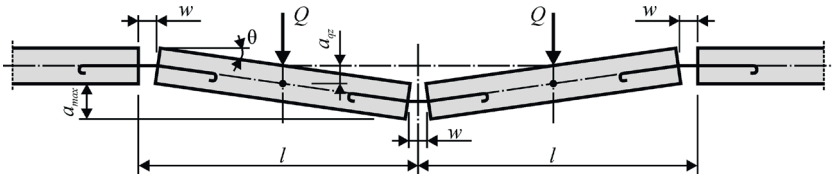

Fig. 1.   Deformed scheme of prefabricated floor for catenary (chain) forces calculation. *Source:* own study

From the conditions of the static equilibrium of the system in a deformed state, we can write:

$$Q \cdot \frac{l}{2} = N(w) \cdot 2 \cdot a_{qz} \qquad (6)$$

For the certain displacements w of the horizontal ties, the vertical deflection a_{qz} can be calculated directly from the deformed geometric scheme (see Fig. 1) as:

$$a_{qz} = \frac{\sqrt{3 \cdot l \cdot w}}{2} \qquad (7)$$

where l is the length of the prefabricated elements.

Considering Eq. 7, static resistance is expressed as:

$$R_{max}\left(a_{qz,max}\right) = 2 \cdot N(w) \cdot \sqrt{\frac{3 \cdot w}{l}} \qquad (8)$$

The maximum value of the static resistance is associated with the maximum displacement $a_{qz,max}$, at which the downward movement of the system must be stopped and which is determined by the formula:

$$R_{max}\left(a_{qz,max}\right) = 2 \cdot N_u \cdot \sqrt{\frac{3 \cdot w_{max}}{l}} \qquad (9)$$

We can express the energy equilibrium condition for the doubled span system as:

$$2Q \cdot a_{qz,\max} = 3\xi\left(w_{\max}\right) \cdot N_u \cdot w_{\max} \tag{10}$$

By introducing Eq. 7 and Eq. 9 into Eq. 10, we obtain the dynamic resistance as:

$$R_{dyn}\left(a_{qz,\max}\right) = \frac{1}{2}\xi\left(w_{\max}\right) \cdot R_{\max} \tag{11}$$

As stated in [2], even if the tie will have an ideally plastic response, the static response of the system based on the chain (catenary) actions increases almost linearly with increasing displacement, therefore Eq. 11 uses a factor of 1/2.

3.2. Modelling of the tie elements. "*N-w*" relationship for reinforcing bar

The "*N-w*" relationship relates the tensile force *N* in the tie connection and its end displacement *w* (local end-slip displacement). To obtain the "*N-w*" diagram, it is necessary to have an adequate local bond-slip relationship "*τ-s*" (Fig. 2). Basing on extensive experimental research [24], including our own, we adopted the dependence in accordance with [8] and [13].
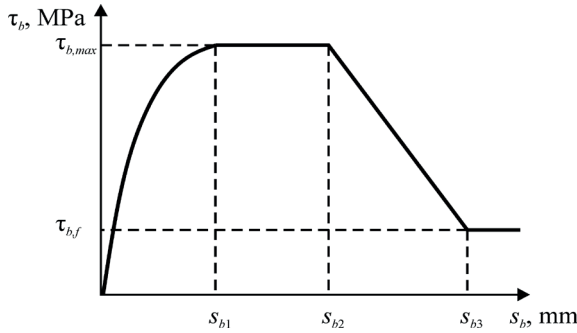

Fig. 2.   Analytical bond stress-slip relationship *Source:* [8], [13]

The advantage of the relationship (Fig. 2) is the applicability for both ribbed and plain bars, as well as an almost complete range of concrete classes, including high-strength ones [8], [13], [24]. The bond-slip behaviour for reinforcement bars is modelled according to [13].

According to [24], for the "*N-w*" diagram development, it is necessary to determine (a) the transmission length l_t, and (b) the strain $\varepsilon_s(x)$ and $\varepsilon_{ct}(x)$ distribution along this length.

In the general case, the transmission zone length increases with increasing tensile stress. In this case, for a steel bar embedded in concrete, the following cases are possible: (1) the length of the transmission zone is shorter or equal to the anchorage length; (2) the transmission zone length is greater than the anchorage length. It should be noted that for continuous tie elements passing through the overlap case (1) is usually valid.

According to [8] and [13], for monotonic loading the reference value of τ_b of the bond stresses between concrete and the reinforcing bar can be calculated as follows:

$$\tau_b = \tau_{b,\max} \cdot s_b^{0.4} \tag{12}$$

where $\tau_{b,\max}$ is the maximum bond-shear stresses between concrete and the reinforcing bar in accordance with [8]; s_b is the current value of the relative slip displacement of the reinforcing bar in concrete.

If the anchorage length is greater than the transmission length, to determine the slip displacement we assume to consider the concrete element rigid in relation to the reinforcing bar. Such an assumption gives a slight overestimation of the designed value of the end slip. According to works [7] and [24], the relation (13) is valid if the following requirements are satisfied: 1) the steel bar works in an elastic stage; 2) the net end-slip is less than 1.0 mm:

$$w_{end} = 0.288 \cdot \left(\frac{\emptyset \cdot \sigma_s^2}{\tau_{b,\max} \cdot E_s} \right)^{0.714} + \frac{\sigma_s}{E_s} \cdot 2 \cdot \emptyset \tag{13}$$

where $\tau_{b,\max} = 2.5\sqrt{f_{cd}}$ for "good" bond conditions; $\qquad$ (14a)

$\tau_{b,\max} = 1.25\sqrt{f_{cd}}$ for "all other" bond conditions; $\qquad$ (14b)

Ø is the bar diameter, in [mm].

In Eq. 13, the first term on the right-hand side describes the end-slip displacement caused by bond stresses along that part of the transmission length where bond stresses appear, here defined as the "net end-slip" $s_{end,net}$:

$$s_{end,net} = 0.288 \cdot \left(\frac{\emptyset \cdot \sigma_s^2}{\tau_{b,\max} \cdot E_s} \right)^{0.714} \tag{15}$$

The last term of Eq. 13 considers the effect of local concrete failure near the free end over a length of approximately 2Ø.

The relationship between stress σ_s and a given end-slip displacement can be rewritten from Eq. 15 as follows:

$$\sigma_s = 2.39 \cdot \sqrt{\frac{\tau_{b,\max} \cdot E_s}{\emptyset} \cdot s_{end,net}^{1.4}} \tag{16}$$

where $s_{end,net} = w_{end} - \dfrac{\sigma_s}{E_s} \cdot 2 \cdot \emptyset$ $\qquad$ (17)

The transmission length according to works [7] and [24] is calculated as:

$$l_t = 0.583 \cdot \frac{\emptyset \cdot \sigma_s}{\tau_{b,\max} \cdot s_{end,net}^{0.4}} + 2 \cdot \emptyset \tag{18}$$

When yielding in steel reinforcement starts, the end-slip $w_{end,y}$ and the transmission length $l_{t,y}$ can be obtained by inserting $\sigma_s = f_{yd}$ into Eq. 16 and Eq. 18. In the general case, the relationship *"N-w_{end}"* is nonlinear before steel yielding is reached. However, the pull-out stiffness of the joint $k_a(w_{end})$ is generally defined as a secant at point $N(w_{end})$:

$$k_a\left(w_{end}\right) = \frac{N\left(w_{end}\right)}{w_{end}} \tag{19}$$

As the first approximation, we can obtain the value of the connection pull-out stiffness based on the stiffness it reached just before yielding:

$$k_a = \frac{N_y}{w_{end,y}} \tag{20}$$

where N_y is the force corresponding to the steel yielding in the tie connection; $w_{end,y}$ is the end-slip corresponding to $\sigma_s = f_{yd}$.

It should be noted that Eq. 19 underestimates the stiffness for loads less than N_y. A more accurate value of the axial stiffness is calculated by Eq. 20 for a given loading range or the end-slip.

According to [7], the "plastic zone length" is defined as the part of the transmission length where the reinforcement bar has reached yielding. Within the "plastic zone length", the bond-shear stress decreases due to steel yielding to [24].

If the anchorage length of the reinforcement bar in the concrete body is sufficient, the maximum value of the "plastic zone length" along the transmission length can be calculated accounting for the fact that the reinforcing steel reaches rupture tensile strength f_u. Along the "plastic zone" length, the tensile stress in reinforcement increases from the value of yield strength f_y to the value of the ultimate tensile strength f_{ud} at the loaded end of the bar.

The ultimate value of the plastic zone length can be calculated according to [24] as:

$$l_{t,pl} = \left(\frac{f_{ud} - f_{yd}}{\tau_{bm,pl}} \right) \cdot \frac{\varnothing}{4} \tag{21}$$

where $\tau_{bm,pl}$ is the average value of bond-shear stress, calculated by Eq. 22.

To calculate the average shear-bond stress for ribbed bars of ductile type (classes B and C according to [8] determined as "*high ductility*") in [7], [24], the following formula has been proposed:

$$\tau_{bm,pl} = 0.27\tau_{b,\max} \tag{22}$$

where $\tau_{b,\max}$ is determined by Eq. 14a or Eq. 14b, depending on the bond conditions.

The ultimate end-slip of the tie bar can be calculated as follows:

$$w_{end,u} = l_{t,pl} \cdot \varepsilon_{sm,pl} + w_{end,y} \tag{23}$$

where $\varepsilon_{sm,pl}$ is the average strain of the reinforcing bar along the plastic zone length, and according to [7] it can be estimated as $\varepsilon_{sm,pl} = 0.5\varepsilon_{su}$.

As follows from Eq. 23, with an increase of the plastic zone length $l_{t,pl}$. the ultimate displacement of the tie increases. An idealized three-line "*N-w*" relationship shown in Fig. 3 can be proposed, basing on the recommendations of [7].
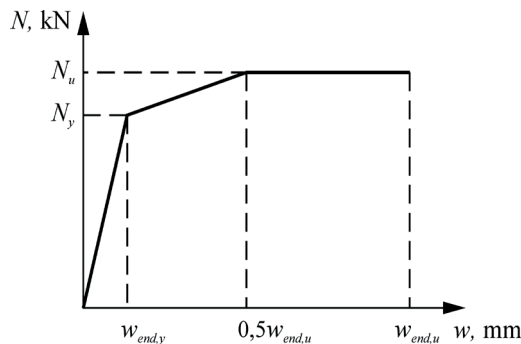

Fig. 3.   Idealized "*N-w*" relationship. *Source:* [7], [24]

4. Example of checking the robustness of precast multi-storey building

4.1. Structural system description, input data for analysis

As an example, we will consider the structural system of an 18-storey building, the plan of which is shown in Fig. 4. In the considered structural system, monolithic (cast-in-place) columns with a section of 300x300 mm (along axes 2, 7) and prefabricated panel walls (along axes 1, 4, 8) are used as supporting vertical elements. Floors are made of prefabricated hollow-core slabs (1.2x6.0x0.22 m) with modification in the support nodes. The slabs are supported on prefabricated girders with a height of 0.26 m (see Fig. 4). At the stage of preliminary analysis and design, an integrated system of horizontal and vertical ties under the requirements of [8] and [10] was designed.

In accordance with the input data, the following characteristic values of actions were adopted for the design: (1) dead load of floor slabs g_{k1} = 3.05 kPa; (2) dead load of the floor finishing g_{k2} = 0.6 kPa; (3) imposed load q_k = 1.5 kPa. An accidental load combination is taken as:

$$p_A = g_{k1} + g_{k2} + \psi_2.q_k = 3.05 + 0.6 + 0.3 \cdot 1.5 = 4.1 \text{ kPa}.$$

According to the proposed analytical model, we check the robustness of the structural system taking into account the chain (membrane) effects.
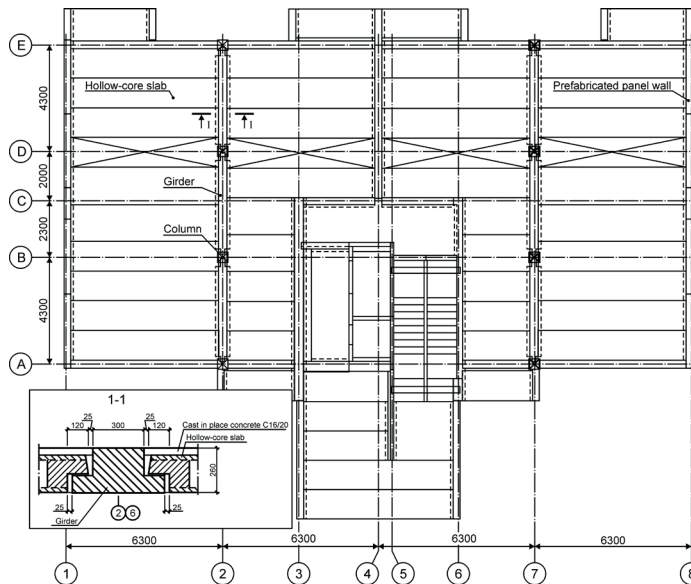
Fig. 4.   The first floor of an analysed 18-storey prefabricated framed building. *Source:* own study

Within the framework of the approaches in the current codes and guidelines [8]–[12], the resistance of precast floor slabs in one direction and resistance of prefabricated girders in the other (transverse) direction are considered separately. To determine the required cross-sectional areas of horizontal ties in girders and slabs, the principle of compatibility of vertical displacements

at the point of the column removal is used. In accordance with this principle (the principle of compatibility), the force-deformation connection parameters of the ties in the beams and slabs are determined in the condition of equality of displacements: $a_{max,p} = a_{max,b}$ (here, $a_{max,p}$ and $a_{max,b}$ are the maximum deflection of slabs and girders at the remote element, respectively).

4.2. Modelling of the horizontal tie

Plain bars Ø28S240, which have significant plastic deformability, are accepted as tie connections. The following reinforcement steel properties are taken: $f_{yk} = 240$ MPa; $(f_u/f_y)_k = 1.3$; $E_s = 200$ GPa; $\varepsilon_{suk} = 1.5 \cdot 10^{-2}$; $A_s = 616$ mm². It is assumed that the tie bar is anchored in confined concrete of compressive strength class C20/25 ($f_{ck} = 20$ MPa; $f_{cm} = 20 + 8 = 28$ MPa), "good" bond conditions. In Tab. 1, the values of the main parametric points of the "N-w" relationship (Fig. 3) for tie connections are presented, which are calculated basing on the proposed end-slip approach.

Table 1.   "N-w" relationship basic points for plain bars Ø28S240. *Source:* own study

№	Reinforcement	Parameters for "N-w" diagram			
		N_y, kN	N_u, kN	$w_{end,y}$, mm	$w_{end,u}$, mm
1	2Ø28S240	295.68	384.38	0.658	28.94
2	4Ø28S240	591.40	768.76	0.658	28.94

Note: general view of the "N-w" diagram see Fig. 3.

4.3. Analytical solution for ties sections area

Let us consider a strip of girders along axis 2 (Fig. 4). We conclude that the internal tie connections in the direction of axis 2 are concentrated in prefabricated girders. The girders are loaded with an accidental loads combination as follows: $Q = 4.1x6.0x4.0 = 98.4$ kN. The girders have a loop connection at the column (2Ø25S500) and have additionally reserved horizontal tie connections (4Ø28S240). The deflection of the middle joint (at the joint with the removed column) should not exceed 2.3 m (free floor space). In Tab. 2, the main design parameters and the results of robustness checking are presented.

Basing on the accepted concept of the deflection compatibility, we will show how to determine the required cross-sectional area of the tie connections for a given type of rein-forcement (S240).

Basing on the results from Table 2, the required ultimate force to break the bar can be calculated from Eq. 9 as:

$$N_u = \frac{R_{max}}{2 \cdot \sqrt{\dfrac{3 \cdot w_{max}}{6.0}}} = \frac{60.86}{2 \cdot \sqrt{\dfrac{3 \cdot 0.0206}{6.0}}} = 299.8 \text{ kN,}$$

where $R_{max} = \dfrac{2 \cdot R_{dyn}}{\xi(w_{max})} = \dfrac{2 \cdot 29,52}{0,97} = 60,86$ kN.

Since 2Ø28S240 $N_u = 384$ kN > 299.8 kN, the required reinforcing bar area equals:

$$A_{s,req} = \frac{N_u}{1.3 \cdot f_{yk}} = \frac{299.8 \cdot 10^3}{1.3 \cdot 240} = 960.9 \text{ mm}^2;$$

we accept 2Ø25S240 ($A_s = 982$ mm²).

Table 2.   Robustness checking results for an analysed precast building (by EBM). *Source:* own study

Calc. step	Design Parameter	Reference	Value	Units
Girders ($l = 4.3$ m)				
1	w_{max}	Tab. 1	0.02894	m
2	$a_{max,b} = 2\,a_{qz,max}$	Eq. 6	0.61	m
3	R_{max}	Eq. 9	218.47	kN
4	R_{dyn}	Eq. 11	218.47	kN
5	$R_{dyn} > Q$	Eq. 5	105.8>98.4	
Hollow-core slabs ($l = 6.3$ m)				
6	$a_{max,s} = a_{max,b}$	see note[1]	0.61	m
7	w_{max}	Eq. 6	0.0206	m
8	R_{max}	Eq. 9	77.94	kN
9	R_{dyn}	Eq. 11	37.80	kN
10	$R_{dyn} > Q$	Eq. 5	37.8>29.52	

Notes:
1) based on the compatibility hypothesis $a_{max,s} = a_{max,b}$.

4.4. Comparison of the required tie sections area and dynamic resistance designed using energy balance method (EBM) and according to current standards

At the first stage, we verified the proposed model based on the results of our own investigations [25] obtained by testing span-to-span hollow-core slab fragments under uniformly distributed load and sudden support removal (see Fig. 5). It was found that the obtained experimental results are in good agreement with the calculation based on EBM.

Fig. 5.   Experimental investigation of hollow-core slab fragment. *Source:* [25]

Let us compare now the calculation results obtained using the proposed model (EBM) and the models included in the codes and standards of various countries. In Tab. 3, the results of calculating the required cross-sectional area of horizontal tie connections according to the current standards are given.

The analysis of standards [8], [10]–[12] shows that all the design models for the calculation of the chain (membrane) force presented in Tab. 3 are based on the equations which are obtained from the condition of static equilibrium of the deflected system at the maximum vertical displacement:

$$T_j = \left(1+\alpha\right) \cdot \frac{\left(g_k + \psi_i \cdot q_k\right) \cdot l_b^2}{2 \cdot \delta_s} \tag{24}$$

where δ_s is the vertical displacement of the joint with the removed element.

In work [2] it is shown that the design model of [10] and [11] is based on the following formula for the determination of the vertical displacement:

$$\delta_s = 18.75 \cdot (1+\alpha) \cdot \frac{l_b}{T_j} \qquad (25)$$

Table 3.　Designing horizontal ties according to current standards. *Source:* own study

№	Reference	Expression	Tie Force, T_j		$a_{max}^{(2)}$	δ_s	Reinforcement (A_s, mm²)
			kN	kN/m	m		
1	[10]	$0.8(g_k^{(1)} + q_k)sL$	75	62.5	1.3	$\leq \dfrac{l_s}{4.8}$	1Ø20S240 (314)
2	[10] [11] [12]	$\dfrac{(g_k + q_k)}{7.5} \cdot \dfrac{l_r}{5} \cdot F_t$ $F_t = 20 + 4n_s$ or 60 kN/m	62.69	51.91	1.97	$\leq \dfrac{l_s}{3.2}$	1Ø20S240 (314)
3	[12] [8]	$3(1.2\,g_k + 0.5q_k)l_b$ $3(g_k + 0.3q_k)l_b$	116.34	96.57	1.05	$\leq \dfrac{l_s}{6}$	1Ø25S240 (491)

Notes:
1) input data $l_b = 6.3$ m; $g_k = 3.65$ kPa; $q_k = 1.5$ kPa;
2) the value of the maximum deflection $a_{max} = \delta_s = (g_k + q_k) \cdot l_b^2 / (2 \cdot T_j)$

When determining α from 0 to 1.5 (according to [2]) and F_t from 24 to 60 kN/m (when the number of floors changes from 1 to 10 or more), we obtain the maximum displacement $a_{max} = \delta_s \leq l_b / 1.28(!)$. The design model of [12] was obtained with $a_{max} = \delta_s \leq l_b / 6$.

Basing on the analysis of the results obtained from testing the full-scale slab-to-slab joint tests carried out by PCA [2], it is implied that the catenary action will stop at an ultimate deflection greater than $\delta s = lb / 6.67$, which agrees well with the [12] requirements and other research studies. Furthermore, experimental studies [2], [18], [23] have shown that in the bar fracture failure mode the system collapses at $\delta s \approx lb / 10$. The discrepancy in the value of an ultimate vertical displacement according to the different standards [8], [10], [11] and another research provision (e.g. energy balance method) is remarkable, and standard [12] is more relaxed.

The comparison of calculation results obtained using the energy balance method and standard methods [8]–[12] (see Tab. 3) shows that the required areas of reinforcing bars used as horizontal ties are significantly different. So, when calculating according to the codes [8]–[11] 1Ø20S240 is required, [12] uses 1Ø25S240 standards (see Tab. 3), while from the calculation according to the energy balance method using the dependences, "N-w" is 2Ø25S240.

Assuming fixed values of maximum vertical deflection (from $l_b / 1.28$ to $l_b / 10$) in the codes [8]–[12] leads to rather optimistic and relaxed results when the horizontal ties are designed.

Tab. 4 compares the values of the parametric points of the "N-w" relationship for the tie connections which were calculated according to standards [8], [9], and Tab. 5 presents robustness criteria checking results of the precast floor using the resistances R_{max}, R_{dyn}, assessed basing on the energy balance method.

The calculation result presented in Tab. 5 shows that checking criterion $R_{dyn} \geq Q$ for horizontal ties designed according to the standards [8], [10]–[12] is not satisfied. At the same time, the designed tie connection, despite the significant plastic deformability of the rein-

forcement S240 (ε_{suk} = 1.5·10⁻²), does not provide the *a priori* assumed vertical deflections without the bar rupture. A sudden failure mode of the structural system occurs. The vertical deflection of the damaged floor a_{max} = 0.73 m with horizontal steel ties 1Ø20S240, determined by the energy balance method considering the ultimate (rupture) steel force, turns out to be insufficient for resisting the accidental action effects. Tie forces determined by the standards [8], [10]–[12] correspond to a_{max} from 1.05 m to 1.968 m, which is not realistic for this type of reinforcement (Ø20S240).

Table 4. "*N-w*" relationship basic parameters for analysed horizontal ties according to [7] and [24]. *Source: own study*

№	Reinforcement	Parameters of the "*N-w*" diagram			
		N_y, kN	N_u, kN	$w_{end,y}$, mm	$w_{end,u}$, mm
1	1Ø25S240	117.84	153.19	0.492	38.49
2	1Ø20S240	75.4	97.97	0.612	30.8

Note: "*N-w*" diagram see Fig. 5.

Table 5. Design values of resistances R_{max}, R_{dyn} for the damaged system. *Source:* own study

№	Reference	Required reinforcement	Resistance of ties, kN		Maximum displacement a_{max}, m		Criterion $R_{dyn} \geq Q$
			R_{max}	R_{dyn}	according to the standards[(1)]	according to the energy balance[(2)]	
1	[10]	1Ø20S240	23.73	11.03	1.3	0.73	not done
2	[10]–[12]				1.968	0.73	not done
3	[8], [12]	1Ø25S240	41.63	19.44	1.05	0.85	not done
4	according to EBM	2Ø25S240	60.87	29.52	-	0.61	done

Note: 1) max deflection corresponding to the ultimate force in the tie calculated by the current standards;
2) max deflection by the energy balance method (EBM)

As follows from Eq. 24 obtained from the equilibrium condition of the deflected system, at a constant value of the tie force $T_j = f_{yd} \cdot A_{st}$ (after yielding of steel), the global resistance of the structure linearly depends on the value of the vertical deflection δ_s. After rewriting the equation (Eq. 24), considering that $(g_k + \psi_i \cdot q_k) = R_{max}$, we obtain:

$$R_{max} = \frac{2 \cdot f_{yd} \cdot A_{st}}{l_b^2} \cdot \delta_s \tag{26}$$

For the considered case of the horizontal tie 1Ø25 S240 at l_b = 6300 mm, A_{st} = 491 mm²:

$$R_{max} = 0.0059 \cdot \delta_{s,max} \tag{27}$$

4.5. Reliability assessment of the load-bearing capacity models

The next stage of the comparison of the proposed energy balance method (EBM) and standard methods considered in actual codes was performed basing on the reliability assessment of the damaged system with the horizontal ties designed according to provisions (requirements) of the codes and EBM. To determine failure probability, the probabilistic model for the dynamic resistance is combined with the probabilistic model for accidental load combination acting on

the typical floor. We calculated failure probabilities for the damaged system according to the following limit state function g(X):

$$g(X) = \theta_R \cdot R_{dyn} - \theta_E \cdot (G + Q) \tag{28}$$

Probabilistic models for the most important basic variables adopted in the probabilistic models for the dynamic resistance and effects of actions which are used in limit state function (Eq. 28) are listed in Tab. 6.

Table 6. Probabilistic models of basic variables for reliability analyses. *Source:* own study

Category of variables	Name of basic variables	Sym. X	Dimension	Distrib.	Mean μ_X	St. dev. σ_X
Actions	Permanent	G	kN	N	$G_k = 27.59$	$0.1\mu_G = 2.759$
	Imposed	Q	kN	GU	$0.2Q_k = 2.268$	$1.1\mu_Q = 2.495$
Material strengths	Concrete (C20/25)	f_c	MPa	LN	28	4,8
	Reinforcement (S240)	f_y	MPa	LN	300	30
	Reinforcement (S500)	f_y	MPa	LN	560	30
Model uncertainties	Load effect factor	θ_E	-	N	1	0.10
	Resistance factor	θ_R	-	N	1	0.05

Notes:
N – normal distribution; LN – lognormal distribution; GU – Gumbel distribution; $l_s = 6.3$ m; $b_s = 1.2$ m; $g_k = 3.65$ kPa; $q_k = 1.5$ kPa; $G_k = g_k$ x l_s x $b_s = 27.59$ kN; $Q_k = q_k$ x l_s x $b_s = 11.34$ kN

The probability density distribution functions for the different analysed design cases are shown in Fig. 6 and Fig. 7. The results of the failure probability calculations are presented in Tab. 7. Probabilistic modelling of the limit state function was performed with the use of the Monte Carlo simulation method ($N=10^8$).
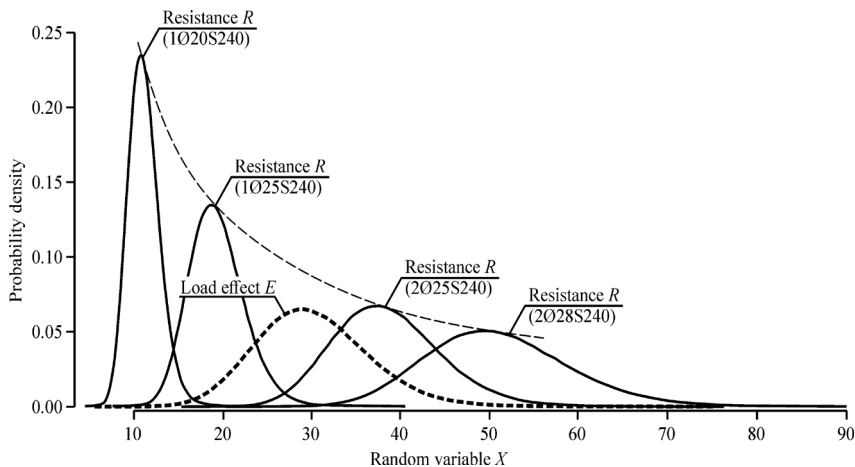

Fig. 6. Load effect E and resistance R as random variables for ties from reinforcement class S240. *Source:* own study
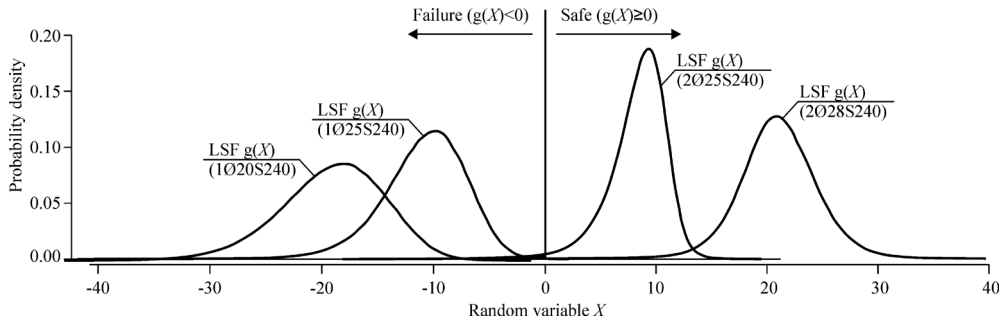
Fig. 7. Limit state function g(X) as random variables for ties from reinforcement class S240. *Source:* own study

Table 7. Results of probability simulation of performance function of damaged system with hollow-core slabs. *Source:* own study

№	Reference	Req. reinforcement	Resistance, R		Load Effect, E		Performance function, g(X)		p_f(g(X)<0)	β
			mean	sd	mean	sd	mean	sd		
Ties from reinforcement of class S240 ($k = 1.3$; $\varepsilon_u = 15\%$)										
1	[10]-[12]	1Ø20 S240	11.03	1.74			-19.12	4.74	0.999999	< -4.8
2	[8], [12]	1Ø25 S240	19.26	3.03	30.14	6.28	-10.88	3.70	0.999971	-4.02
3	according to EBM	2Ø25 S240	38.53	6.07			8.39	2.53	0.007649	2.42
Force-equivalent ties from reinforcement of class S500 ($k = 1.08$; $\varepsilon_u = 5\%$)										
1	[10]-[12]	1Ø20 S500	7.25	0.64			-22.89	5.70	0.999999	< -4.8
2	[8], [12]	1Ø25 S500	12.67	1.12	30.14	6.28	-17.47	5.28	0.999998	-4.6
3	according to EBM	2Ø25 S500	25.34	2.23			-4.80	4.33	0.877255	-1.16

Notes: sd – standard deviation; $k = f_u / f_y$; β is reliability index according to the Laplace function.

As can be seen from the results presented in Tab.7, only the energy balance method (EBM) in which ductility of the steel ties is considered allows to design a reliable structural system in damaged state (failure probability p_f(g(X)<0) = 0.007649 in case 2Ø25S240). From the analysis of the numerical results (see Tab. 7) one can conclude that the design under the actual design regulations according to codes [8], [10]–[12] is non-robust and would collapse in case of the notional column removal, even if the requirements are fulfilled according to the codes. The very close conclusions were formulated in [26] basing on own numerical investigations ("*It is concluded that in case of the removal of an inner column, the original design according to the Eurocodes is very likely to fail.*"). We relate the main reason of this problem of the non-robust designing with the requirements of the actual codes which neglect the ductility and rotation capacity of the slab elements in the damaged system.

5. Brief algorithm for simplified calculation of the dynamic resistance

As shown earlier, one of the main issues in the tie force assessment is to determine the value of deflection at which the catenary effect is mobilized. For a statically indeterminate structural system, this point can be determined using a simplified approach. As the deflection at which the catenary effect starts, point a_0 of the "F-δ" relationship should be taken as shown in Fig. 8. It was assumed as the point where the nonlinear flexural response crosses with a straight-line response of the catenary effect (see Fig. 8).
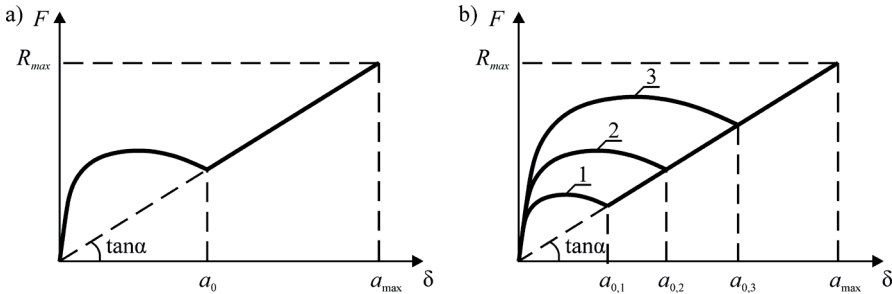

Fig. 8.　For the assessment of point a_0 position. *Source:* own study

It should be borne in mind that the horizontal tie in the structure is either unloaded before being put into operation (when it is designed as an independent link), or has the compressive strained (when it is part of the reinforcement). The amount of horizontal tie reinforcement should be designed in such a way that a chain (membrane) effect is provided for the perception of an accidental combination of actions and that a smooth transition from a disengaging flexural plastic hinge to an engaging tensile tie is ensured. Here, the amount and ductility properties of flexural reinforcement should provide a sufficient length of the plastic deformation branch of the "F-δ" response to achieve the deflection a_0 (see Fig. 9). We should base the structural design procedure for robustness checks on ensuring a smooth and consistent transition to the mobilization of alternative loading paths.
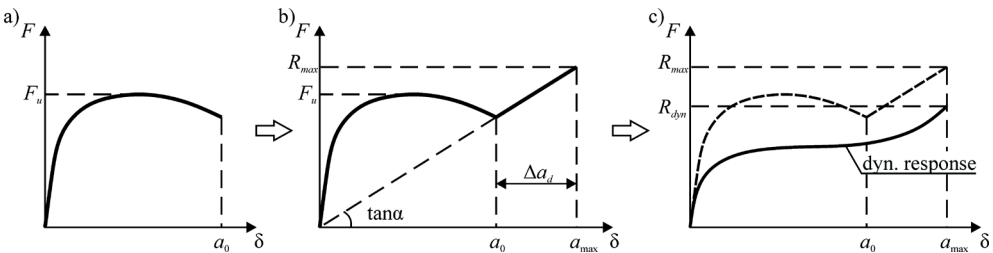

Fig. 9.　Calculation steps to determination of horizontal tie system parameters : a) the response "F-δ" when a flexural plastic hinge is realized; b) common response "F-δ" for the flexural joint and horizontal tie connection; c) the dynamic response of the damaged system. *Source:* own study

In this case, the maximum deflection a_{max} and the resistance R_{max} should be determined basing on the energy balance equations, as shown earlier. To ensure compatibility (consist-

ency) in the response of flexural hinges and horizontal tensile ties in statically indeterminate systems, the following procedure can be proposed:

1) a nonlinear calculation of the modified structural system is performed and the nonlinear reaction "F-δ" is determined taking into account only flexural plastic hinges behaviour (Fig. 9a). A linear reaction "F-δ" will pass through this point (a_0), which describes, with an acceptable approximation, the operation of the horizontal tie. The slope tangent is the axial stiffness of the horizontal tie;

2) the parameters of the horizontal tie connections necessary to ensure the resistance of the accidental combination are calculated. For a given R_{max}, the deformation parameters of the ties are determined, which will ensure the achievement of the maximum displacement a_{max} (Fig. 9b);

3) to perform complex nonlinear analysis of the damaged structural system with flexural and tension plastic hinges using computer software;

4) to calculate parametric points of a dynamic diagram and determine the global resistance of the damaged structural system (Fig. 9c), accounting for the value of the global safety factor according to [11].

5. Conclusions

Basing on the obtained results, the following conclusions can be drawn:

1. The proposed method for determining membrane (chain) forces based on the provisions of the energy balance method of the damaged structural system (EBM) is a promising method for calculating its maximum dynamic response. This method for the determination of the system total dynamic response can be successfully applied both in the case of simple analytical models and for complex nonlinear finite element models instead of a cumbersome nonlinear dynamic analysis (NLD) which contains a number of uncertainties (for example load history, damping coefficient, modelling error etc.).

2. Comparison of the calculation results according to the current standards [8]–[12] with the proposed energy balance method has shown that the calculation models of the codes can give an unsafe result, for example, underestimating the required cross-sectional area of horizontal ties. This is because all dependencies for calculating the tie force were based on constant values of the ultimate deflection (usually from 1/6 to 1/10 of the span), without checking the ultimate deformability of horizontal ties. As follows from the performed analysis, with the unchanged value of the accidental combination of actions, the calculated tie force (for which its cross-section is selected) will change in inverse proportion to the deflection. The approach adopted in the standards [8]–[12] can lead to unrealistic results when the adopted reinforcement in horizontal tie cannot ensure the achievement of the *a priori* maximum deflection due to insufficient deformability. The model included in [12], in which the constant deflection of 1/10 span is used to derive the design equations, is most similar to the solutions based on the energy balance. Changes should be made to the current standards [8]–[10] in terms of the application of methods based on the energy balance of the system for the design of horizontal ties.

3. Taking into account a number of assumptions made in the formulation of the basic provisions of the method based on the energy approach, it is necessary to perform

a statistical analysis of the uncertainty modelling basing on the results of experimental studies, but not on the results of dynamic calculations of the finite element model as done in [23].

References

[1] Adam J.M., Parisi F., Sagaseta J.,Lu X., "Research and practice on progressive collapse and robustness of building structures in the 21st century", *Engineering Structures*, vol. 173, (2018), pp. 122–149. https://doi.org/10.1016/j.engstruct.2018.06.082

[2] Tohidi M., *Effect of floor-to-floor joint design on the robustness of precast concrete cross wall buildings*. PhD dissertation, University of Birmingham, UK, 2015.

[3] El-Tawil S., Li H. and Kunnath S., "Computational simulation of gravity-induced progressive collapse of steel-frame buildings: Current trends and future research needs", *Journal of Structural Engineering,* vol. 140, no. 8, (2014), A2513001. https://doi.org 10.1061/(ASCE) ST.1943-541X.0000897

[4] Byfield M., Mudalige W., Morison C. and Stoddart E., "A review of progressive collapse research and regulations", *Proceedings of the Institution of Civil Engineers-Structures and Buildings,* vol. 167, no. 8, (2014), pp. 447–456.

[5] Fang Z.X. and Fan H.T., "Redundancy of structural systems in the context of structural safety", *Procedia engineering*, vol. 14, (2011), pp. 2172–2178. https://doi.org/10.1016/j.proeng.2011.07.273

[6] Folić R., "Structural Robustness of monolithic and precast RC building", in *First Scientific-applied Conference with International Participation Reinforced Concrete and Masonry Structures-Theory and Practice*, Sofia, 2015.

[7] *fib* Bulletin 43. Structural connections for precast concrete buildings. Guide to good practice, 2008. https://doi.org 10.35789/fib.BULL.0043

[8] SP 5.03.01-2020. Concrete and reinforced concrete structures. Minsk, Belarus, 2020. (In Russian)

[9] SN 2.01.01-2019. Basis of structural design. Minsk, Belarus, 2020. (In Russian)

[10] EN 1991-1-7. Eurocode 1 – Actions on structures – Part 1-7: General actions – Accidental actions, 2006.

[11] BS 8110-1. The structural use of concrete in building – Part 1: Code of practice for design and construction, 1997.

[12] Department of Defense (DoD) Unified Facilities Criteria (UFC-04-023-03). Design Building to Resist Progressive Collapse. Washington, D.C., 2005

[13] MC2010. *fib* Model Code for Concrete Structures, International Federation for Structural Concrete (*fib*), 2010.

[14] ISO 2394:2015. General principles on reliability of structures. International Standard, 2015.

[15] Qian K. and Li B., "Research advances in design of structures to resist progressive collapse", *Journal of Performance of Constructed Facilities*, vol. 29, no. 5, (2015), B4014007. https://doi. org10.1061/(ASCE)CF.1943-5509.0000698

[16] Tur A. and Tur V., "Reliability Approaches to Modelling of the Nonlinear Pseudo-Static Response of RC-structural Systems in Accidental Design Situations", *Journal of Sustainable Architecture and Civil Engineering*, vol. 22, no. 1, (2018), pp. 76–87.

[17] Herraiz B., Vogel T. and Russell J., "Energy-based method for sudden column failure scenarios: theoretical, numerical and experimental analysis", in *IABSE Workshop Helsinki 2015: Safety, Robustness and Condition Assessment of Structures. Report,* International Association for Bridge and Structural Engineering IABSE, 2015, pp. 70-77. https://doi.org/10.3929/ethz-a-010389549

[18] Izzuddin B.A., Vlassis A.G., Elghazouli A.Y. and Nethercot D.A., "Progressive collapse of multi-storey buildings due to sudden column loss – Part I: Simplified assessment framework", *Engineering structures*, vol. 30, no. 5, (2008), pp. 1308–1318. https://doi.org/10.1016/j.engstruct.2007.07.011

[19] Vlassis A.G., Izzuddin B.A., Elghazouli A.Y. and Nethercot D.A., "Progressive collapse of multi-storey buildings due to sudden column loss – Part II: Application", *Engineering Structure*, vol. 30, no. 5, (2008), pp. 1424-1438. https://doi.org/10.1016/j.engstruct.2007.08.011

[20] ASCE. Minimum design loads for buildings and other structures. American Society of Civil Engineers, 2013.

[21] Tur V., Tur A., Lizahub A. and Derechennik S., "Accidental actions values and combinations for key-elements checking", in *E3S Web of Conferences*, vol. 212, EDP Sciences, 2020. https://doi.org 10.1051/e3sconf/202021202019

[22] Van Coile R., Hopkin D., Elhami Khorasani N., Lange D. and Gernay T., "Permanent and live load model for probabilistic structural fire analysis: a review", in *3rd International Conference on Structural Safety under Fire and Blast Loading*, Brunel University, London, 2019, 2nd – 4th September 2019.

[23] Ding L., Van Coile R., Botte W. and Caspeele R., "Quantification of model uncertainties of the energy-based method for dynamic column removal scenarios", *Engineering Structures*, vol. 237, (2021), pp. 112057. https://doi.org/10.1016/j.engstruct.2021.112057

[24] *fib* Bulletin 72. Bond and anchorage of embedded reinforcement: Background to the *fib* Model Code for Concrete Structures 2010. Technical report. fib-Fédération internationale du béton, 2014. https://doi.org 10.35789/fib.BULL.0072

[25] Tur A.V., Petsold T.M., Tsimbarevich T.A., "Experimental research of the robustness of disk of overlapping from the hollow core slabs with removing the carrier element", *Bulletin of the Brest State Technical University*, vol. 1, (2018), pp. 104–109.

[26] Droogné, D., Caspeele, R., Taerwe, L., and Herraiz, B., "Parametric study and reliability-based evaluation of alternate load path design in reinforced concrete slabs", In *39th IABSE Symposium-Engineering the Future*, (2017), pp. 1106-1113. IABSE.